UNIVERSITÀ DEGLI STUDI DI PADOVA

Dipartimento di Geoscienze

TESI DI LAUREA MAGISTRALE IN GEOLOGIA E GEOLOGIA TECNICA

INTEGRATED BENTHIC FORAMINIFERAL AND CALCAREOUS NANNOFOSSIL RECORDS FROM IODP SITE U1506: THE BIOGENIC BLOOM

Il record integrato di foraminiferi bentonici e nannofossili calcarei del Site IODP U1506 durante il "biogenic bloom"

Relatore: Dott.ssa Claudia Agnini, Dipartimento di Geoscienze

Correlatore: Dott.ssa Laia Alegret, Department of Earth Science, University of Zaragoza

Laureanda: Maria Elena Gastaldello

ANNO ACCADEMICO 2018/2019

RIASSUNTO

In questo elaborato di tesi viene presentata l'analisi biostratigrafica, biocronologica e paleoambientale di una successione miocenica-pliocenica recuperata al Site U1506, perforato nel corso della spedizione IODP 371 (Mar di Tasman, Pacifico sud-occidentale). La successione studiata va da una profondità di 233.50 a 81.75 m CSF-A (Core depth below Sea Floor-A).

Nell'intervallo dal Miocene superiore al Pliocene un aumento nelle mass accumulation rates (MARs) delle componenti biogeniche, importanti cambiamenti nelle associazioni planctoniche e bentoniche, e una diminuzione marcata delle condizioni redox nei sedimenti sono stati documentati al di sotto delle zone di upwelling sia nell'Oceano Pacifico e nell'Oceano Indiano. Queste particolari condizioni sono conosciute con il nome di "biogenic bloom". Lavori precedenti hanno suggerito che questo evento paleoceanografico è caratterizzato da un aumento della produttività primaria tra 9.0 e 3.5 Ma.

Un primo risultato di questa tesi è la classificazione biostratigrafica della successione basata sulla biostratigrafia a nannofossili calcarei. A questo scopo, sono state utilizzate le biozonature standard di Martini (1971) e di Okada and Bukry (1980). Inoltre, per migliorare la risoluzione biostratigrafica, è stata utilizzata la recente biozonatura di Backman et al. (2012). Secondo le biozonature disponibili, la sezione si estende dalla Zona NN10 fino alla Zona NN13 (Martini,1971), dalla Subzona CN8b alla Subzona CN10c (Okada and Bukry, 1980) e, infine, dalla Zona CNM15 alla Zona CNPL2 (Backman et al., 2012). Dal punto di vista cronostratigrafico la successione si estende dal Tortoniano (Miocene superiore) allo Zancleano (Pliocene inferiore). Sulla base della biocronologia a nannofossili calcarei è stato sviluppato un modello che ha permesso di stimare l'intervallo di tempo coperto dalla base della sezione (8.45 Ma) al top della stessa (4.53 Ma) come pure le velocità di sedimentazione lungo la successione. Inoltre, il frame cronologico disponibile per il Site U1506 ha fornito una stima precisa del timing e della durata del biogenic bloom, che inizia a 7.28 e si conclude a 6.50 Ma (0.78 Myr). Questo nuovo dato riduce in maniera significativa le prime stime della durata di questo evento (5.5 Myr).

I foraminiferi bentonici sono stati utilizzati per ricostruire le condizioni paleoambientali sul fondale in termini di disponibilità di nutrienti, condizioni trofiche e concentrazione di ossigeno lungo la successione sulla base delle differenti affinità ecologiche dei taxa presenti nelle associazioni. La successione studiata è stata divisa in tre intervalli in base alle associazioni di foraminiferi e alla detrended correspondence analysis (DCA). L'Intervallo 1 è caratterizzato dalla presenza di taxa tipici di ambienti ad alta produttività, caratterizzati da alto apporto di nutrienti e bassi livelli di ossigeno, che sono stati interpretati come la documentazione del biogenic bloom (tra 192.91 e 168.00 m CSF-A). Invece gli intervalli 2 e 3 suggeriscono condizioni più oligotrofiche e caratterizzate da più alti livelli di ossigeno al fondo.

Il prossimo passo per meglio comprendere questo evento sarà quello di integrare i dati paleontologici con quelli geochimici ($\delta^{13}C$) così da correlare i cambiamenti paleontologici con quelli del ciclo del carbonio.

INDEX

ABSTRACT

This Master thesis is a biostratigraphic, biochronologic and paleoenvironmental study of a Miocene-Pliocene section retrieved at Site U1506, drilled during IODP Exp. 371 (Tasman Sea, southwest Pacific). The studied succession spans from 233.50 to 81.75 m CSF-A (Core depth below Sea Floor-A).

During the latest Miocene-early Pliocene, increases in the mass accumulation rate (MAR) of biogenic components, major changes in planktic and benthic fauna assemblages, and marked decreases in sedimentary redox conditions have been documented both in the Indian and Pacific Ocean beneath upwelling zones. These conditions are referred to as the "biogenic bloom". Previous works have suggested that this paleoceanographic event is characterized by a prominent increase in primary productivity between ca. 9.0 and 3.5 Ma.

A first result of this thesis is the biostratigraphic classification of the study succession based on calcareous nannofossil biostratigraphy using appearance and disappearance biohorizons of a number of taxa proposed in standard (Martini, 1971; Okada and Bukry, 1980) and alternative biozonations (Backman et al., 2012).

According to the biostratigraphic zonation available, the study section extends from Zone NN10 to Zone NN13 (Martini, 1971), from Subzone CN8b to Subzone CN10c (Okada and Bukry, 1980) and from Zone CNM15 to Zone CNPL2 (Backman et al., 2012). From the chronostratigraphic point of view, the analysed section thus spans from the Tortonian (late Miocene) to the Zanclean (early Pliocene). Based on calcareous nannofossil biochronology an integrated age model has been constructed which allows to estimate the time interval spanned from the Base of the section (8.45 Ma) to the Top of the section (4.53 Ma) as well as the sedimentation rates along the section. Moreover, the chronological framework available for Site U1506 also permits to evaluate the precise timing and duration of the biogenic bloom that is from 7.28 to 6.50 Ma (0.78 Myr). This datum consistently shortens the previous estimates for the duration of the event (5.5 Myr).

Benthic foraminifera have been used to reconstruct the paleoenvironmental conditions at the sea floor in terms of nutrient availability, trophic conditions and oxygen concentrations along the study section, based on the different paleoecological affinity of the taxa present in the assemblages.

The succession has been divided into three intervals based on changes observed in the foraminiferal assemblages and detrended correspondence analysis (DCA). Taxa typical of high nutrient influx and low oxygen conditions, indicative of high productivity environmental conditions, were observed in Interval 1 and are interpreted to document the biogenic bloom between 192.91 and 168.00 m CSF-A. Instead, Interval 2 and 3 are suggestive of more oligotrophic environmental conditions likely characterized by a higher oxygen availability.

The next step in order to better understand this event will be to integrate paleontological and geochemical (δ^{13}C) data in order to correlate paleontological changes with modifications in the carbon cycle.

INTRODUCTION

Carbon is a vital element on Earth and is essential for the chemical processes that support life. The carbon cycle is a biogeochemical cycle by which carbon is exchanged between four different reservoirs: the atmosphere, the biosphere, the hydrosphere and the lithosphere. Carbon is constantly cycling by means of CO_2 fluxes and is stored in the different reservoirs as inorganic or organic C. It is important to study and understand the carbon cycles since if its balance is not maintained, it can cause dramatic effects (Ruddiman, 2007). One of the most important C reservoir on our planet is the deep ocean, where ca. 38.000 Gt of C is stored. This definitely has a higher capacity with respect to both atmosphere (600 Gt of C) and the upper ocean (1000 Gt of C) (Ruddiman, 2007). The fluxes of carbon among reservoirs always occur through CO_2 exchanges and when the carbon enters in the ocean it is usually found as dissolved inorganic carbon (HCO_3^-, CO_2 and HCO_3^{2-}), carbonates and organic matter. If the CO_2 concentration in the ocean waters increases, this causes an enrichment in H^+ concentration, which means a decrease in ocean pH, that eventually lead possible dissolution of deep-water carbonates, in other words to the so-called acidification. There are several proxies that can be used to get information about the carbon cycle and the paleoceanographic conditions in the oceans. For instance, deep-sea benthic foraminiferal assemblages and bulk $\delta^{13}C$ carbonate could help in reconstructing variations in paleo-marine productivity and export production (Coxall and Pearson, 2007).

In this thesis we investigate a particular long-lived event occurred between ca. 9 and 3.5 Ma, the so-called biogenic bloom (Dickens and Owen, 1999). This event is interpreted as an increase in primary paleo-productivity that is associated with a change in the marine carbon cycle, possibly related to variations in deep water circulation, carbon supply to the ocean, or both (Grant and Dickens, 2002).

Understanding these types of events can actually help to understand the dynamics of modern oceans, in particular the biogenic bloom is interesting to study because is relatively recent and paleoceanographic data for this time interval are well constrained allowing for a detail description of the successive steps of event (timing) as well as the processes involved.

Since the oceanography/paleoceanography is relatively well known for more recent intervals (Neogene), it becomes easier to understand the causes, the mechanisms and effects of the variations recorded in the geological record. This is of particular importance because the geological record represents the only opportunity we have to test processes that lasted millions of years that may have happened in the past and, more interestingly, can reoccur in the future.

Another important bonus in studying the biogenic bloom is that, though it is a relatively recent event (with thus a strong chronological frame and straightforward paleoceanographic contest), we still know very little about how and why it happened and which processes are involved.

1. THE PALEOCLIMATIC CONTEXT

1.1. Paleoclimatic evolution during the Neogene

The Neogene is a geological period that spans from 23.03 Ma (Oligocene-Miocene boundary) to 2.58 Ma (Pliocene-Pleistocene boundary), it includes the Miocene and Pliocene epochs and witnessed several major paleoclimatological changes. This period went from a warm climatic optimum in the late early Miocene through rapid cooling during the middle Miocene, to the onset of Northern Hemisphere Glaciation (NHG) in the Pliocene (Gornitz, 2008).

A dataset of oxygen isotopes ($\delta^{18}O$) (Zachos et al., 2001; Zachos et al., 2008), based on data obtained from more than 40 DSDP (Deep Sea Drilling Project) and ODP (Ocean Drilling Program) Sites, has made possible to carefully observe the trend of temperatures and ice caps variations in the last 65 million years. Of equal importance is the $\delta^{13}C$ data, available for the same time window, which documents the evolution of the carbon cycle throughout the Cenozoic (Fig. 1.1).

A brief rationale of stable isotopes theory and, in particular, on $\delta^{18}O$ is necessary in order to explicit their importance and their present role in reconstructing paleotemperatures values. $\delta^{18}O$ notation is the proxy used, under certain circumstances, to evaluate paleotemperatures and is calculated as specified in the following equation. $\delta^{18}O$ is equal to $^{18}O/^{16}O$ measured in the sample divided by $^{18}O/^{16}O$ of a standard, minus 1 and finally per mill.

$$\delta^{18}O = \left(\frac{\left(\frac{^{18}O}{^{16}O} \right)_{sample}}{\left(\frac{^{18}O}{^{16}O} \right)_{standard}} - 1 \right) * 1000 \text{ ‰}$$

These values are used in the paleotemperature of Epstein et al. (1951) to determine the temperature at which the carbonate precipitated.

$$T = 16.5 - 4.3 \, (\delta^{18}O_{sample} - \delta^{18}O_{sea\ water}) + 0.14 \, (\delta^{18}O_{sample} - \delta^{18}O_{sea\ water})^2$$

T = temperature, $\delta^{18}O_{sample}$ = isotopic value measured in the sample (benthic or planktonic foraminifera, bulk,…) and $\delta^{18}O_{sea\ water}$ = value of water isotope composition. If the temperature is the only factor controlling the isotope composition, the decrease of 1 ‰ in $\delta^{18}O$ values accounts for an increase of ca. 4.2°C in temperature.

It is important to note that variations in $\delta^{18}O$ values are controlled not only by changes in the ocean water temperature but also, and even more importantly, by the changes in ice sheet volume. This is because the waxing and waning of ice sheets allows for larger or smaller amount of water to be stored at poles. During a glacial time, the isotopic fractionation due to the latitudinal effect results in a progressive lighting of the isotopic snow composition that is eventually stored in the ice cap, conversely during an interglacial phase the isotopic fractionation takes place anyway but the amount of ^{16}O stored in the ice sheet is smaller and this results in relatively lighter $\delta^{18}O$ sea water values, if compared with glacial phases.

During the last 65 million years, the Earth's climate system has passed, from warm periods with ice-free poles (greenhouse), to cooler periods with polar ice caps and massive continental ice-sheets (icehouse). During ice-free phases, $\delta^{18}O$ values are exclusively controlled by temperature changes while when at least one ice sheet is present the main factor that influenced $\delta^{18}O$ values is by far the so-called glacial effect. This implies that $\delta^{18}O$ values can be used as paleothermometer only during greenhouse phases, instead, in intervals with documented presence of polar caps the value of $\delta^{18}O$ is used to analyse the evolution of the ice sheets.

Miocene and Pliocene lie in an icehouse phase (Fig. 1.1), with presence of a polar cap in Antarctica, and therefore measured $\delta^{18}O$ values can not be used to analyse temperature changes over time (Ruddiman, 2007). During the Miocene, the Earth went through several major climatic and tectonic changes. The climatic changes included a gradual cooling, started about 15 Ma, and the establishment of major ice sheet on Antarctica around 10 Ma (Zachos et al., 2001), as well as significant changes in global carbon cycling and deep ocean circulation. The Miocene is characterized by several glaciation intervals based on analysis on microfossil stable oxygen isotope composition (Miller et al., 1991).

However, after a major glacial episode at the Oligocene/Miocene boundary, average surface water and deep-water temperatures trended slightly higher (Zachos et al., 1997; Zachos et al., 2001). This warm phase peaked in the late middle Miocene climatic optimum (17 to 15 Ma), at this time deep-water and high-latitude surface water temperature were up to 6°C warmer than present-day (Shackleton and Kennet, 1975; Savin et al., 1975). Around 15 Ma ago, temperature started to cool down, proxies show a rapid deep-water cooling and an expansion of the east Antarctic ice-sheet. The presence of ice-rafted debris from late Miocene indicate the start of the glaciation in the Nordic seas and Arctic regions. The early Pliocene instead is characterized by a slight warming trend until ca. 3.2 Ma, when $\delta^{18}O$ increased again reflecting the onset of Northern Hemisphere Glaciation (NHG).
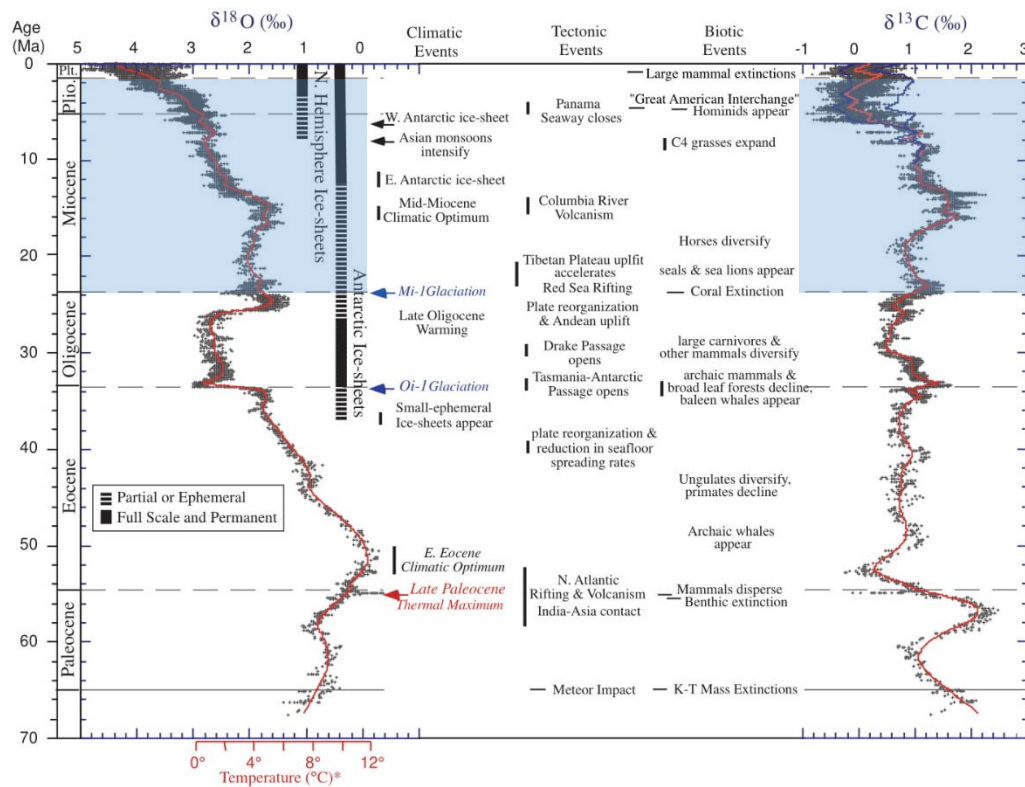
Fig. 1.1 Global deep-sea oxygen and carbon isotope records based on data compiled from more than 40 DSDP and ODP sites. Most of the data are derived from analyses of two common and long-lived benthic taxa, *Cibicidoides* and *Nuttallides*. The absolute ages are relative to the GPTS (Berggren et al., 1995). The $\delta^{18}O$ temperature scale, on the right axis, was computed on the assumption of an ice-free ocean; it therefore applies only to the time preceding the onset of large-scale glaciation on Antarctica (about 34 million years ago). From the early Oligocene to present, much of the variability (ca. 70 %) in the $\delta^{18}O$ record reflects changes in Antarctica and Northern Hemisphere ice volume (Zachos et al., 2001). The blue band marks the Neogene.

1.2. The latest Miocene–early Pliocene biogenic bloom

The interval comprised between the late Miocene and the early Pliocene is a period of important paleoclimatic and paleoceanographic changes such as the expansion of ice caps at both poles, the gradual uplifting of the Isthmus of Panama (Farrell et al., 1995), the evolution and domination of the global deep circulation by the North Atlantic deep water (NADW), and the "Messinian salinity crisis" caused by the isolation of the Mediterranean from the Atlantic Ocean (Hodell et al., 1994; Krijgsman et al., 1999).

There is another event occurred in the latest Miocene-early Pliocene that has been documented over the last 40 years in a series of investigations in the Pacific Ocean. Sediments deposited beneath upwelling zones during this interval of time show pronounced anomalies, in particular there are significant increases in the mass accumulation rate (MAR) of the biogenic components, major changes in planktic and benthic fauna assemblages, and marked decreases in sedimentary redox conditions. (e.g. Van Andel et al., 1975; Leinen, 1979; Theyer et al., 1985; Woodruff, 1985; Kennett and Von der Borch, 1986; Berger et al., 1993; Delaney and Filippelli, 1994; Farrell et al.,. 1995a; Rea et al., 1995; Dickens and Owen, 1996). These conditions have been recognized in a number of different successions located in different areas, as for instance: the ODP Leg 115 in the equatorial Indian Ocean (Peterson and Backman, 1990), the ODP Site 756 from the southern Ninetyeast Ridge (Indian Ocean; Brumer and Van Eijden, 1992), the ODP Sites 752, 754, and 757 on Broken and Ninetyeast ridges, central Indian Ocean (Dickens and Owen, 1994). Many authors (Peterson et al., 1992; Berger et al., 1993; Delaney and Filippelli, 1994; Dickens and Owen, 1994, 1996; Farrell et al., 1995; Rea et al., 1995) have tried to explain these anomalies as the result of an increased productivity in the Indo-Pacific divergence zones.

These particular conditions are referred to as "biogenic bloom" hypothesis (Farrell et al., 1995; Dickens and Owen, 1999).

The Indian Ocean area

In the modern oceans, biogenic blooms are episodes of unusual high biological productivity that typically occur beneath divergence and upwelling zones. These events are characterized by:

- increased accumulation rates of biogenic components to the seafloor associated with enhanced supply of organic carbon;
- major changes in the benthic and planktic fauna assemblages;
- pronounced decrease in sedimentary redox conditions and low dissolved O_2 content in intermediate waters, which result in a more expanded oxygen minimum zone (OMZ) (Dickens and Owen, 1999).

High rates of surface productivity in the Indo-Pacific divergence zone produce a significant organic carbon flux to the seafloor. The organic matter usually sinks and is decomposed along the water column. This process consumes oxygen and, if enhanced, causes an expansion of the OMZ at intermediate water depths beneath the present-day Indo-Pacific divergence zone (Reid, 1965; Wyrtki, 1971).

The OMZ in the modern Indian Ocean has a wedge-shape form and extends ca. 5000 km in a southeast direction (Fig. 1.3a). If compared with the late Miocene-early Pliocene conditions recorded during the biogenic bloom (between 9.0 and 3.5 Ma), modern oceans are characterized by significantly lower productivity than those observed in the past oceans, and the oxygen minimum zone (OMZ) appears less expanded (Olson et al., 1993; Dickens and Owen, 1994) (Fig. 1.3).

Based on oceanographic models, an increase in surface productivity during the latest Miocene-early Pliocene should have produced an intensification of the underlying intermediate water OMZs (Olson et al., 1993). According to these models (Dickens and Owen, 1994), the increase in primary productivity associated to the biogenic bloom hypothesis in the Indian Ocean has produced an intensified OMZ that expanded further than 5000 km in a southeast direction (Fig. 1.3b) (Dickens and Owen, 1999). The intensification of these paleoceanographic conditions between 6.0 and 5.0 Ma in the Pacific Ocean suggests that the biogenic bloom was time-coincident in the Indian and Pacific Oceans. The biogenic bloom, therefore, implies an important change in global nutrient cycling occurred during the latest Miocene-earliest Pliocene, although a satisfactory explanation for this change remains elusive (Dickens and Owen, 1999).
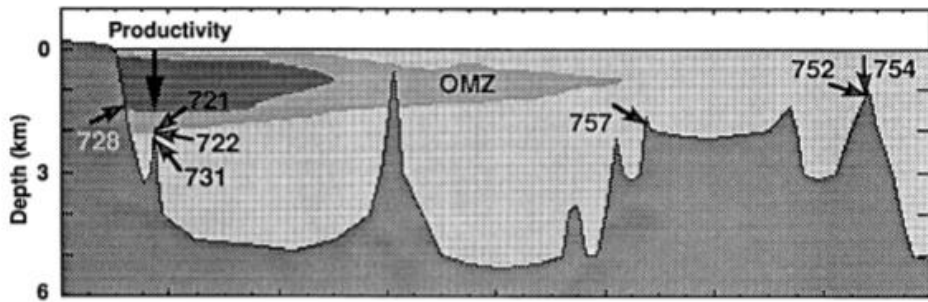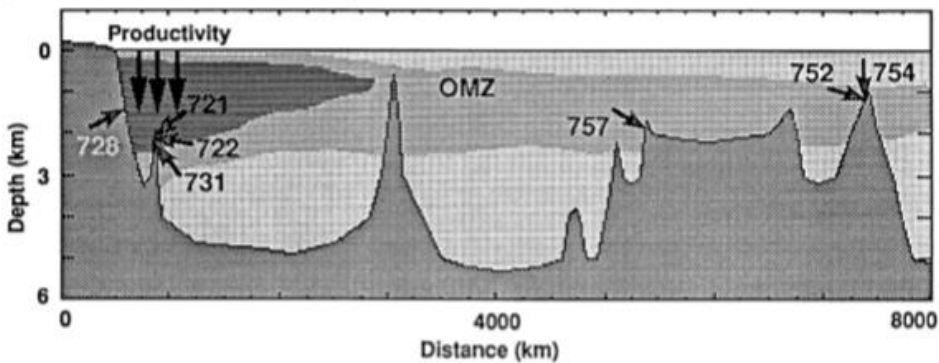
Fig. 1.3 (a) Bathymetric profile of the present-day Indian Ocean. The present locations of ODP sites 721, 722, 728, 731, 752, 754, and 757 are shown on this profile as well as the present dimensions of the Indian Ocean OMZ. (b) Model of the Indian Ocean during the latest Miocene-early Pliocene, productivity in the north and west Indian Ocean was significantly elevated, and the underlying OMZ was greatly expanded. Note that the OMZ dimensions in the lower figure are highly schematic (Dickens and Owen, 1999).

Evidence of the biogenic bloom in the Indian Ocean

The biogenic bloom hypothesis in the Indian Ocean is mainly supported by the mass accumulation rates (MARs) calculated on Neogene carbonate sequences at relatively shallow (< 3000 m) depths and seat under areas of high productivity (Peterson and Backman, 1990; Peterson et al., 1992; Farrell and Janecek, 1991; Brummer and Van Eijden, 1992; Seisser, 1995). In the latest Miocene-early Pliocene, bulk carbonate MARs were 150 to 250 % higher than those of present-day at ODP sites 707, 709, 710 on the Mascarene Plateau (Fig. 1.4), at ODP Sites 721, 722 and 728 in the western Arabian Sea, and at Site 758 on the northern end of Ninety-east Ridge. Since the carbonate in these locations is composed mostly by calcareous nannofossil and planktic foraminifera, the increase in bulk carbonate MARs points to increased supply or decreased removal of biogenic carbonate (Dickens and Owen, 1999).

10

At Sites 707, 709, 710, the high abundance of diatom, which are indicative of high productivity conditions (Fig. 1.4) (Mikkelsen, 1990; Nigrini, 1991), and low magnetic susceptibility, suggestive of Fe reduction likely related to an increase in organic carbon supply (Backman et al., 1988; Robinson, 1990), are the main evidences that observed elevated MARs reflect enhanced organic supply due to increased paleoproductivity rather than diminished dissolution (Peterson and Backman, 1990, Peterson et al., 1992).

In additions to MARs values, another evidence to support this view is represented by the increase in carbonate dissolution at deep to intermediate water depths (Farrel and Janecek, 1991; Peterson et al., 1992), which testifies the shoaling of the lysocline as a consequence of the elevated paleoproductivity (e.g., Broecker and Peng, 1982).
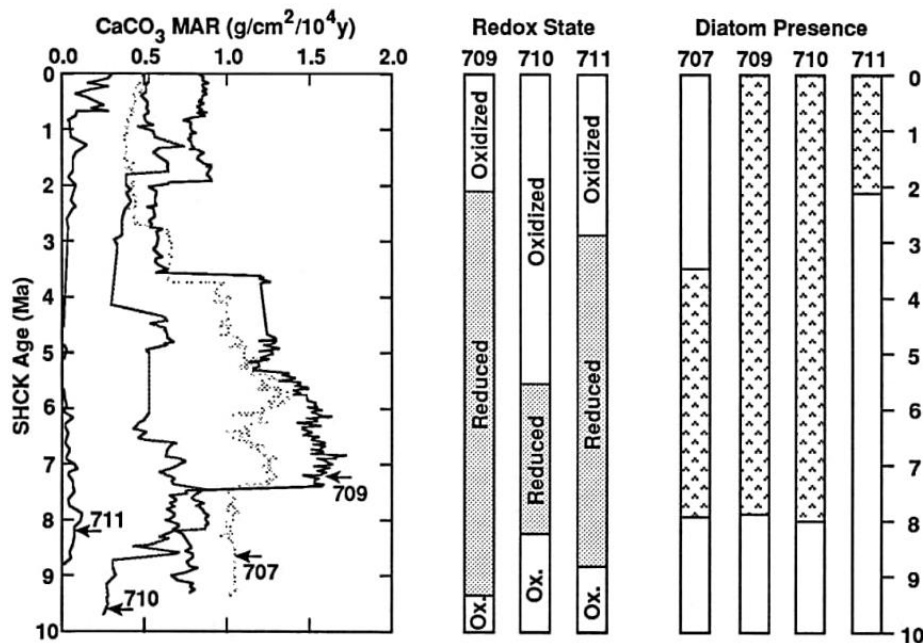
Fig. 1.4 Calculated carbonate MARs, sedimentary redox conditions, and diatom presence at ODP sites 707, 709, 710, and 711 on the Mascarene Plateau. Carbonate percentages, DBD, and LSRs for carbonate MARs are from Backman et al. (1988) and Peterson, Backman (1990) and Dickens and Owen (1999). Intervals of reduced facies are from Backman et al. (1988) and Robinson (1990). Intervals with diatoms are from Mikkelsen (1990). Depths of all parameters have been converted to the SHCK time scale (Cande and Kent, 1995; Shackleton et al., 1995) (Dickens and Owen, 1999).

The biogenic bloom in the Pacific Ocean

The main evidence for the recording of the biogenic bloom in the Pacific Ocean is the same observed in the Indian Ocean, in particular: high MARs of biogenic components ($CaCO_3$, SiO_2), which lead to an increase in the amount of sediment deposited during the latest Miocene-early Pliocene beneath the divergence zone (e.g., Van Andel et al., 1975; Leinen, 1979; Theyer et al., 1985; Berger et al., 1993; Delaney and Filippelli, 1994; Farrell et al., 1995).

At Sites 849 and 885/886 (Pacific Ocean ODP) there are also other lines of evidence such as: the inferred high surface productivity based on high abundance of biogenic calcite (Berger et al., 1993; Farrell et al., 1995); the Fe mobilization likely produced by higher organic carbon fluxes (Tarduno, 1994; Arnold et al., 1995; Dickens and Owen, 1996); and the foraminiferal assemblages typical of low dissolved O_2 conditions (Woodruff and Douglas, 1981; Woodruff, 1985; Resig, 1993).

Dickens and Owen (2002) also reported the occurrence of the biogenic bloom in New Zealand, beneath the Tasman Front, and at DSDP Site 590 in the Tasman Sea on the eastern flank of the Lord Howe Rise, close to IODP Site U1506, the site studied in this thesis. At Site 590, sediments deposited between ca. 9 and 3.8 Ma shows clear evidences for elevated primary productivity, such as increased carbonate MARs, increase in bulk sediment Ca/Ti, Ba/Ti, and Al/Ti ratios, and a significant increase in the $\delta^{13}C$ gradient through the water column (Grant and Dickens, 2002). However, the record of the biogenic bloom at this location is unusual because the different productivity proxies available as well as the $\delta^{13}C$ records show important time offsets (Grant and Dickens, 2002).

1.3. The significance of the biogenic bloom

This event, if global, represents an intriguing mystery in the geological record because the conditions observed during the biogenic bloom need to hypothesize a different system or, at least, a radical change in global nutrient cycling of the oceans in the late Miocene-early Pliocene. The primary productivity in the oceans is limited by the availability of nutrients and, their residence time is usually short ($< 10^5$ years, Delaney and Filippelli, 1994; Treguer et al., 1995) so that in the oceans high productivity conditions can not be maintained for long periods, however, the biogenic bloom lasted for ca. 5.5 Ma (Dickens and Owen, 1999).

Possible explanations to these persisting and anomalously high productivity conditions are (1) the increase in gross productivity related to an enhanced supply of nutrient to the ocean (Filippelli, 1997; Hermovian and Owen, 2001), or (2) a major redistribution of nutrient within the oceans, or (3) both.

In any case, the biogenic bloom is related to an increase in nutrient delivery to, at least part, of the ocean.

To sustain the first hypothesis, the so-called "increase in nutrients supply theory", several authors (Berger et al., 1993; Berger and Stax, 1994; Delaney and Filippelli, 1994; Farrell et al., 1995) have proposed that the biogenic bloom was caused by an increased delivery of nutrients through rivers, as a result of intensified continental weathering. This would suggest an increase in net supply of nutrients and sediment burial in the oceans between 9.0 and 3.5 Ma.

Another evidence supporting this theory is the increase in seawater $^{87}Sr/^{86}Sr$ that may indicate elevated riverine fluxes to the oceans (Farrell et al., 1995), and a general increase in terrigenous deposition associated with increased riverine outflow (Rea, 1992; Dobson et al., 1997). An additional datum to take into account is the difference in benthic foraminifera $\delta^{13}C$ between the Atlantic and Pacific Oceans that could suggest higher mean nutrient levels in the Pacific Ocean (Wright and Miller, 1996).

It should be noted that a problem emerges while correlating the increase in seawater $^{87}Sr/^{86}Sr$ and the increase in terrigenous content to the biogenic bloom because these two proxies reached their maximum 3.5 Ma after termination of the biogenic bloom (Rea, 1992; Farrell et al., 1995b; Dobson et al., 1997).

To sustain the second hypothesis, the so-called "redistribution of nutrient theory" it is necessary to hypothesize some prominent changes in the oceanic global circulation. Between 9.0 and 3.5 Ma, the formation of deep waters intensified (Wright and Miller, 1996) and high-latitude warming (Hays and Opdyke, 1967; Koizumi, 1986) could have accelerated the deep-water conveyor belt (Rind and Chandler, 1991). Simple box models have demonstrated that enhanced deep-water flow can lead to increased productivity at divergence zones (Lyle and Pisias, 1990). Hence, Dickens and Owen (1996) have proposed that the biogenic bloom was related to the transport of nutrients from other regions (e.g. the Atlantic Ocean, continental margins, and central gyres) thanks to accelerated deep-water flows.

A comprehensive explanation of the processes involved in this event still remains mostly unclear, however, all the authors agree on the fact that the main driving mechanism must have worked at global scale (Peterson et al., 1992; Berger and Stax, 1994; Berger et al., 1993; Delaney and Filippelli, 1994; Dickens and Owen, 1994, 1996; Farrell et al., 1995; Rea et al., 1995).

In this context, the aims of this thesis therefore are to:

- construct a firm framework for IODP Site U1506 based on calcareous nannofossil biostratigraphy through semi-quantitative estimation of selected taxa to chronologically frame the study section;

- implement the age model proposed by Sutherland et al., (2019) thus allowing to put the benthic foraminiferal assemblage data into a more reliable chronological framework;

- shed light on the paleoenvironmental conditions at the sea floor especially in terms of nutrient availability, trophic conditions and oxygen concentrations, through quantitative studies on benthic foraminiferal assemblages and statistical analysis;

- recognise the presence of the biogenic bloom through the interpretation of the benthic foraminiferal data in terms of paleoecological and paleoenvironmental changes, and derive the precise timing and duration of this event by using the integrated age model.

2. THE OCEAN DRILLING PROJECT AND EXPEDITION IODP 371

2.1. Brief history of the ocean drilling project

The first oceanographic cruise was organised by the English *Royal Society* between 1872 and 1876 when the *H.S.M. Challenger* carried out the first systematic recovery of sediments from the ocean bottom. After more than a century, in 1964 several American research institutes formed the JOIDES consortium (*Joint Oceanographic Institution of Deep Earth Sampling*) that in 1968 was transformed in the DSPD (*Deep Sea Drilling Project)*, a project coordinated by an American research agency that used the *Glomar Challenger* as a scientific vessel. In 1975, this consortium finally allowed the entry of other national states, leading to the IPOD (*International Phase of Ocean Drilling*), which lasted until 1983. From 1985, the project was renamed ODP (*Ocean Drilling Program*) and started to use a new drilling vessel, the *JOIDES Resolution* (Fig. 2.1). In 2003, the IODP (*International Ocean Drilling Program*) project began with the introduction of new and more efficient techniques that allowed obtaining data with better quality. Lastly in 2013 a new ten-year phase of the program called IODP (*International Ocean Drilling Program*) started.

Fig. 2.1 The research vessel JOIDES Resolution at the start of expedition 371 in Townsville, Australia, on 27 July 2017 (Credit: Tim Fulton, IODP JRSO).

2.2. The *JOIDES Resolution* and the technologies used

The *JOIDES Resolution* (Fig. 2.1) has been used for 35 years as the main vessel of the ODP/IODP projects though other vessels (e.g. Chikyū) have also served the project in the most recent times. The JR has a total length of 144 m and is 21 m wide, this vessel is equipped with a derrick, the drilling tower, which has a height of 64 m; it also has a battery of rods (pipe drill) that could reach a total length of 9144 m. The routine drilling operations are described in the following:

Once the drilling site is reached, an acoustic transponder is lowered on the ocean floor and, the vessel uses a computer-controlled, acoustic dynamic positioning system to maintain location over the drilling site. During normal operations, the crew lowers the assembled drill pipe from the drill floor through the moonpool, a ca. 7 m opening that extends through the bottom of the ship. The process of lowering the drill string takes ca. 12 hours in 5,500 m of water. After the crew lowers the drill string to the seafloor, coring operations begin. The drill crew lowers core barrels through the drill pipe. To core through the seafloor, the entire drill string is rotated. The core barrels retrieve and store the core material cut by the drill bit. After the drilling is deemed complete and the drilling equipment is taken out from the hole, the work at the site is not over. Next, comes the logging, which is the part of the operation where instrumentation is lowered to measure a number of characteristics surrounding the newly drilled hole. The drilling method is chosen according to the objectives and lithology of the seabed to be studied.

Rotary Core Barrel (RCB) is used in the case of strongly lithified rocks or ocean floor made of igneous rocks.

For paleoclimatic or paleoceanographic the favourite drilling method is **Advanced Piston Core** (APC), because it allows the recovery of undisturbed and orientated cores with both poorly consolidated sediments and consolidated sediments.

When sediments have intermediate features, the preferred method is **Extended Core Barrel** (XCB). This method allows the recovery of whole cores (9.5 m) of slightly, to moderately lithified sediments; it is chosen if sediments are too hard for APC or, if are not hard enough to allow the use of RCB.

Lastly, if the recovery of sediments is not necessary for research purposes, the **Wash Coring** is used, which is characterized by a higher drilling speed.

In this case, sediments are not recovered but rather they are pushed into the space between the drill pipe and the wall of the well (wall of the hole) by pumping of high-pressure water.

Cores are extracted from the drilling shaft by the core barrel, they usually have an average length of 9.5 m and are divided into section of approximately 1.5 m.

Sections are numbered from the top to the base of the core and put to rest in a refrigerator to avoid any shock, after a few hours they can be cut into two halves: a working half (w), on which the studies will be done and an archive half (a), which is usually preserved. The two halves are stored inside dedicated repositories (i.e., Bremen (Germany), Kochi (Japan), College Station (USA)) in order to guarantee the best preservation of the material (Fig. 2.2).
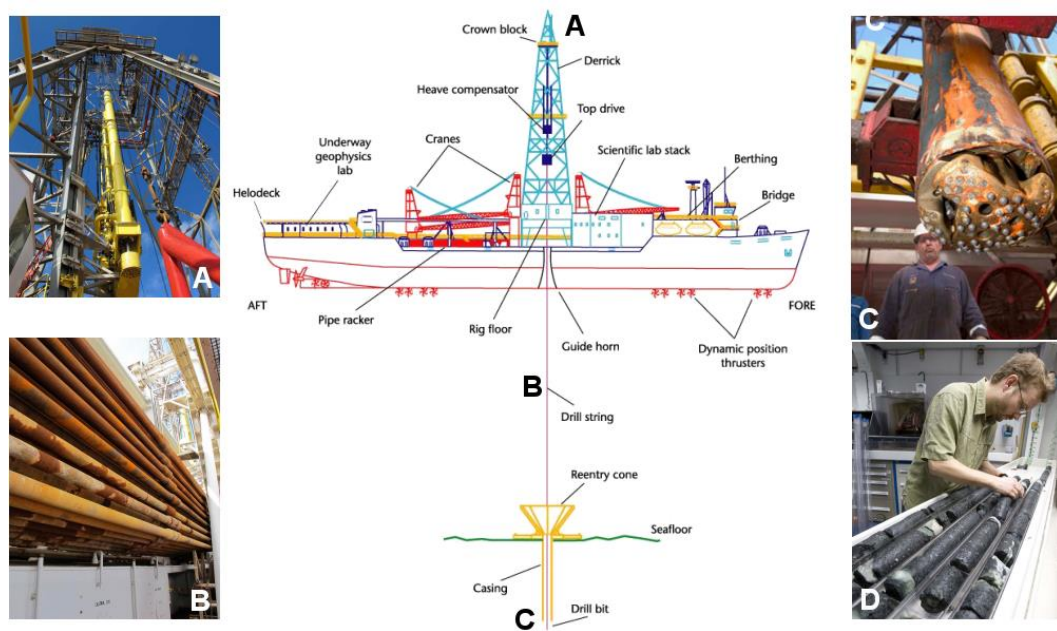
Fig. 2.2 Graphic representation of the JOIDES Resolution: A. Derrick; B. Drilling string; C. Drill bit; D. drill cores studied in laboratory.
(http://raymond.rodriguez1.free.fr/Textes/1s23.htm)

2.3. Expedition IODP 371: the main targets

The primary target of Expedition IODP 371 was to understand Tonga-Kermadec subduction initiation through the recovery of Paleogene sediment records and to complement results from Expeditions 350, 351, and 352; the secondary target was to understand regional climate and oceanography through intervals of the Cenozoic, especially the Eocene (Fig. 2.3).

During this expedition, six sites were drilled (U1506-U1511) in the Tasman Frontier (Tasman Sea, southwest Pacific) (Fig. 2.4), all the sites provided new stratigraphic and paleogeographic information that were put into contest through regional seismic stratigraphic interpretation.
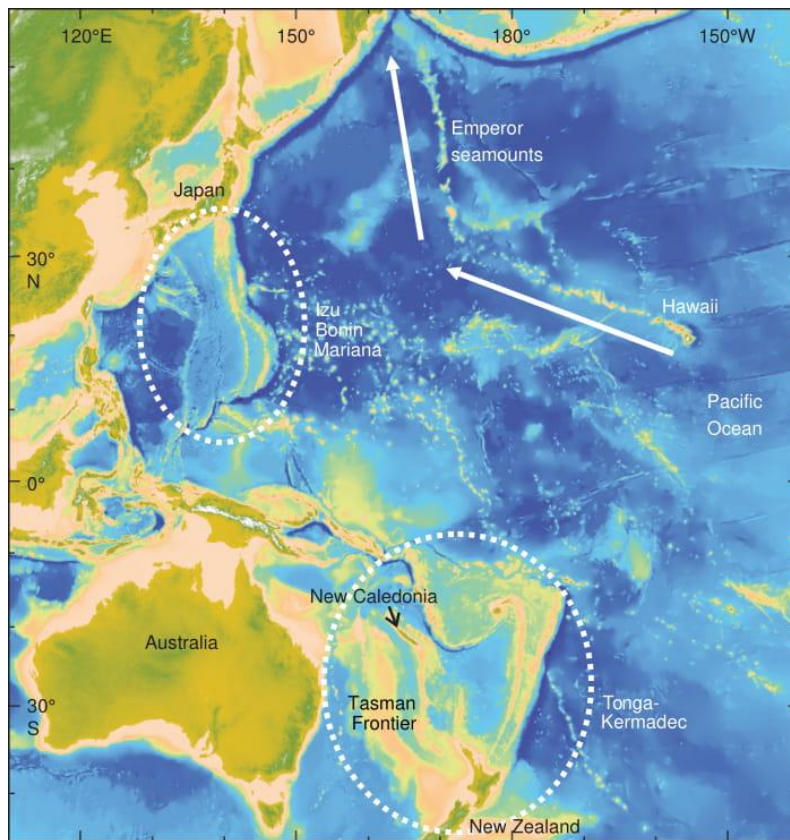
Fig. 2.3 The dashed circles point the location of Izu-Bonin-Mariana and Tonga-Kermadec subduction system in western Pacific (Sutherland et al., 2017).
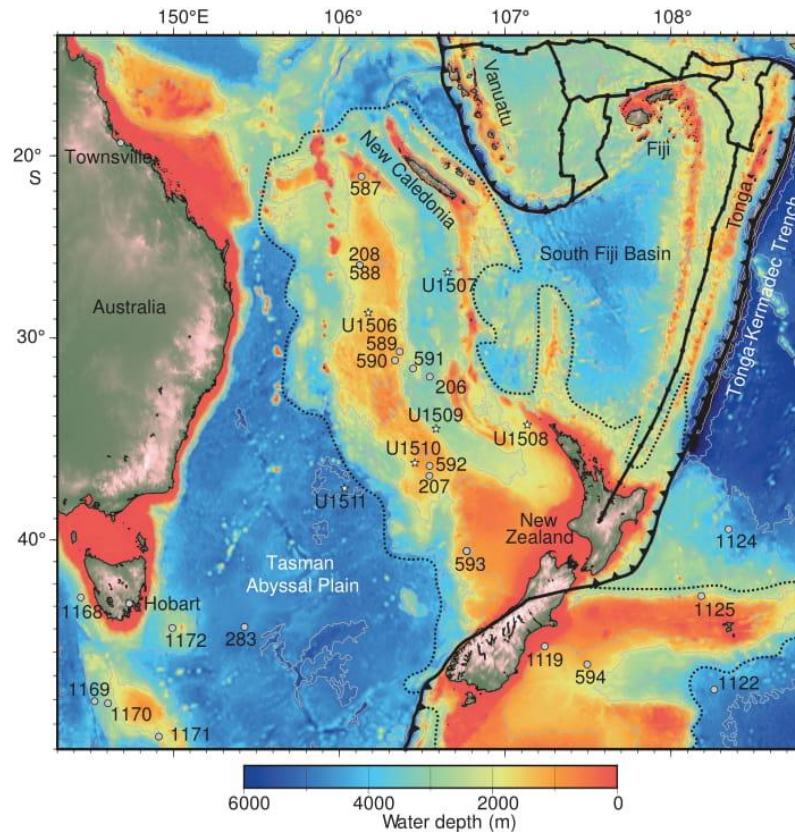
Fig. 2.4 Location of Sites U1506-U11 (stars) in the southwest Pacific. Dots = relevant DSDP and ODP sites. The expedition departed from Townsville and returned to Hobart. Dashed line = approximate location of Zealandia (modified after Mortimer et al., 2017).

In detail, IODP Expedition 371 aimed to address the following questions:

1. How and why does subduction initiation occur?

2. Was the Eocene southwest Pacific anomalously warm, and why?

3. How does post-Eocene oceanography and climate compare with elsewhere in the Pacific?

The Tasman Frontier is an extensive, geologically complex, and underexplored area of the ocean between Australia, New Zealand and New Caledonia. It includes portion of the Zealandia continent (Mortimer et al., 2017) and it is located on the western side of the Tonga-Kermadec Trench system (Fig. 2.3). Understanding how subduction initiation occurs is important since subduction systems are the main drivers of plate motions, mantle dynamics, and global geochemical cycles; though they are important processes, it is still not very clear how a subduction initiation works. In the western Pacific, the Eocene subduction was accompanied by tectonic changes, these events occurred at a crucial moment for the Cenozoic climate.

The long-term global warming though the Paleocene-Eocene transition culminated in the Early Eocene Climatic Optimum (EECO; ca. 53-49 Ma), which was followed by overall cooling thought the rest of the Cenozoic. An unknown number of geologically fleeting events of extreme warmth, biological turnover, and geochemical change commonly named "hyperthermals" also characterized the Paleocene and Eocene (Zachos et al., 2008; Westerhold et al., 2018). The first objective was successfully completed by coring at six sites that were optimally located based on local and regional seismic reflection lines and from consideration of regional structure and plate motion history (Fig. 2.4) (Sutherland et al., 2019).

The second scientific goal of this expedition was to understand the long-term and short-term transitions during the early Paleogene and, if the climate's shifts between greenhouse and icehouse states were somehow related to tectonic change, in particular to the widespread initiation of subduction zones in the western Pacific. The studied location, the Tasman Frontier, was chosen since global climate models are not able to simulate the extreme warmth conditions recorded in the southwest Pacific and Southern Ocean (Bijl et al., 2009; Hollis et al., 2009, 2012; Pross et al., 2012; Douglas et al., 2014). In addition, the EECO and some hyperthermals are located throughout several uplifted marine section of New Zealand (Nicolo et al., 2007; Hollis et al., 2009, 2012; Slotnick et al., 2012).

During the expedition were also recovered Neogene sediments, which have been used in this thesis.

3. METHODS AND MATERIALS

3.1. Studied material: IODP Site U1506

Site IODP U1506 is located at 28.66°S, 161.74°E in the Tasman Sea (South Pacific), at a water depth of 1505 m. This site is situated on the northern part of the Lord Howe Rise, approximately 290 km south of the Deep Sea Drilling Project (DSDP) Sites 208 and 588 (Sutherland et al., 2019) (Fig. 3.1).

This site, identified using seismic reflection data, was interpreted as a small-mounded structure with a relief of about 100 m above the regional unconformity surface. It has been hypothesized that this structure could have been a coral reef (Sutherland et al., 2019).

The type of drilling chosen was rotary drilling since the seismic data showed that the material may have been too hard for advanced piston core (APC) or extended core barrel (XCB) systems.
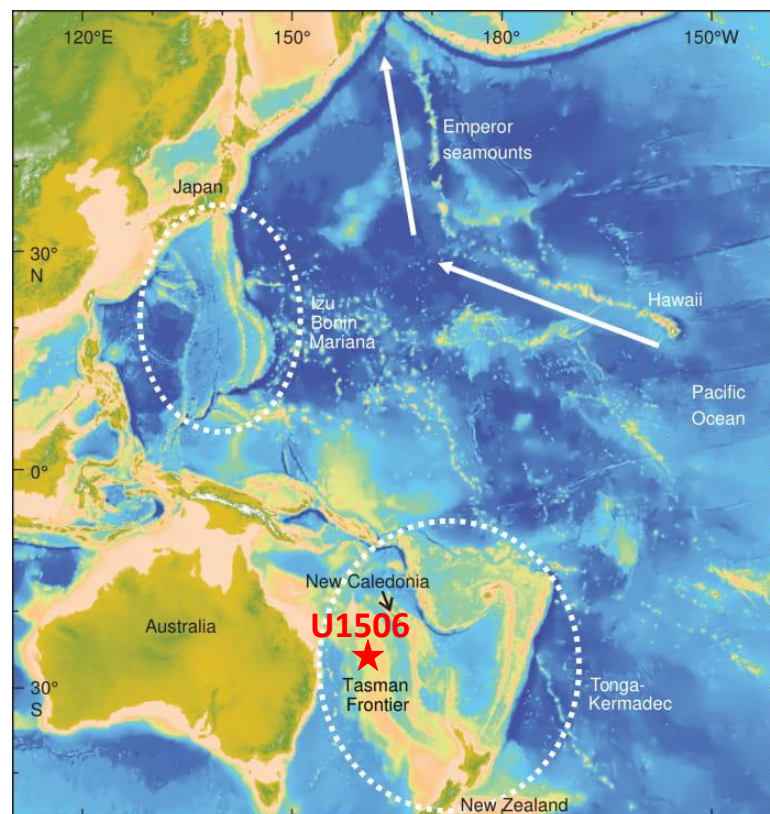
Fig. 3.1 Location of Site U1506 (red star) in the Tasman Frontier (Sutherland et al., 2019).

3.1.1. Lithostratigraphy

At Site U1506 a total of 306.07 m was retrieved, the material has been divided into two different lithostratigraphic units. Lithostratigraphic Unit I was further divided into Subunits Ia, Ib and Ic (Table 3T). These lithologic units differ one to each other in lithology and sedimentological features that were identified using both macroscopic and microscopic description (smear slide, thin section and scanning electron microscope [SEM]) of the cores and with the additional aid of carbonate content and X-ray diffraction (XRD) analysis (Sutherland et al., 2019).

All the following results are available at Proceedings of the International Ocean Discovery Program Volume 371 (Sutherland et al., 2019), and the measurement unit used for the depths is CSF-A (m), Core depth below Sea Floor-A.

Visual colour determination was performed using Munsell soil colour charts (Munsell Color Company, Inc., 1994), the nomenclature consists of two components: colour name and the Munsell notation of colour. The Munsell notation consists of separate notations for hue, value, and chroma, combined to form the colour designation. The symbol for hue is the letter abbreviation of the color of the rainbow (i.e. R for red, YR for yellow-red, Y for yellow) and it is preceded by a number from 0 to 10, for each letter range, the hue becomes more yellow and less red as the number increase. For example, 5YR is in the middle of the yellow-red hue, which extends from 10R (zero YR) to 10YR (zero Y). Value is represented by a number from 0, absolute black, to 10, absolute white, i.e. a color with 5/ as value, is midway between absolute white and absolute black. The notation for chroma consists of numbers beginning at 0 for neutral greys, and increasing at equal intervals to a maximum of 20, which is never approached in soil. White, black and pure grey have zero chroma and no hue so the letter N (neural) takes the place of a hue designation.

Lithostratigraphic Unit I

The lithostratigraphic Unit I is a sequence about 265 m thick of Pleistocene-middle Eocene nannofossil ooze and chalk overlie ~40 m of volcanic rocks. It is subdivided into three subunits, the Subunit Ib is distinguished from Ia by its pale yellow (2.5Y 8/2) colour, Ic instead is marked by the presence of glauconite. The boundaries between the subunits coincide with stratigraphic hiatuses.

Subunit Ia (from 0 to 258.23 m CSF-A)

The Subunit Ia is a 258 m thick sequence of Pleistocene-middle Miocene white (N 8.5 and N 9) nannofossil ooze and chalk with foraminifers. The carbonate content range between 88 % and 95 %. It is characterized by the presence of pyrite crystals throughout all the subunit, identified with XRD and SEM (Fig. 3.2).

The upper 48 m (Cores 1R through 6R) is variably soupy as a result of drilling disturbance, Cores 8R through 26R are variably slightly to moderately biscuited and fractured. The ooze-chalk transition happens over Cores 24R (ooze), 25R (firmer ooze) and 26R (chalk). Chalk is characterized by structures and textures that are better preserved with respect to those present in the nannofossili ooze. Bioturbations are generally slightly darker (10YR 8/1), than the surrounding material and include *Zoophycos*, *Planolites*, *Skolithos* and *Chondrites* ichnofacies. All these features also occur in ooze but were partially destroyed during the drilling.

Subunit Ib (from 258.23 to 264.29 m CSF-A)

Subunit Ib is a sequence of about 6 m of pale yellow (2.5Y 8/2) to white (2.5Y 8/1) Oligocene nannofossil chalk with foraminifers. The contact with the above Subunit Ia is marked by a change in colour, from white grey (GLEY 1 8/N) to pale yellow (25Y 8/2) and by a minor increase in magnetic susceptibility. This contact occurs across a 2 cm thick interval of sediment disturbed by the drilling process. This transition was incompletely recovered (Fig. 3.2) but corresponds to a hiatus covering an interval from the late Miocene to the late Oligocene. This subunit is characterized by abundant bioturbations, including *Zoophycos* and *Planolites* ichnofacies.

Subunit Ic (from 264.29 to 264.63 m CSF-A)

The subunit Ic is a 34 cm thick sequence of middle Eocene glauconitic nannofossil chalk with foraminifers. The contact with overhead Subunit Ib is marked by the appearance of glauconite and by a prominent colour change, the sediments become light greenish grey (5GY 9/1). The contact between Subunit Ib and Subunit Ic corresponds to a hiatus spanning from the late Oligocene to middle Eocene.

This subunit is profoundly bioturbated, and chalk from the above Subunit Ib is abundantly present in the upper 20 cm of Subunit Ib.

Lithostratigraphic Unit II (from 264.63 to 306.070 m CSF-A)

The lithostratigraphic Unit II is a sequence about 40 m thick of mafic crystalline volcanic rocks, with a wide range of textures and mineralogy, and it includes carbonate veins and infills (neptunian dyke) (Fig. 3.2).

Lith. Unit	Depth CSF-A (m)	Thickness (m)	Lithology	Stage
Ia	0.00-258.23	258.23	Nannofossil ooze and chalk with varying amounts of foraminifers	Pleistocene to middle Miocene
Ib	258.23-264.29	6.06	Nannofossil chalk with foraminifers	upper Oligocene
Ic	264.29-264.63	0.34	Glauconitic nannofossili chalk with foraminifers	middle Eocene
II	264.63-306.07	41.44	Basalt	Minimum estimate middle Eocene

Table 3T Summary of the lithostratigraphic units at Site U1506.

The samples analysed in this thesis come from Subunit Ia, the analysed interval range between 81.75 and 233.50 m CSF-A, for a total of 151.75 m. The material come from core 10R to 25R (Fig. 3.3).
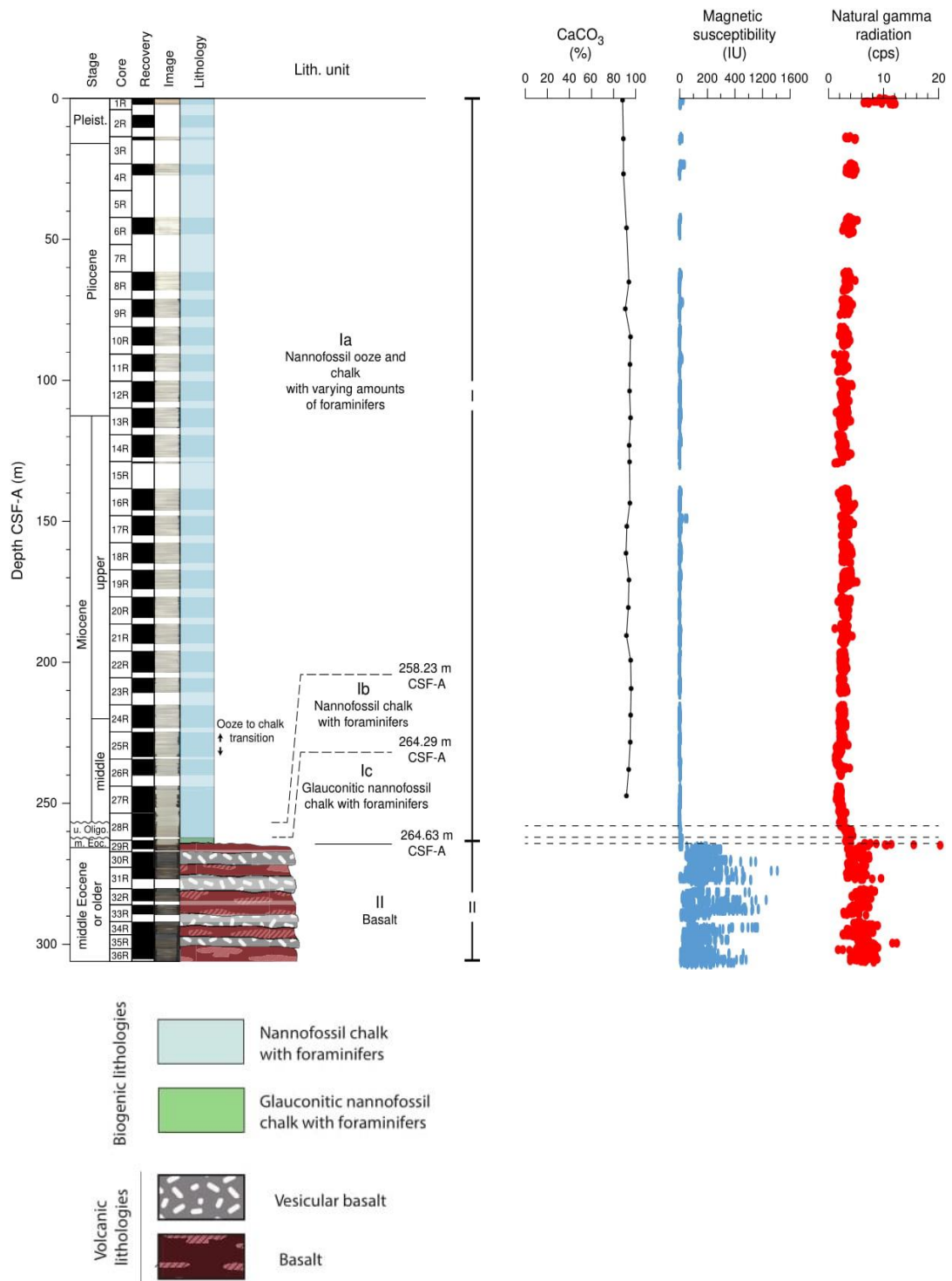
Fig. 3.2 Lithostratigraphic summary of sediments and volcanic rocks of Site U1506 (Sutherland et al., 2019). On the right are reported: carbonate content (CaCo$_3$ [%]), magnetic susceptibility (IU) and natural gamma radiation (cps = counts per second). Magnetic susceptibility is low throughout Unit I thus does not provide any useful information for the interval of interest.
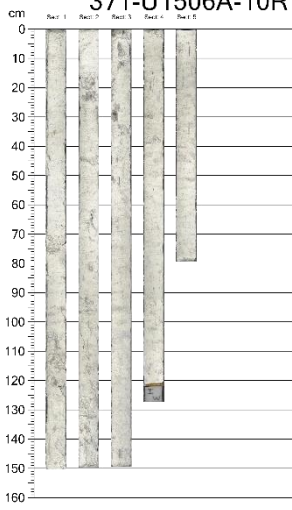
371-U1506A-10R   371-U1506A-11R   371-U1506A-12R
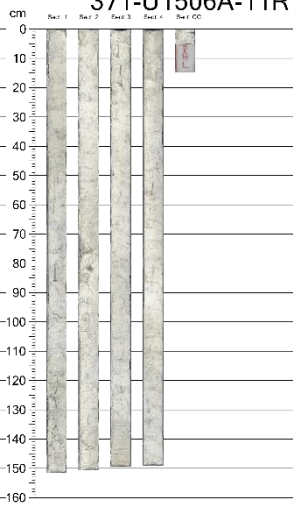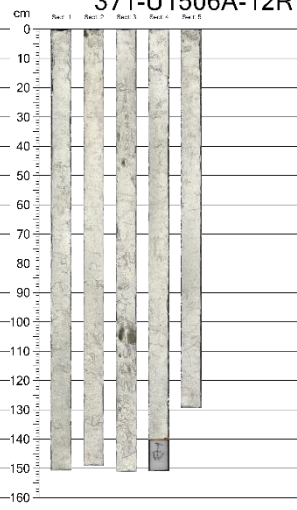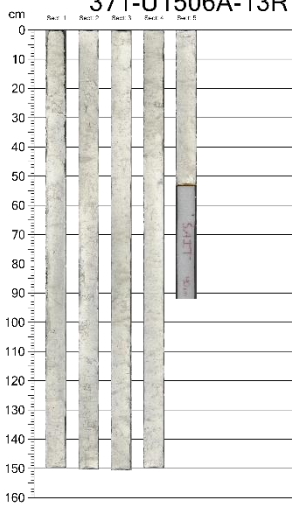
371-U1506A-13R   371-U1506A-14R   371-U1506A-15R
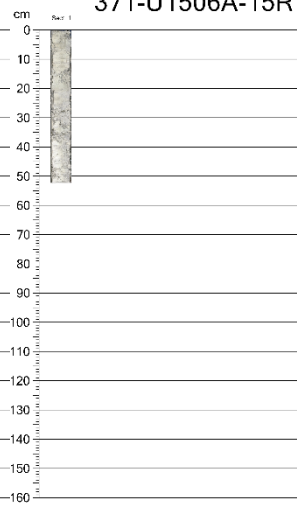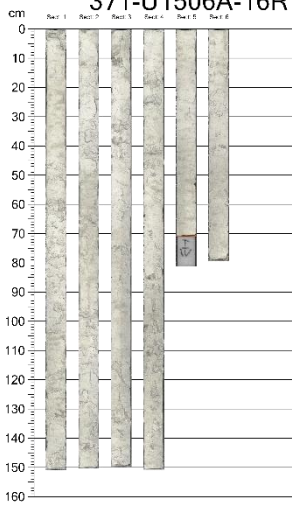
371-U1506A-16R   371-U1506A-17R   371-U1506A-18R
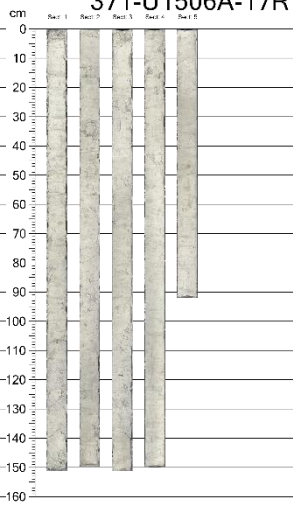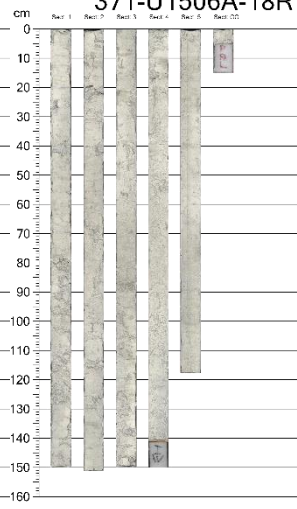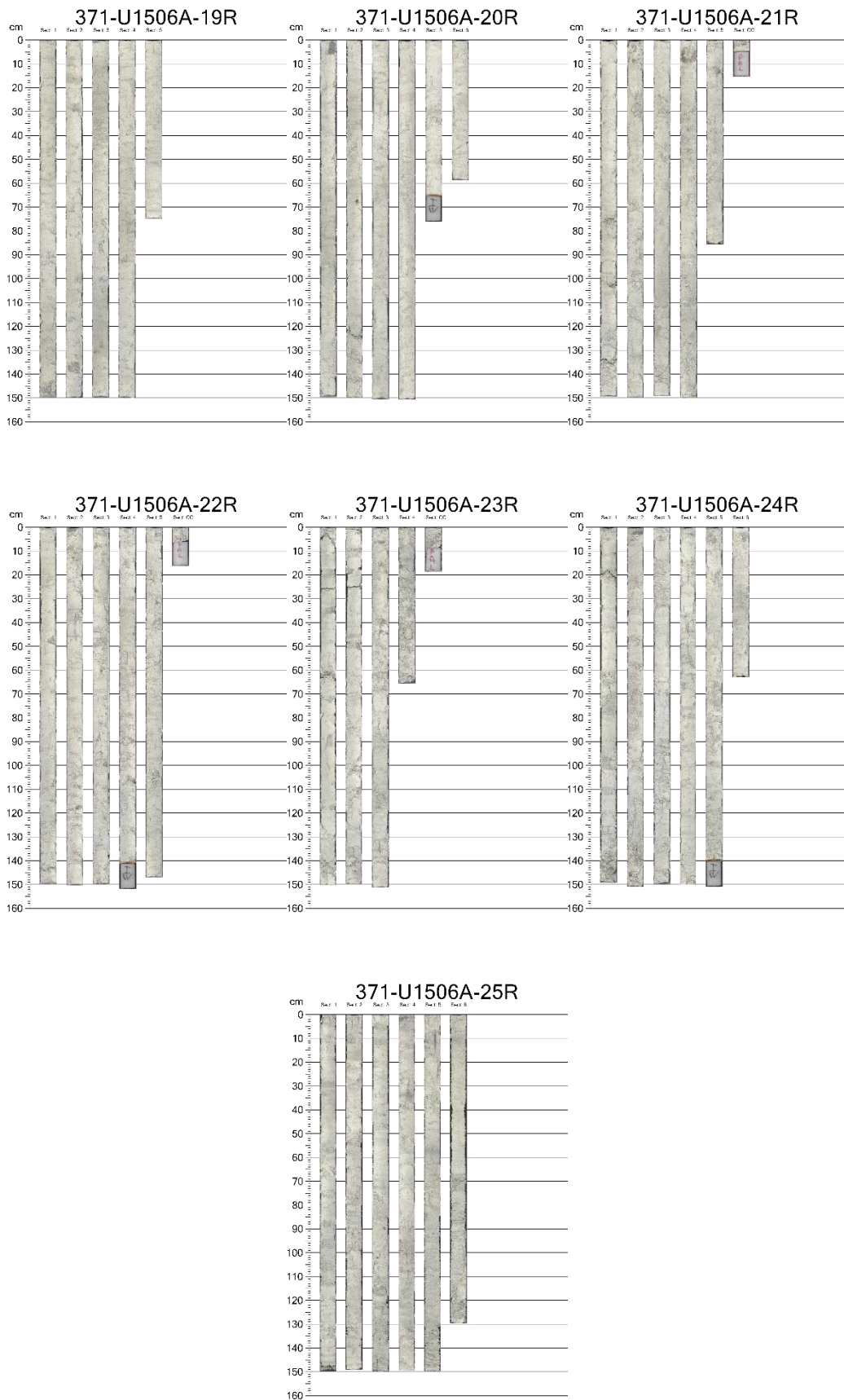
Fig. 3.3 Pictures of the cores from which comes the studied material. (Online dataset LIMS Reports, http://web.iodp.tamu.edu/LORE/).

3.2. Micropaleontological analysis

In this work, I have analysed the paleontological content in terms of small benthic foraminifera and calcareous nannofossils.

3.2.1. Benthic foraminifera

Foraminifera are single-celled organisms (protists), formed within a complex cell (Eukaryotes), and composed of genetic material within a cell nucleus. They have thread-like extensions of the ectoplasm called granuloreticulose pseudopodia, which often includes grains or tiny particles of various materials. They are heterotroph organisms, they do not use photosynthesis to produce energy but they eat dissolved organic molecules, bacteria, diatoms and other single-celled algae, small animals such as copepods. Foraminifera are typical of marine environments and can be distinguished into planktic and benthic, the latter is further divided into small benthic and large benthic. Foraminifera secrete an organic or shell-like outer protective layer, called a test, and they are classified primary on its composition and morphology:

- Organic: protinaceous mucopolysaccharide (tectin), e.g. *Allogromia laticollaris*;
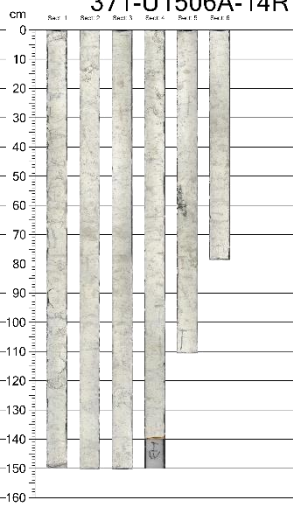- Agglutinated: made from small pieces of sediment cemented together, e.g. *Sigmoilina schlumbergeri*;
- CaCO$_3$: calcit, e.g. *Cibicidoides mundulus*, or more rarely aragonite, e.g. *Hoeglundina elegans*;
- Silica: e.g. *Silicoloculinina;*
- No test: e.g. *Xenophyophores, Arthrodendron.*

The benthic foraminifera and their ecology

The identification and characterization of the biogenic bloom at Site U1506A was one of the main goals of this thesis. To this aim, we have investigated the foraminiferal assemblages, which are able to provide paleo-ecological proxies that can be used to reconstruct the paleoenvironmental condition at the sea floor (Ruddiman, 2007). The comparison between recent and fossil benthic foraminiferal taxa allows us to derive environmental parameters such as nutrient supply, seawater oxygenation and seasonality (e.g. Bernhar, 1986; Jorissen et al., 1995; Fontanier et

al., 2002). Though this a routinely used tool it is worth to remind that this approach should be used with a critical attitude because the ecology of present-day foraminifera is still not fully understood and the morphologic features, used to compare fossil and recent foraminifera to infer similar ecological affinities are, at least in some cases, are not straightforward (Murray, 2001).

Ninety-one different species of benthic foraminifera were identified in the investigated samples, the most common species (with abundance > 5 % at least in one sample) are described in term of both morphological and ecological characteristics in the following:

Abditodentrix asketocomptella **Patterson 1985**

This species has an elongate rectangular test, flattened sides, truncated margins, deep sutures, elliptical aperture with a toothplate and the chambers have a biserial arrangement. The wall is calcareous, hyaline, perforated with medium-size pores (Patterson, 1985).

Bolivina finlayi **Hornibrook 1961**

This species characterized by the crooked, more or less limbate sutures and fine longitudinal convergent ribs (Hayward and Buzas, 1979). It is associated with low oxygen concentration and high nutrient supply (Gooday, 1994; Mackensen et al., 1995; Schmiedl et al., 1997; Bernhard and Gupta, 1999).

Bulimina elongata **d'Orbigny 1846**

The test of this taxon has an elongate shape and is triserial and circular if observed in cross-section; the chambers are moderately inflated, increase rapidly in height and are separated by distinct sutures. This species presents smooth calcareous wall finely perforated. The aperture is loop-shaped on the final chamber and it has a lip that merge with an internal toothplate (Hayward amd Buzas, 1979). This species is typical of low oxygen, muddy environments and is associated with high influx of organic carbon to the seafloor (Verhallen, 1991; Bernhard and Sen Gupta, 1999).

Bulimina truncana **Gümbel 1868**

This taxon has a globose to ovate test with calcareous, hyaline wall; the coiling is triserial, the chambers are pyriform and the sutures are depressed and curved. It usually an arcuate aperture in the basal zone of the test (Hayward and Buzas, 1979). It is typical of eutrophic and suboxic environments (Hayward et al., 2010).

Cassidulina crassa **d'Orbigny 1839**

This species is characterized by a globose to ovate test, biserial coiling and a calcareous hyaline walls; it has an aperture in the basal zone, typically a slit (Hayward et al., 2014). Abundant from littoral and bathyal muds with peaks between 120 and 650 m depth (Parker, 1958; Sgarrella and Moncharmont Zei, 1993). The increase in abundance of this species may indicate an increase in oxygen concentration and/or a decrease in the influx of organic matter to the seafloor, or strong bottom currents (Mackensen et al., 1995; Smart, 2008).

Cibicidoides bradyi **Trauth 1918**

The test of this taxon is trochospiral, unequally biconvex in cross-section with an involute umbilical side and an evolute, more convex spiral side. The chambers are inflated and each chamber is separated by sutures, which are radial on the umbilical side and curved in the spiral side. The maximum number of chambers is at most 9 to 10, and their size increases gradually in the last whorl (Holbourn et al., 2013). The wall is calcareous, coarsely perforated on the spiral side, smooth on the umbilical side. The aperture is located in the spiral side and it is typically a slit (Holbourn et al., 2013). *C. bradyi* is usually found below the upper middle bathyal zone in the western Pacific Ocean (Igle and Keller, 1980) but Schnitker (1971) reported the presence of this taxon also in the neritic zone. Genus *Cibicidoides* is indicative of oxic conditions (Hermelin, 1989).

Cibicidoides mexicanus **Nuttall 1932**

The test of this taxon is trochospiral, and planoconvex in cross-secton, with a flattened spiral side and a convex umbilical side. This species has ten chambers that are inflated and separated by raised sutures. The wall is calcareous, coarsely perforated on both sides. It has an aperture, a narrow slit (Holbourn et al., 2013).

Cibicidoides mundulus **Brady, Parker and Jones 1888**

This species has a biumbonate trochospiral shape, the general outline is subcircular and nearly biconvex in cross-section; the umbilical side is involute and convex, instead the spiral side is evolute. The chambers are inflated, separated by sutures. The wall is calcareous and perforated, finely on the umbilical side, coarsely on the spiral side. The primary aperture is a narrow slit (Holbourn et al., 2013).

Ehrenbergina carinata **Eade 1967**

This species has a triangular test, the wall is thin, perforated and hyaline. Typical of this species is the well-developed peripheral keel, non-perforated, with large spine departing from each chamber. The dorsal side is almost flat, slightly concave, while the ventral side has a raised central keel. The aperture is a narrow, elongate slit (Eade, 1967).

Epistominella exigua **Brady 1884**

The test is convex on both side, the periphery is acute and lobulated; it is composed of three convolutions, the outermost has usually five segments. The sutures are thickened on the spiral side and slightly depressed on the umbilical side (Brady, 1884). This species is a deep-water form, and it is considered an "index species" for Antarctic Bottom Water (ABW) and lower North Atlantic Deep Water (NADW) (Hermelin, 1989). The abundance of this species in benthic assemblage may indicate inputs of seasonal phytodetritus and reflect seasonality in paleoproductivity. It is a useful indicator of high nutrient supply and high oxygen concentration (Thomas et al., 1995; Thomas and Gooday, 1996).

Globocassidulina subglobosa **Brady 1881**

The test of *G. subglobosa* is subglobular in side view, coiled biserial, the peripheral margin is rounded and in cross-section is ovate to globular. Chambers are inflated and separated by distinct sutures, sometimes slightly depressed. The wall is calcareous, hyaline, smooth, and finely perforate. It has a narrow aperture, in a depression of the apertural face (Hermelin, 1989).

This species is present in the middle bathyal zone as suggested by data reported from the Gulf of California (Hermelin, 1989).

Gyroidina orbicularis d'Orbigny in Parker, Jones and Brady 1865

This species has a trochospiral test, the spiral side is flat and the umbilical side is strongly convex; the outline is circular with rounded periphery. The chambers are indistinct, all visible on the spiral side. The wall is calcareous, hyaline, smooth and finely perforated. It has an interiomarginal slit as aperture (Hermelin, 1989). This species shows a strong correlation with low oxygen condition (Hayward et al., 2014).

Melonis barleeanum Williamson 1858

The test of *M. barleeanum* is planispiral, involute, compressed, deeply biumbilicate, the periphery is rounded and the chambers are clearly distinct. The wall is calcareous, hyaline, smooth and coarsely perforated, except for the apertural face. The aperture is an interiomarginal slit (Holbourn et al., 2013).

This species is typical of bathyal depths, though this species has been found from the neritic zone, down to the middle bathyal zone but in the Gulf of Mexico (Pflum and Frerichs, 1976).

Oridorsalis umbonatus Reuss 1851

The test of this species is trochospiral, lenticular, compressed and it is circular in side view; it has a keel in the periphery. All the chambers are visible on the spiral side, instead on the umbilical side, only those of the last whorl can be seen. The sutures are radial, slightly curved on the spiral side and sinusoidal on the umbilical side. The wall is calcareous, hyaline, smooth and finely perforated. The aperture is an interiomarginal slit (Holbourn et al., 2013).

This species occurs with relative high abundances (5-20 %) at lower bathyal to abyssal depths (1500-4000 m). Assemblages with *O. umbonatus/G. subglobosa* co-dominance are indicative of high oxygen environments (Muray, 1988; Mackensen et al., 1995; Hayward et al., 2004b). It may indicate low labile carbon flux and oxic bottom conditions.

Osangularia culter Parker and Jones 1865

The test of this taxon is trochospiral, unequally biconvex, the umbilical side is more convex. The chambers are distinct and the sutures are oblique on the spiral side, radial and depressed on the umbilical side. The wall is calcareous, hyaline, smooth and finely perforated. The aperture is an interiomarginal slit (Holbourn et al., 2013). In the Gulf of Mexico *O. culter* is present in the upper middle bathyal zone (Pflum and Frerichs, 1976), but upper depth limit for this species suggests deeper environments > 350-400 m (Hayward et al., 2014).

Planulina wuellestorfi Schwager 1866

The test of this taxon has plano-convex shape and its periphery shows a distinct keel. The sutures are recurved on both sides, limbate on the spiral side. The wall is calcareous, coarsely and densely perforated. It has an aperture, a low arch, on the final chamber (Holbourn et al., 2013). It is common at bathyal to abyssal depths and it typical of oligotrophic conditions and oxic environments (Hayward et al., 2014).

Spiroplectammina spectabilis (Grzybowski, 1989), emend. Kaminski, 1984

One of the best-known and widely distributed Paleogene species among deep-water agglutinated foraminifera; the test of this species is initially planispiral with 4 to 7 chambers, then the chamber arrangement changes into biserial with up to 36 chambers. The biserial part has a rhomboidal shape in cross-section and presents nearly parallel sides (Grzybowski, 1989). This species is common in "Flysch-type" assemblages, typical of detritic deep-sea environments. In the eastern Atlantic, this taxon is absent in oligotrophic sites.

In general, *S. spectabilis* is known as a "disaster species" because it appeared above the Cretaceous/Paleogene boundary at ODP Site 959 (Kuhnt et al., 1998) and at Gubbio, Italy (Kuhnt & Kaminski, 1996). Its presence in deep-sea sites is mostly linked to increased sea-floor carbon flux (Kaminski and Gradstein, 2005).

Uvigerina occidentalis Cushman 1923

The test is elongated, slender, and fusiform with a smooth periphery; chambers are compact and indistinct in the lower part, slightly inflated in the upper part. The wall is calcareous, thin, and with weak, longitudinal costae. It has an aperture relatively large, at the end of a short neck (Sen Gupta et al., 2009).

Uvigerina peregrina s.l. Cushman 1923

This taxon has a triserial and elongated test, the sutures are indistinct and depressed. The wall is calcareous, perforated, ornamented by blade-like costae on each chamber, this ornamentation does not continue from one chamber to another. The aperture is in the last chamber, on a short neck, with a lip (Hermelin, 1989).

High abundance of this species is usually associated with glacial periods (Schnitker, 1974; Corliss, 1982) and increase in organic carbon in the sediments (Douglas, 1981; Miller and Lohmann, 1982). The presence of *U. peregrina* in benthic assemblage can indicate low oxygen content and/or high nutrient supply (Lohmann, 1978; Streeter and Shackleton, 1979; Schnitker, 1979; Douglas, 1981; Miller and Lohmann, 1982).

Uvigerina proboscidea Schwager 1866

Uvigerina proboscidea has a triserial arrangement in the initial part of the test, that becomes biserial in the rest of the test, and it is circular in cross-section. The test is characterized by the presence of small spines, tapering toward the apertural neck. The aperture is located at the end of a long neck with a distinct collar. The wall is calcareous, hyaline, finely perforated (Holbourn et al., 2013).

Data on this species reported from the Gulf of Mexico indicated a distribution from the lower neritic zone to the upper middle bathyal zone (Pflum and Frerichs, 1976). Higher percentages of this taxon are related to low oxygen concentrations and/or high nutrient supply (Hermelin, 1989).

Methods

Samples were disaggregated in water with diluted sodium hexametaphosphate, were washed through a sieve to isolate the fraction larger than 63 µm, and dried in an oven at 50°C. For the quantitative studies and the calculation of the species richness, approximately 200-300 specimens of benthic foraminifera larger than 63 µm were selected and mounted on microslides.

Most of specimens were identified at the specific level; the names of the common species with original author are listed in Appendix II - taxonomic list. Data counts on benthic foraminifera are included in supplementary material (see attached CD). In this study I analysed the > 63 µm fraction because this fraction is more appropriate for a detailed analysis of the benthic foraminiferal assemblages. In fact, according to Schroeder et al. (1987) the study of larger-size fractions is not sufficient to interpret the obtained results in term of environmental changes. Several species, particularly those in Arctic waters, produce small adult tests that would be lost using larger sieve sizes (125 µm, 150 µm, 250 µm). The 63 µm limit should be chosen because it produces larger assemblages, which are likely to provide more reliable statistical analyses, and leads to minimal loss of specimens. For example, a study on foraminifera collected by DSDP Leg 90 in the Southwest Pacific on 63-150 µm and > 150 µm fractions has shown that the foraminiferal test smaller than 150 µm constitute 50-99 % (average 78-89 %) of the benthic assemblage. Therefore, studying only the large side fraction would have resulted in a significant loss of benthic foraminifera.

Each taxon has been allocated in different morphogroups following Corliss (1985, 1991), Jones and Charnock (1985) e Corliss e Chen (1988). Epifaunal foraminifera, living near the sediment surface or in its upper few centimetres, are characterized by plano-convex, biconvex and rounded trochospiral tests, tubular and coiled flattened, and also milioline and palmate tests. Infaunal foraminifera instead usually have cylindrical or flattened tapered, spherical, rounded planispiral, flattened ovoid, globular unilocular or elongated multilocular tests, and overall live deeper into the sediment (4-10 cm depth; deep infaunal in Corliss, 1991). The comparison of fossil taxa with recent benthic foraminifera along with the morphotype analysis (e.g. Corliss 1985; Corliss and Chen, 1988; Jones and Charnock, 1985), allows to likely infer microhabitat preferences and possibly reconstruct paleoenvironmental

parameters such as sea-water oxygen content, nutrient supply and seasonality (e.g., Bernhar, 1986; Jorissen et al., 1995; Fontanier et al., 2002). Though we now have a conspicuous number of studies available, it is always worth to take into account that these interpretations could be not always straightforward because the ecology of the present-day foraminifera is complicated and still not wholly understood (e.g. Murray, 2001). Furthermore, the ecological preference of fossil taxa are only based on their morphology, which means that for a number of taxa the expected relationship between the morphology of the test and the inferred microhabitat has not been directly observed, but rather extrapolated from data based on similar taxa, this is particularly the case for extinct taxa. The bathymetric divisions used in this thesis are based on those defined in Van Morkhoven et al. (1986) and Berggren and Miller (1989), that are: neritic (0-200 m), upper bathyal (200-600 m), middle bathyal (600-1000 m), lower bathyal (1000>2000 m). A total number of 55 samples were analysed using a binocular stereoscopic microscope (Olympus SZX12) (Fig. 3.4), counting at least 300 specimens. Ideally, when possible, the specimens were identified at the specific level, and then reported in an Excel file (see attached CD). Quantitative data are used to calculate the relative abundance of taxa that have been plotted using *Grapher,* and then improved with *Adobe Illustrator.*

Multivariate analyses of quantitative data were performed to assess the benthic foraminiferal assemblages, using PAST software v. 3.04 (Hammer et al., 2001). These techniques allowed identification of the main assemblages and their most typical benthic foraminifera. The species diversity has been determined through the Fisher-α diversity index plot (Fisher et al., 1943) using the number of species and the number of individuals per samples; the Shannon-Weaver heterogeneity index H(S) was also determined, high values of H(S) indicate high heterogeneity and high diversity (Murray, 1991). The whole work on benthic foraminifera has been carried out at the Universidad de Zaragoza (Spain) under the supervision of Professor Laia Alegret, during a period of study abroad subsidised by the Erasmus+ traineeship project. Pictures of benthic foraminifera were taken using OLYMPUS Stream Image Analysis Software at the Departamento de Ciencias de la Tierra (Appendix I, Plate I to IV) (Fig. 3.5), and by SEM (scanning electron microscope, Zeiss Merlin) imaging, at the Departamento de Ingeniería - Universidad de Zaragoza (Appendix I, Plate V and VI, Credit Lucía Rivero-Cuesta) (Fig. 3.6-3.7).

Fig 3.4 Binocular stereoscopic microscope used to analyse the benthic foraminifera (University of Zaragoza, image by Maria Elena Gastaldello).
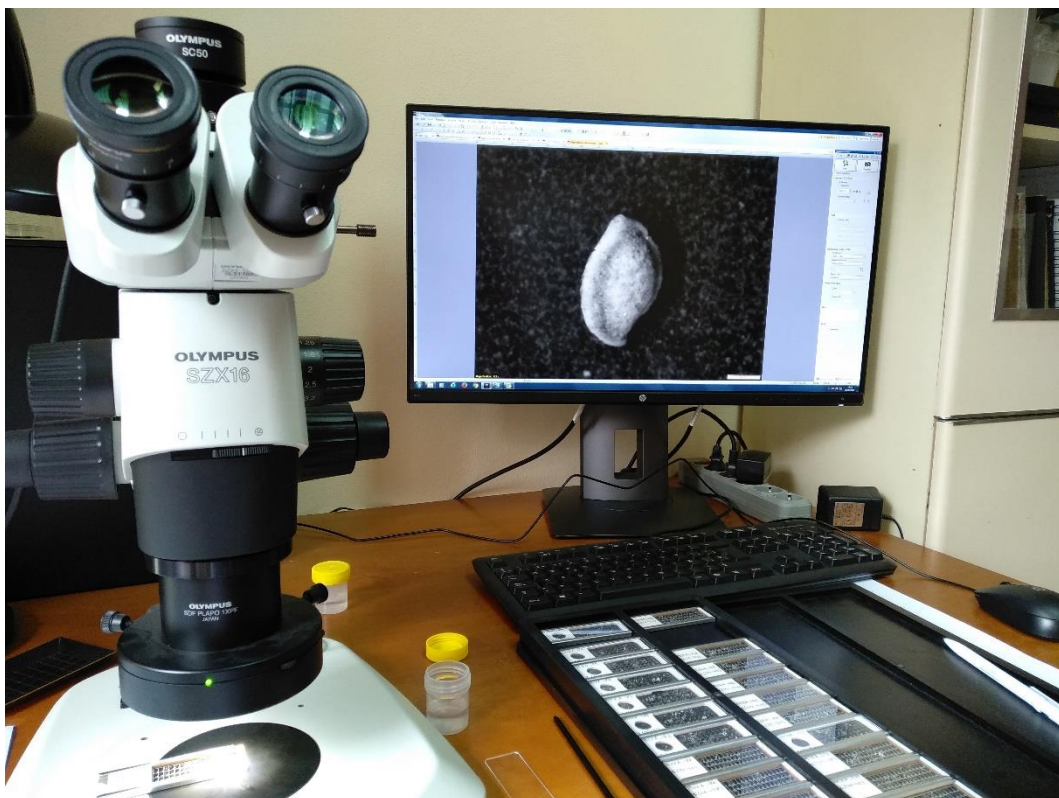
Fig. 3.5 Binocular stereoscopic microscope used to take pictures of the benthic foraminifera (University of Zaragoza, image by Maria Elena Gastaldello).
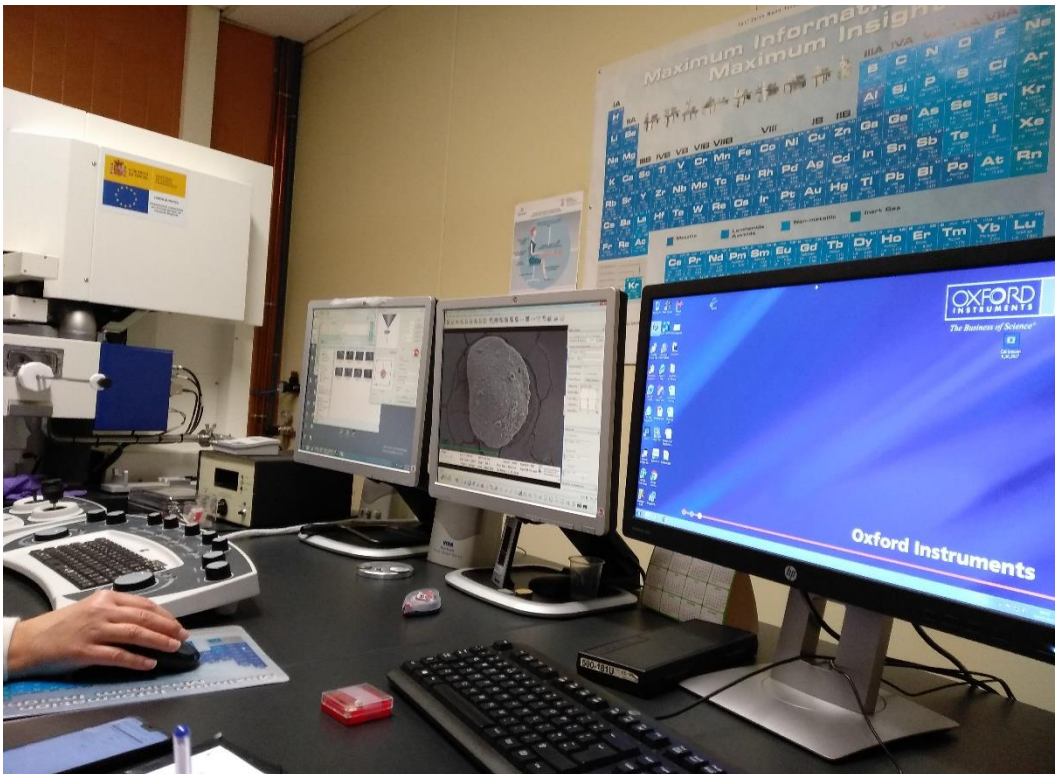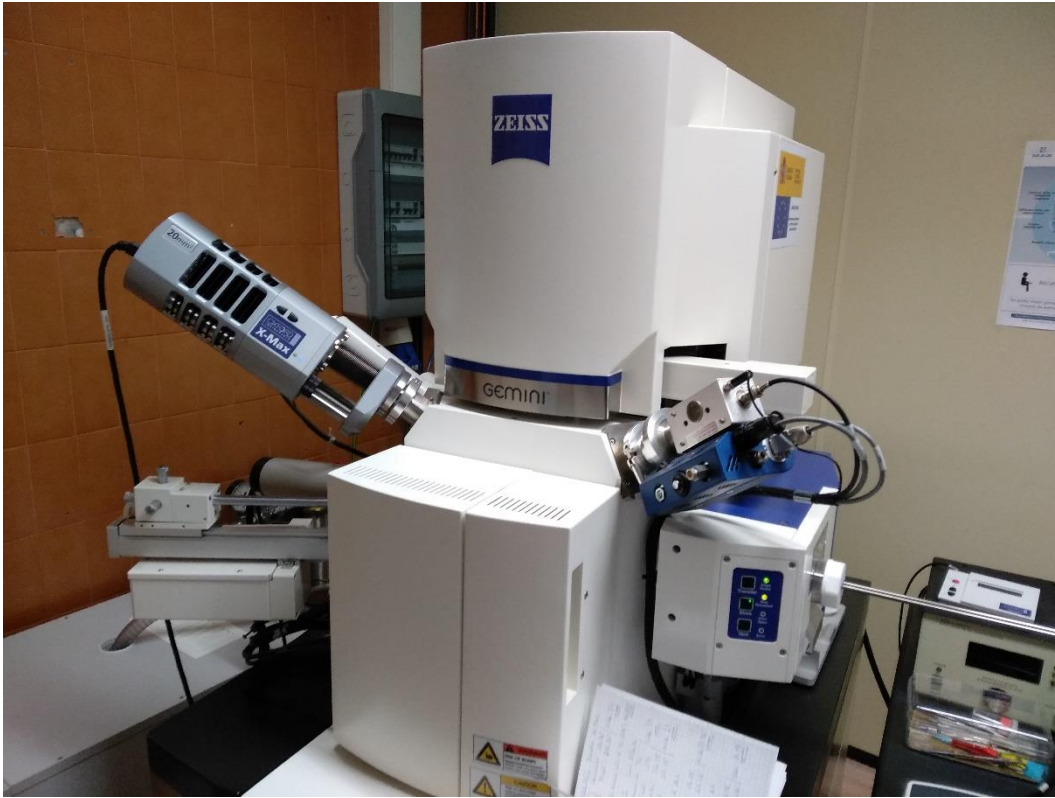
Fig. 3.6-3.7 SEM (scanning electron microscope, Zeiss Merlin, University of Zaragoza) used to take pictures of some specimen of benthic foraminifera (images by Maria Elena Gastaldello).

3.2.2. Calcareous nannofossils

Calcareous nannofossils are single-celled eukaryotic algae and they use photosynthesis to produce energy (photosynthetic autothrops). These organisms are made of soft organic materials generally encased within a hard calcite exoskeleton ($CaCO_3$), the coccosphere. The coccosphere consists of miniscule calcite plates that form a protective covering around their delicate cell walls, some taxa have organic scale covering while some others are completely naked. Calcareous nannoplankton are typical of marine environments and they are planktic organisms, they live in the photic zone. These organisms are responsible for 40 % of the total carbonate production in the modern oceans (Milliman, 1993; Falkowski et al., 2004).

Methods

The study material was prepared using the "smear slides" standard method (Bown, 1998). A small amount of the material has been collected from the sample bag and placed on a microscope slide, already signed with the sample ID. Successively, a drop of distilled water was added to the slide and mixed with a plastic straw. The material was then smeared on the slide and bands of different density were obtained. After drying the sample on a preheated plate at approximately 100°C for few seconds, the slide was sealed with a cover slip with the aid of an optical adhesive (Norland). Finally, the slide was exposed to the radiation of an ultraviolet lamp to activate the optical glue. (Fig. 3.8).

The samples are ready to be analysed with an optical polarizing microscope at 1250 magnifications, Zeiss (Fig. 3.9). The preparation of the slides as well as the calcareous nannofossil analyses were performed at Dipartimento di Geoscienze – Università di Padova under the supervision of Prof. Claudia Agnini.

In addition, microphotographies of the most significant taxa were taken using DeltaPix digital camera and *DeltaPix Insight* software, and are provided in order to further clarify the taxonomic concepts used here (Appendix I, Plate VII).

Calcareous nannofossil analyses were performed in order to determine taxa present in the fossil assemblages, to this aim samples were observed both at parallel and crossed nicols, which has allowed for both a structural and morphological investigation.

Crossed nicols analysis reveals the optical characterization of different taxa. For those taxa that are not extinct at crossed nicols, their extinction figure is a fundamental diagnostic character, which allows to determine and distinguish different taxa.

Due to the lack of time, the estimation of relative abundances of the taxa present in the assemblage (in %; Pospichal, 1991) has not been carried out. In this study, I have performed semi-quantitative estimations of selected taxa, which consist of counting the number of specimens belonging to the same taxon present on an area of 1 mm^2 (Backman & Shackleton, 1983). This method is usually applied for biostratigraphic purposes to highlight the presence of marker species that are typically rare within the assemblages.

The biostratigraphic schemes adopted in this thesis are those proposed by Martini (1971), Okada and Burky (1980) and Backman et al. (2012). The taxonomic concepts used for determining taxa are those of Perch-Nielsen (1985), Farinacci (1969-1989) "Catalogue of Calcareous Nannofossils" and online atlas nannotax (http://www.mikrotax.org/Nannotax3/index.php?dir=Coccolithophores), unless otherwise specified. Data obtained from sample counts were analysed in order to biostratigraphically frame the study succession, graphs were developed with the *Grapher* software and elaborated with *Adobe Illustrator*.

Fig. 3.8 Work desk for the preparation of the smear slides (image by Maria Elena Gastaldello).

Fig. 3.9 Optical polarizing microscope used to analyse the samples and to take pictures through DeltaPix digital camera and *DeltaPix Insight* software (image by Maria Elena Gastaldello).

4. CALCAREOUS NANNOFOSSIL BIOSTRATIGRAPHY AND BIOCHRONOLOGY

Biostratigraphy is a subdiscipline of stratigraphy that describes all rock bodies forming the Earth's crust and their organization into distinctive units based on their fossil content.

4.1. Biozones

The base unit in biostratigraphy is the biozone, this consists of a package of geological strata defined based on its particular fossil content. It can be defined based on the range occurrence of a particular taxon or combination of two taxa (range zone), assemblage of three or more fossil taxa (assemblage zone), the relative stratigraphic distribution of taxa (interval zone), the abundance patterns of taxa (abundance zone), and the successive segments of an evolutionary lineage (lineage zone), (http://www.stratigraphy.org/index.php/ics-stratigraphicguide).

Based on the biohorizons used, the same interval could in principle be subdivided with different type of zones. According to Agnini et al. (2014), calcareous nannofossils biozones are usually defined using different biohorizons thus resulting in the following five different type of biozones (Fig. 4.1): Taxon Range Zone (TRZ), Concurrent Range Zone (CRZ), Base Zone (BZ), Top Zone (TZ) and Partial Range Zone (PRZ)
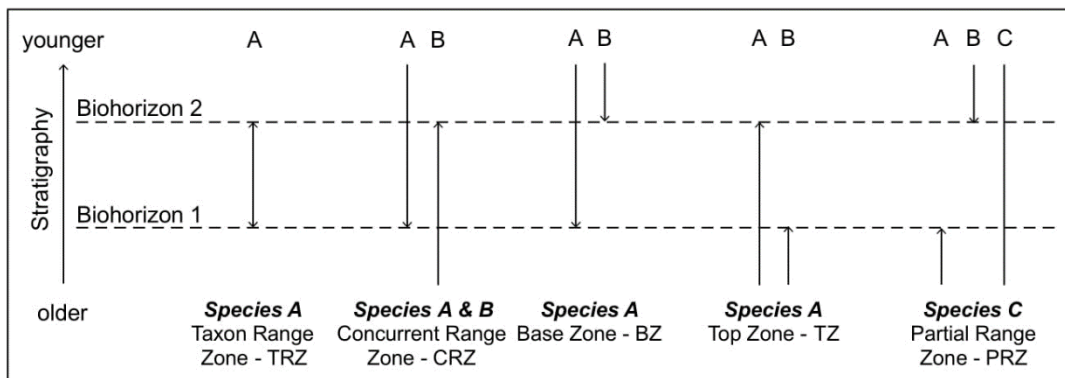
Fig. 4.1 Scheme of the biozones commonly used for calcareous nannofossils biostratigraphic subdivisions (Backman et al., 2012)

4.2. Biohorizons

A biohorizon is a stratigraphic boundary or surface through which there is a meaningful change in biostratigraphic characters (http://www.stratigraphy.org/index.php/ics-stratigraphicguide). Biostratigraphic events can be controlled by organic (non-repetitive) evolution or by environmental (possibly repetitive) evolution. The former type includes evolutionary events of speciation and extinction (e.g. First Appearance Datum, Last Appearance Datum, Fig. 4.2), while the latter includes events controlled by local factors such as:

- Events of appearance or disappearance caused by migration or environmental exclusion
- Intervals of abundance or absence
- Morphological variations
- Abundance fluctuations

Biohorizons are usually termed as first occurrence (FO)/last occurrence (LO) or lowest occurrence (LO)/highest occurrence (HO) or base (B)/top (T) (Fig. 4.2).
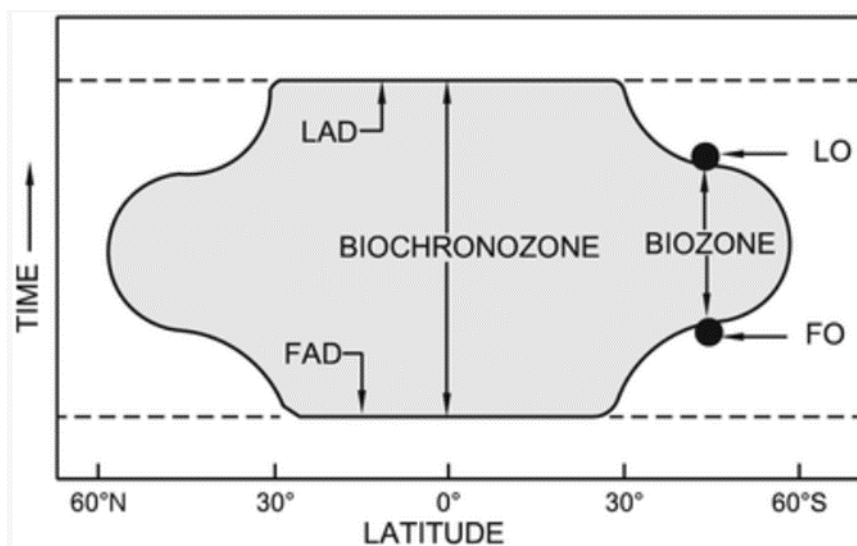
Fig. 4.2 The figure explains first occurrence (FO), last occurrence (LO), first appearance datum (FAD) and last appearance datum (LAD) of a species (Saraswati and Srinivasan, 2016).

A reliable biostratigraphic event has to maintain the same temporal spacing (*spacing*) and the same relative position (*ranking*) between different successions and within the same succession, among different authors.

The features that discriminate whether an event is reliable or not are:

- Easy recognition of the species that defines the event
- Taxon abundance
- Continuous distribution of the taxon
- The presence of reworking
- The preservation potential of the taxon
- Traceability
- Correlations across or with basins

The term used to define the appearance and disappearance of a taxon are multiple. In literature, First Occurrence (FO) and Last Occurrence (CO) are often used, but Lowest Occurrence (LO) and Highest Occurrence (HO) are also commonly found (Wade et al., 2011). The problem is that LO may refer both to Last Occurrence or to Lowest Occurrence of a taxon (Backman et al., 2012). For this reason, in this thesis, I use Base (B) and Top (T) to describe appearance and disappearance of taxa in order to avoid any misunderstanding caused by previous acronyms (Backman et al., 2012; Agnini et al., 2014). First appearance of calcareous nannofossil taxa are initially often followed by low and in many cases sporadic occurrences, prior to becoming well-established members of the assemblages.

Correspondingly, extinctions of taxa are often preceded by low and sporadic occurrences prior to their final demise. This is why the first or last continuous and relatively common occurrence of a taxon may represent a better biohorizon than the absolute first or last occurrence, and is why the concepts Base common (Bc) and Top common (Tc) are possibly employed here for biozone boundary definitions (Agnini et al., 2014.) Two other terms are adopted by Backman et al. (2012) which are: Base absence (Ba) for defining the temporary disappearance of taxon and thus the beginning of a paracme interval, and Top absence (Ta) for identifying the re-entrance of a taxon, which coincides with the end of the paracme interval.

In this thesis the position of each biohorizon has been calculated using the midpoint method. For example, in the case of the appearance of a taxon (x), the B(x), the biohorizon has been placed at the midpoint between the last sample in which the taxon is absent and the first sample in which the taxon is present.

The same has been done for T(x), which has been placed between the last sample in which the taxon is still present and the first sample in which the taxon is absent. In the following, the list of the biohorizons and biozones used in the biozonation adopted in this study are reported (Backman et al., 2012) (Fig. 4.3):

Marker Taxon for Base of Zone	Type of Event	Marker Taxon for Top of Zone	Type of Event	Biozone*	Code
Discoaster quinqueramus	Top	Ceratolithus acutus	Base	T. rugosus PRZ	CNM20
Nicklithus amplificus	Top	Discoaster quinqueramus	Top	D. quinqueramus TZ	CNM19
Nicklithus amplificus	Base	Nicklithus amplificus	Top	N. amplificus TRZ	CNM18
Amaurolithus primus	Base	Nicklithus amplificus	Base	A. primus BZ	CNM17
Discoaster berggrenii	Base	Amaurolithus primus	Base	D. berggrenii BZ	CNM16
Reticulofenestra pseudoumbilicus	Base absence	Discoaster berggrenii	Base	D. bellus BZ	CNM15
Discoaster hamatus	Top	Reticulofenestra pseudoumbilicus	Base absence	R. pseudoumbilicus PRZ	CNM14
Discoaster hamatus	Base	Discoaster hamatus	Top	D. hamatus TRZ	CNM13
Ceratolithus coalitus	Base	Discoaster hamatus	Base	C. coalitus BZ	CNM12
Discoaster kugleri	Top common	Ceratolithus coalitus	Base	C. exilis PRZ	CNM11
Discoaster kugleri	Base common	Discoaster kugleri	Top common	D. kugleri TRZ	CNM10
Calcidiscus premacintyrei	Base	Discoaster kugleri	Base common	D. variabilis PRZ	CNM9
Sphenolithus heteromorphus	Top	Calcidiscus premacintyrei	Base	C. premacintyrei TZ	CNM8
Discoaster signus	Base	Sphenolithus heteromorphus	Top	D. signus / S. heteromorphus CRZ	CNM7
Sphenolithus heteromorphus	Base common	Discoaster signus	Base	S. heteromorphus BZ	CNM6
Sphenolithus belemnos	Base	Sphenolithus heteromorphus	Base common	S. belemnos BZ	CNM5
Helicosphaera euphratis / H. carteri	Cross-Over	Sphenolithus belemnos	Base	H. carteri PRZ	CNM4
Triquetrorhabdulus carinatus	Top common	Helicosphaera euphratis / H. carteri	Cross-Over	H. euphratis PRZ	CNM3
Sphenolithus disbelemnos	Base	Triquetrorhabdulus carinatus	Top common	S. disbelemnos / T. carinatus CRZ	CNM2
Sphenolithus delphix	Top	Sphenolithus disbelemnos	Base	S. conicus PRZ	CNM1

Fig. 4.3 Biohorizons used for definitions of Miocene biozones (modified after Backman et al., 2012). The orange band marks the interval investigated in this thesis.

4.3. Miocene through Pleistocene calcareous nannofossil biozonations

The calcareous nannofossili biozonations adopted for the Miocene are those of Martini (1971), Okada and Bukry (1980), and the more recent proposed by Backman et al. (2012). The first two biostratigraphic schemes are based on the pioneering papers of Hay et al. (1967), Bramlette and Wilcoxon (1967), Roth (1970, 1973), Roth et al. (1971) and Bukry (1973, 1975). For the time interval investigated in this thesis, Martini (1971) codifies the biozones using the acronym "NN" (Neogene Nannoplankton) followed by a progressive number for each biozone, starting from the base.

An alternative biozonation was proposed by Bukry (1973), based on the studies he carried out in the context of the international Deep Sea Drilling Project (DSDP) (Bukry, 1970, 1971, 1973, 1975a), which was eventually republished after minor revisions (Okada and Bukry, 1980).

The coding system of this biostratigraphic scheme uses the acronym "CN" (Neogene Coccolith), followed by a progressive number and, if needed a letter (a, b or c), to identify the subzones.

In 2012, Backman et al. (2012) have published a new calcareous nannofossil biozonation for Miocene-Pleistocene interval. This recent scheme obviously relies on the previous fundamental contributions of Erlend Martini and David Bukry, however several of their zonal boundary have proven to be poorly reliable and this explains the need for a revised biozonation. (Fig. 4.4) This biozonation is composed of 31 biozones that span over 23 million years: 20 for the Miocene, 6 for the Pliocene and 5 for the Pleistocene; each biozone is defined by a single biohorizon to give stability to the zonal scheme and keep it simple. The biozone code system is inspired to Berggren and Pearson (2006) and Wade et al. (2011) biozonation.

In particular, Backman et al. (2012) introduced a new code system which is formed by letter for denoting series (M=Miocene; PL=Pliocene/Pleistocene) followed by a progressive number starting at the base of the series.

The biozonation proposed by Backman et al. (2012) consists of:

- 11 biozones (CNPL1 to CNPL11) covering the Pliocene through Pleistocene interval;
- 20 biozones (CNM1 to CNM20) spanning the Miocene.

4.4. Calcareous nannofossil biochronology

Biochronology is the sequencing of geologic events, based on evolution (Berggren and Van Couvering, 1974, 1978) and allows us to estimate/calibrate an absolute age for the considered biohorizons (Salvador, 1994).

In this thesis, we adopted the biochronology proposed by Backman et al. (2012), based on different methods. For the Miocene through Pleistocene interval, the age estimates derive from improved astronomically tuned cyclostratigraphy based on the work of Raffi et al. (2006).

The age of the biohorizons were estimated from correlation to Pleistocene Marine Isotope Stages (MIS), using the work of Lisiecki and Raymo (2005). Age estimates derived from two types of orbitally-tuned lithologic cyclicities: at ODP Sites 925 and 926, Shackleton and Crowhurst (1997) used magnetic susceptibility; at ODP Leg 138 sites Shackleton et al. (1995) derived the age estimates from gamma ray wet-bulk densities, in Backman et al. (2012) the estimates from Shackleton et al. (1995) data has been converted to the timescale of Lourens et al. (2004).

For age estimates derived from the lower Miocene cyclostratigraphies in ODP Hole 926B and ODP Site 1218, Backman et al. (2012) used orbitally-tuned data produced by Pälike et al. (2006, 2007). In addition to astronomically tuned cyclostratigraphic age data, it was also used magnetostratigraphy for a few late Miocene biohorizons (Schneider, 1995). The biochronologic data used to construct our age model (Fig. 4.5) has been calibrated to GTS2012.

Calcareous Nannofossil Zones and Biohorizons chart

Age (Ma)	GPTS	Epoch	Stage	Okada & Bukry 1980	Martini 1971	this study		Biohorizons — primary and additional
5.0	C3n		Zancl.	CN10b	NN12	CNPL1	C. acutus TRZ	B Ceratolithus acutus (5.36); B Ceratolithus atlanticus (5.39)
	C3r			CN10a		CNM20	T. rugosus PRZ	T Discoaster quinqueramus (5.53)
6.0		Messinian				CNM19	D. quinqueramus TZ	T Nicklithus amplificus (5.98)
	C3An			CN9b	NN11	CNM18	N. amplificus TRZ	B Nicklithus amplificus (6.82)
7.0	C3Ar					CNM17	A. primus BZ	Ta R. pseudoumbilicus (7.09); B Amaurolithus primus (7.39)
	C3Br							
8.0	C4n			CN9a		CNM16	D. berggrenii BZ	T Minylitha convallis; Bc Discoaster surculus; B Discoaster berggrenii (8.20)
	C4r	late	Tortonian	CN8b	NN10	CNM15	D. bellus BZ	Ba R. pseudoumbilicus (8.80); B Discoaster loeblichii / Discoaster neorectus; B Discoaster pentaradiatus; B Minylitha convallis
9.0	C4An			CN8a		CNM14	R. pseudoumbilicus PRZ	T Discoaster hamatus (9.65) / T Catinaster calyculus (9.65); T Catinaster coalitus (9.70)
	C4Ar							
10.0	C5n			CN7	NN9	CNM13	D. hamatus TRZ	B Discoaster neohamatus (10.47)
				CN6	NN8	CNM12	C. coalitus BZ	B Discoaster hamatus (10.49); B Discoaster bellus; T Coccolithus miopelagicus (10.61); B Catinaster calyculus (10.71); B Catinaster coalitus (10.79); T Coccolithus miopelagicus (10.94)
11.0	C5r			CN5b	NN7	CNM11	C. exilis PRZ	Tc Discoaster kugleri (11.60)
12.0	C5An		Seravallian			CNM10	D. kugleri TRZ	Bc Discoaster kugleri (11.88)
		middle		CN5a	NN6	CNM9	D. variabilis PRZ	T Cyclicargolithus floridanus; T Coronocyclus nitescens
13.0	C5Ar, C5AAn, C5AAr, C5ABn, C5ABr					CNM8	C. premacintyrei TZ	Tc Calcidiscus premacintyrei (12.57); Tc Cyclicargolithus floridanus; Bc Reticulofenestra pseudoumbilicus
14.0	C5ACn, C5ACr, C5ADn, C5ADr		Langhian	CN4	NN5	CNM7	D. signus CRZ	T Sphenolithus heteromorphus (13.53)
15.0	C5Bn							T Helicosphaera ampliaperta (14.86)
16.0	C5Br							Tc Discoaster deflandrei (15.69); B Discoaster signus (15.73)
	C5Cn			CN3	NN4	CNM6	S. heteromorphus BZ	
17.0	C5Cr		Burdigalian					
	C5Dn							B Sphenolithus heteromorphus (17.75)
18.0	C5Dr, C5En			CN2	NN3	CNM5	S. belemnos BZ	T Sphenolithus belemnos (17.96)
	C5Er	early						
19.0	C6n							B Sphenolithus belemnos (19.01); T Triquetrorhabdulus carinatus (19.18)
20.0	C6r					CNM4	H. carteri PRZ	B Helicosphaera ampliaperta (20.43)
21.0	C6An, C6Ar			CN1c	NN2			X Helicosphaera euphratis / H. carteri (20.89)
	C6AAr		Aquitanian			CNM3	H. carteri PRZ	
22.0	C6Bn					CNM2	S. disbelemnos / T. carinatus CRZ	Tc T. carinatus (22.10); B Sphenolithus disbelemnos (22.41); B Discoaster druggii (22.59)
23.0	C6Br, C6Cn			CN1b	NN1	CNM1	S. conicus PRZ	T Sphenolithus delphix (23.06); T Helicosphaera recta; B Sphenolithus delphix (23.38)
24.0	C6Cr	late (Oligocene)	Chattian	CN1a	NP25		Oligocene biozone	Ta Cyclicargolithus abisectus

Fig. 4.4 Miocene through Pleistocene biozones and biohorizons of Backman et al., (2012) are plotted versus the biozonations of Martini (1971) and Okada and Bukry (1980), and the Geomagnetic Polarity Time Scale (GPTS; Lourens et al. 2004) (modified after Backman et al., 2012). The orange band marks the interval investigated in this thesis.

Event	Species	Reference	mcd	± m	Hole	Upper Depth	Lower Depth	Younger Age	Older Age	m/myr	Ma	
			Depth		ODP	Interpolation between		Interpolation between		Rate	Age	
						SC97	SC97	SC97	SC97			
B	*C. larrymayeri*	Backman & Raffi, 1997	161.46	0.05	926A	161.21	161.41	5.32	5.34	10.0	5.35	
B	***C. acutus***	Backman & Raffi, 1997	162.16	0.05	926A	161.71	162.71	5.34	5.39	20.0	**5.36**	
B	*C. atlanticus*	Backman & Raffi, 1997	162.66	0.05	926A	161.71	162.71	5.34	5.39	20.0	5.39	
T	***D. quinqueramus***	Backman & Raffi, 1997	165.49	0.10	926C	165.46	165.91	5.53	5.55	22.5	**5.53**	
T	***N. amplificus***	Backman & Raffi, 1997	175.66	0.05	926C	175.56	176.06	5.98	6.00	25.0	**5.98**	
B	***N. amplificus***	Backman & Raffi, 1997	190.94	0.05	926B	190.71	191.01	6.80	6.82	15.0	**6.82**	
						DAS95	DAS95	LL04	LL04			
						C3An.2n (o)[1]	C3Bn (y)	C3An.2n (o)	C3Bn (y)			Mean age
B	*N. amplificus*	Raffi & Flores, 1995	39.19	0.15	844B	38.65	41.00	6.73	7.140	5.8	6.83	844/845
B	*N. amplificus*	Raffi & Flores, 1995	96.50	0.22	845A	96.28	101.18	6.73	7.140	12.0	6.75	6.79
						SC97	SC97	SC97	SC97			
Ta	*R. pseudoumbilicus*	Backman & Raffi, 1997	195.14	0.05	926B	195.11	195.76	7.09	7.14	13.0	7.09	
						DAS95	DAS95	LL04	LL04			
						C3An.2n (o)	C3Bn (y)	C3An.2n (o)	C3Bn (y)			Mean age
Ta	*R. pseudoumbilicus*	Raffi & Flores, 1995	40.99	0.15	844B	38.65	41.00	6.73	7.140	5.8	7.14	844/845
Ta	*R. pseudoumbilicus*	Raffi & Flores, 1995	99.26	0.28	845A	96.28	101.18	6.73	7.140	12.0	6.98	7.06
						SC97	SC97	SC97	SC97			
B	***A. primus***	Backman & Raffi, 1997	199.79	0.05	926A	198.91	200.01	7.35	7.40	22.0	**7.39**	
						DAS95	DAS95	LL04	LL04			
						C3Bn (y)	C4n.1n (y)	C3Bn (y)	C4n.1n (y)			Mean age
B	*A. primus*	Raffi & Flores, 1995	42.65	0.30	844B	41.80	43.15	7.140	7.528	3.5	7.38	844/845
B	*A. primus*	Raffi & Flores, 1995	106.18	1.50	845A	101.18	108.06	7.140	7.528	17.7	7.42	7.40
						SC97	SC97	SC97	SC97			
B	***D. berggrenii***	Backman & Raffi, 1997	217.60	0.56	926B/C	198.91	200.01	7.35	7.40	22.0	**8.20**	
						DAS95	DAS95	LL04	LL04			
						C4n.2n (o)	C4An (y)	C4n.2n (o)	C4An (y)			Mean age
B	*D. berggrenii*	Raffi & Flores, 1995	53.30	1.15	844C	49.95	56.75	8.108	8.769	10.3	8.43	844/845
	D. berggrenii	Raffi & Flores, 1995	126.41	0.25	845A	119.28	129.71	8.108	8.769	15.8	8.56	8.50
						SC97	SC97	SC97	SC97			
Ba	***R. pseudoumbilicus***	Backman & Raffi, 1997	225.51	0.20	926B	225.31	225.71	8.79	8.81	20.0	**8.80**	
T	***D. hamatus***	Backman & Raffi, 1997	237.77	0.35	926B	237.51	238.16	9.63	9.67	16.3	**9.65**	

Fig. 4.5 Age estimates of biohorizons. Biohorizons defining biozone boundaries are marked in bold. mcd – meters composite depth. Acronyms used for depth and age columns are: SC97 – Shackleton and Crowhurst 1997; DAS95 – Schneider 1995; LL04 – Lourens et al. 2004; PÄL06 – Pälike et al. 2006; PÄL07 – Pälike et al. 2007.

# 5. RESULTS AND DISCUSSIONS

5.1. Calcareous nannofossil

General characteristics of calcareous nannofossil assemblages at IODP Site 1506

Calcareous nannofossil are generally abundant and moderately to moderately well preserved throughout the studied succession, however, the Core Catcher samples (CC) show a much higher number of specimens than the others likely because they were prepared by a different operator.

Within the assemblage, *Reticulofenestra* is the most abundant genus (Fig. 5.1) and display an increased abundance in the upper part of the section, which is likely related to the re-entrance of *Reticulofenestra pseudoumbilicus* after the Top absence (Ta) around 7.09 Ma (Backman et al., 2012). *Discoaster* and *Amaurolithus* are also present and show scarce to common abundance. *Calcidiscus*, *Ceratolithus, Coccolithus* and *Nickilithus* are present, however their abundance is much lower than those of the taxa mentioned above. Semiquantitative counts have not been performed for *Calcidiscus leptoporus* and *Discoaster bellus* for which we only provide presence-absence data in all the study samples.

5.1.1. Biohorizons of the standard biozonations

In the following paragraph, biohorizons used in the standard biozonations (Martini, 1971; Okada and Bukry, 1980) are described in stratigraphic order and commented. Some of these biohorizons are used also in Backman et al. (2012). The age of the biohorizons are calibrated to GTS2012. Top and Base samples in which the biohorizons were identified and their corresponding depth (CSF-A) are reported in Table 5.1 and Fig. 5.1-5.2, from now on we will simply use m for CSF-A depth. The ID samples consists of IODP Site, Hole, Core, Top Interval, e.g. U1506A-25R-6W, 75 cm. Microphotographs of most of the taxa on which the biostratigraphic analysis are based, are included on Appendix I, Plate VII.
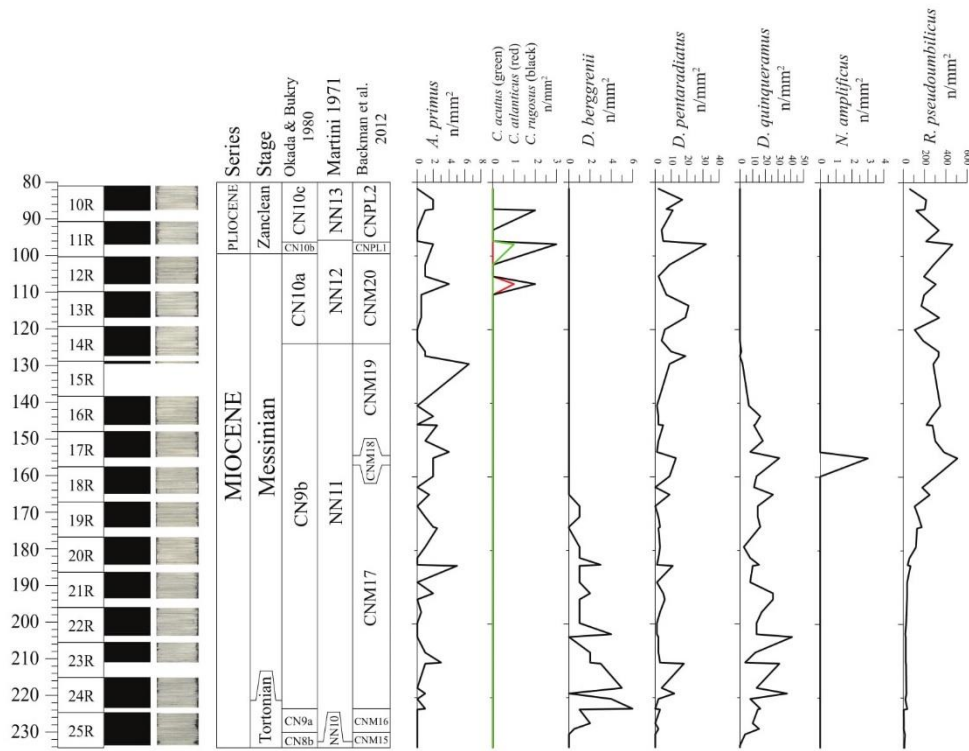
Fig. 5.1 Number of specimens of selected taxa in a specific area (n/mm2). On the left depth (CSF-A), Core, Recovery and the images of the study cores. Calcareous nannofossil biozonations (Martini, 1971; Okada and Bukry, 1980; Backman et al., 2012) and chronostratigraphy are also reported.
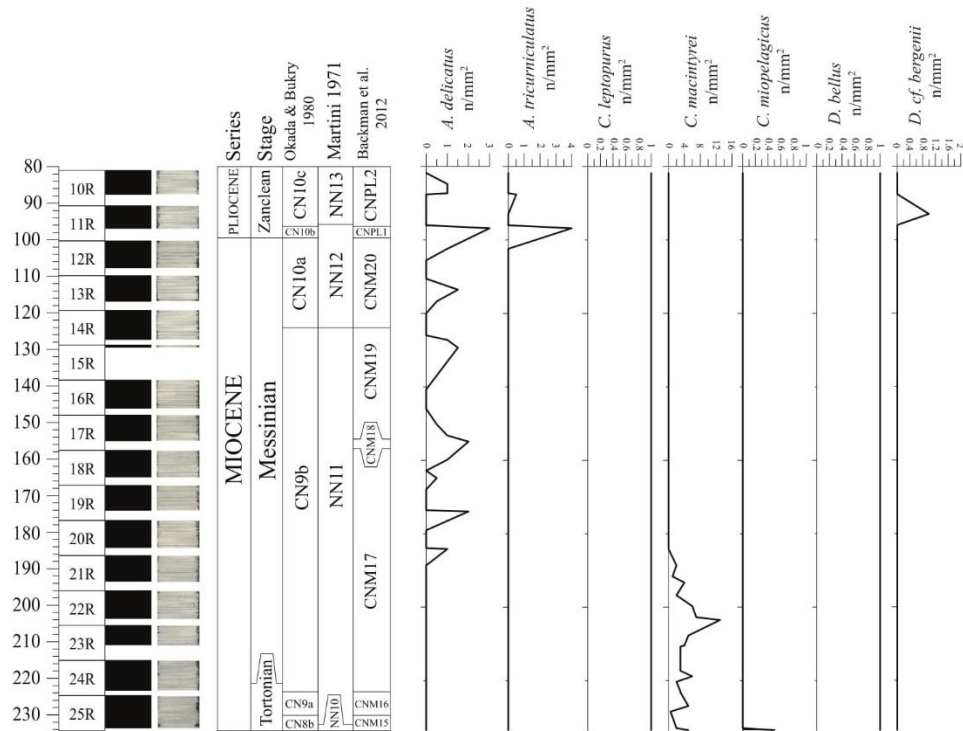
Fig. 5.2 Number of specimens of selected taxa in a specific area (n/mm2). On the left depth (CSF-A), Core, Recovery and the images of the study cores. Calcareous nannofossil biozonations (Martini, 1971; Okada and Bukry, 1980; Backman et al., 2012) and chronostratigraphy are also reported.

Base *Discoaster quinqueramus* (base Zone NN11)

The appearance of *D. quinqueramus* marks the base of Zone NN11 of Martini (1971). In this study, this event occurs slightly before the appearance of *D. berggrenii* that marks the base of Zone CN9a (Okada and Bukry, 1980) and CNM16 (Backman et al., 2012). Site U1506, the base of *D. quinqueramus* is neat and occurs between sample U1506A-25R-6W, 75 cm and sample U1506A-25R-4W, 75 cm at 231.45 m (± 1.5 m) (Fig. 5.1). The pattern of this taxon is continuous and common with abundances fluctuating between 10 and 40 specimens for mm^2. The estimated age for this biohorizon is 8.11 Ma (Backman et al., 2012).

Base *Discoaster berggrenii* (base Subzone CN9a and Zone CNM16)

The appearance of *D. berggrenii* marks the base of Subzone CNM9a of Okada and Bukry (1980) and of Zone CNM16 of Backman et al. (2012). Raffi et al. (1998) proposed that both *D. quinqueramus* and *D. berggrenii* originated from *Discoaster bellus*, its simple structure evolved toward more ornamented morphotypes such *as D. berggrenii* and *D. quinqueramus*. The development of this lineage is gradual and thus characterized by the presence of intermediate forms, which makes sometime difficult to precisely determinate the first appearance of *D. berggrenii* and the degree of synchrony/diachrony of this event in different areas (see discussion in Backman and Raffi, 1997 for details). In this study *D. berggrenii* appears slightly after *D. quinqueramus* between sample U1506A-25R-4W, 75 cm and U1506A-25R-3W, 75 cm at 229.20 m (± 0.75 m) (Fig. 5.1). Backman et al. (2012) provided an age of 8.29 Ma, very similar to that of *D. quinqueramus*, however the relatively low resolution of these datums could, at least partially, account for this discrepancy. The abundance of this taxon is rare and ranges between 1 and 6 specimens for mm^2.

Base *Amaurolithus primus* (base Subzone CN9b and Zone CNM17)

The base of *A. primus*, which coincides with the base of the genus, marks the base of Subzone CN9b of Okada and Bukry (1980) and the base of Zone CNM17 of Backman et al. (2012). At Site U1506, this event is positioned between sample U1506A-24R-CC, 5 cm and sample IODP-U1506A-24R-6W, 37 cm at 223.10 m (± 0.13 m) (Fig. 5.1). The abundance of this taxon is rare to very rare and fluctuates between 0 and 6.5 specimens for mm^2.

Because of the low and sporadic abundance of this taxon, counts were performed on 2 mm^2 and then normalized to 1 mm^2. The age of this biohorizon is 7.42 Ma (Backman et al., 2012).

Top *Discoaster quinqueramus* (base Zone NN12, Subzone CNM10a and Zone CNM20)

The disappearance of *D. quinqueramus* marks the base of Zone NN11 (Martini, 1971), Subzone CNM10a (Okada and Bukry, 1980) and Zone CNM20 (Backman et al., 2012). At Site U1506, this is clear and neat and occurs between sample U1506-14R-5W, 70 cm and U1506-14R-3W, 71 cm at 124.50 m (± 1.5 m) (Fig. 5.1). The estimated age of this taxon is 5.59 Ma (Backman et al., 2012).

Base *Ceratolithus acutus* (base Subzone CN10b and Zone CNPL1)

The appearance of *C. acutus* marks the base of Subzone CN10b (Okada and Bukry, 1980) and Zone CNPL1 (Backman et al., 2012). The Miocene–Pliocene boundary at 5.333 Ma (GTS2012) falls shortly (ca. 20 ka) after the onset of the base of Zone CNPL1 (5.35 Ma). *Ceratolithus acutus* is characterized by a short stratigraphic range, and disappeared in the lowermost Pliocene, at 5.04 Ma (Backman et al., 2012). During the counts performed in this thesis, no specimens of this taxon were encountered, however IODP Exp. 371 shipboard data reported the presence of a single specimen in sample U1506A-11R-CC, 5 cm. At Site U1506 the abundance pattern of this taxon is thus highly unreliable, however the position of this event was tentatively placed at 99.59 m (± 2.79 m) (Fig.5.1).

Top *Ceratolithus acutus* (base Subzone CN10c and Zone CNPL2)

The disappearance of *C. acutus* marks the base of Subzone CN10c of Okada and Bukry (1980) and of Zone CNPL2 of Backman et al. (2012). The single specimens recognized in the entire succession does not allowed for a precise positioning of this taxon. Nevertheless, the depth for this event is 96.40 m (± 0.41 m), which is the midpoint between sample U1506A-11R-CC, 5 cm and U1506A-11R-4W, 75 cm (Fig.5.1). The age of this taxon recalibrated to GTS2012 is 5.04 Ma (Backman et al., 2012).

5.1.2. Additional biohorizons

Recently Backman et al. (2012) revised the Miocene through Pleistocene biozonations proposed by Martini (1971), and Okada and Bukry (1980), substituted those biohorizons that have proven to be poorly reliable and added some new biohorizons to increase the resolution of the previous biozonations.

In the following, these events are described and commented (Fig. 5.1 and 5.2).

Base absence of *Reticulofenestra pseudoumbilicus* (Base Zone CNM15)

The Ba of *R. pseudoumbilicus* defines the base of Zone CNM15 (Backman et al., 2012). At Site 1506, the abundance of *R. pseudoumbilicus* is very low in the basal part of the succession up to 186.41 m ($\pm$ 2.25 m) when this taxon suddenly increases in abundance (Fig.5.1). This abundance pattern suggests that the lower part of the section belongs to Zone CNM15 because of the simultaneous low abundance (paracme interval) of *R. pseudoumbilicus* and the absence of *D. berggrenii*.

Top absence of *Reticulofenestra pseudoumbilicus*

The Top absence of *R. pseudoumbilicus* marks the end of the para-acme interval of this taxon. This biohorizon is not used by any of the biozonation adopted in this thesis but is reported to occur within Zone CNM17 with an estimated age of 7.09 Ma (Backman et al., 2012). The para-acme interval of *R. pseudoumbilicus* during the Messinian (late Miocene) has been observed in the equatorial Indian Ocean by Rio et al. (1990) and in the equatorial Pacific Ocean by Takayama (1993) and Raffi and Flores (1995). At Site U1506, *R. pseudoumbilicus* shows a low abundances in the lower part of the studied interval with values on average around 20-30 specimen for mm^2. The end of the para-acme event is located between sample U1506A-21R-2W, 75 cm and sample U1506-20R-CC, 5 cm at 186.41 m ($\pm$ 2.25 m) where the abundance of *R. pseudoumbilicus* starts to increase significantly up to reach values around 200-400 specimens for mm^2 (Fig. 5.1).

Base _Nickilithus amplificus_ (base Zone CNM18)

The appearance of _N. amplificus_ defines the base of Zone CNM18 (Backman et al., 2012), this zone corresponds to the middle part of Subzone CN9b of Okada and Bukry (1980) and to an interval in the upper part of Zone NN11 of Martini (1971). The restricted range of _N. amplificus_ within the upper part of NN11 reported by Bergen (1984) is confirmed by Rio et al. (1990), and is proven to be a useful event. Raffi et al. (1995) and Backman and Raffi (1997) proved that he first appearance of this taxon is a reliable biostratigraphic event in the low-latitude oceanic environment and appear to be isochronous among the equatorial Indian, Pacific and Atlantic oceans. At Site U1506, this taxon is very rare and only one specimen of _N. amplificus_ has been observed throughout the studied section in sample U1506A-17R-CC, 5 cm. We very tentatively define the base of Zone CNM18 between sample U1506A-18R-2W, 75 cm and sample U1506A-17R-CC, 5 cm though the scarcity of this taxon suggests that the position of this taxon is more a minimum estimate that a real datum (Fig. 5.1). The estimated age of this species is 6.91 Ma (Backman et al., 2012).

Top _Nickilithus amplificus_ (base Zone CNM19)

The disappearance of _N. amplificus_ defines the base of Zone CNM19 of Backman et al. (2012). Because of the single specimen of _N. amplificus_ observed at Site U1506, the placement of Top of this taxon is highly tentative and is considered a minimum estimate for this biohorizon at 154.09 m ($\pm$ 0.83 m) (Fig. 5.1). The age of this bioevent is estimated of 5.94 Ma (Backman et al., 2012).

Base _Ceratolithus atlanticus_

The appearance of _C. atlanticus_ does not define the base of any biozone, however this species is characterized by a short stratigraphic range spanning the Miocene/Pliocene boundary and its appearance has an estimated age of 5.35 Ma (Backman et al., 2012). The use of this biohorizon could in principle implement the resolution of our age model, nevertheless its scarcity, only one specimens found in sample U1506A-12R-CC, 5 cm during counts on board IODP Exp. 371, suggests caution in using this datum (Fig. 5.1).

5.1.3. Biostratigraphic classification of the study succession at Site U1506

The studied section spans from the late Miocene to the early Pliocene.

The simultaneous absence of *D. hamatus* and of *D. quinqueramus* at the lower portion of the section indicates that the base of the section belongs to Zone NN10, while the absence of *D. quinqueramus* and the absence of *C. acutus* in the uppermost samples indicate that the top of the section lies with Zone NN13 (Martini, 1971). Therefore, the study section spans Zone NN10 to Zone NN13. The simultaneous absence of *D. berggrenii* and *D. neorectus* in the basalmost sample suggests that this part of the section belongs to Subzone CN8b, whereas the absence of *C. acutus* in the upmost investigated sample indicate Subzone CN10c (Okada and Bukry, 1980).

Finally, based on the absence of *R. pseudoumbilicus* and *D. berggrenii* in the first investigated sample, the base of the succession lies with Zone CNM15, while the absence of *C. acutus* and the presence of *A. primus* at the top of the section indicate that this portion belongs to Zone CNPL2 (Backman et al., 2012).

Event	Species	Biozone Okada and Bukry 1980	Biozone Martini 1971	Biozone Backman et al. 2012	Depth (CSF-A) base	Depth (CSF-A) top	Depth (CSF-A) midpoint	Depth err (m)	Samples base	Samples top	Age (Ma) Backman et al. 2012
T	*Ceratolithus acutus*	CN10c		CNPL2	96.80	95.99	96.39	0.41	U1506A-11R-CC, 05 cm	U1506A-11R-4W, 75 cm	5.04
B	*Ceratolithus acutus*	CN10b		CNPL1	102.37	96.80	99.59	2.79	U1506A-12R-2W, 57 cm	U1506A-11R-CC, 05 cm	5.33
B	*Ceratolithus atlanticus*				110.55	107.61	109.08	1.47	U1506A-13R-1R, 75 cm	U1506A-12R-CC, 05 cm	5.35
T	*Discoaster quinqueramus*	CN10a	NN12	CNM20	126.00	123.01	124.51	1.50	U1506A-14R-5W, 70 cm	U1506A-14R-3W, 71 cm	5.59
T	*Nickilithus amplificus*			CNM19	154.92	153.26	154.09	0.83	U1506A-17R-CC, 05 cm	U1506A-17R-4W, 76 cm	5.94
B	*Nickilithus amplificus*			CNM18	159.85	154.92	157.39	2.47	U1506A-18R-2W, 75 cm	U1506A-17R-CC, 05 cm	6.91
Ta	*R. pseudoumbilicus*				188.65	184.16	186.41	2.25	U1506A-21R-2W, 75 cm	U1506A-20R-CC, 05 cm	7.09
B	*Amaurolithus primus*	CN9b		CNM17	223.23	222.97	223.10	0.13	U1506A-24R-CC, 05 cm	U1506A-24R-6W, 37 cm	7.42
B	*Discoaster berggrenii*	CN9a		CNM16	229.95	228.45	229.20	0.75	U1506A-25R-4W, 75 cm	U1506A-25R-3W, 75 cm	8.29
B	*Discoaster quinqueramus*		NN11		232.95	229.95	231.45	1.50	U1506A-25R-6W, 75 cm	U1506A-25R-4W, 75 cm	8.11

Table 5.1 Biohorizons used to biostratigraphically classify the studied section. From the left to the right are reported: the type of event (T, B, Ta), the species and the biozones they define (Martini, 1971; Okada and Bukry, 1980; Backman et al., 2012), the samples and their depths and the age associated to each biohorizon (Backman et al., 2012).

5.1.4. Age model and sedimentation rates

The age model for Site U1506 was developed on board IODP Exp. 371 using biostratigraphic datums (i.e., calcareous nannofossils and planktic foraminifera) and polarity chrons (obtained only between 240 and 270 m) (Table 5.2).

The magnetostratigraphic signal obtained on board does not provide any useful information for the interval of interest so that our age model is based on calcareous nannofossili biostratigraphy and biochronology. (Sutherland et al., 2018; 2019).

Based on the biostratigraphic datums, the entire section recovered at Site U1506 covers an interval from 1.93 (Pleistocene) to 44.12 Ma (middle Eocene).

The original age model was implemented with data obtained from this study, each bioevent has been placed on the model, based on the age from the literature (x-axis) and the stratigraphic position (mid-point in CSF-A) within the studied section (y-axis). Data obtained from this study (Fig. 5.3, green triangles) do not show any significant variation from the age model of Sutherland et al. (2019), with which actually fits quite well. The bonus of this new age model is the higher resolution of the study section that in fact allows for an implementation of the proposed age model at least for the interval of interest (from Core 10 to Core 25).

The age model provided is constructed based on a number of tie points but below and above these constrains the sedimentation rate is assumed to remain constant and equal to the sedimentation rate of the last segment of the age model. Based on this assumption, we have extrapolated the age for the base, 8.45 Ma (233.50 m), and for the top, 4.53 Ma (81.75 m), of the investigated section. The inclinations of the curve allowed to calculate the linear sedimentation rates (LSRs) of the different segments of the investigated section (Fig. 5.3). The entire section of Site U1506 shows different LSRs and includes two stratigraphic intervals, the first one spans ca. 20 Ma and separates subunit Ib from subunit Ic, and the second one covers ca. 10 Ma and separates subunit Ia from subunit Ib. In the lower part of subunit Ia, between the late Serravallian and early Tortonian LSRs range between ca. 10 and 20 m/Myr, and they decrease to 5 m/Myr in the late Tortonian (Sutherland et al., 2019). Between late Tortonian and late Piacenzian, LSRs increase considerably and reach values of ca. 40 m/Myr.

The section investigated lies in this interval of increased LSRs from the late Miocene to the early Pliocene. These increased LSRs are likely related to an increase in productivity, which possibly accounts for an enhanced rate in the biogenic accumulation that correlated with the biogenic bloom (Dickens and Owen, 1999).

Marker event	Zone	Top core, section, interval (cm)	Bottom core, section, interval (cm)	Age (Ma)	Top depth CSF-A (m)	Bottom depth CSF-A (m)	Midpoint depth CSF-A (m)	± (m)
Calcareous nannofossils		371-U1506A-	371-U1506A-					
T *Discoaster brouweri*	NN19	1R-CC	3R-1, 75	1.93	2.12	14.35	8.24	6.12
T *Discoaster tamalis*		3R-CC	4R-CC	2.80	14.67	27.05	20.86	6.19
T *Sphenolithus moriformis*		6R-CC	7R-CC	3.54	48.07	51.80	49.94	1.86
T *Reticulofenestra pseudoumbilicus*	NN16	7R-CC	8R-1, 75	3.70	51.80	62.25	57.03	5.23
T *Amaurolithus primus*		9R-CC	10R-CC	4.50	77.51	84.75	81.13	3.62
B *Ceratolithus rugosus*	NN13	12R-CC	13R-CC	5.12	107.61	116.72	112.17	4.56
T *Discoaster quinqueramus*	NN12	15R-CC	16R-CC	5.59	129.34	146.01	137.68	8.33
B *Discoaster quinqueramus*		24R-3, 75	24R-CC	8.12	218.85	223.23	221.04	2.19
B *Discoaster hamatus*	NN9	25R-3, 75	25R-CC	10.55	228.45	233.50	230.98	2.53
B *Calcidiscus macintyrei*		28R-3, 75	28R-4, 75	13.36	257.25	258.75	258.00	0.75
T *Sphenolithus ciperoensis*	NN1	29R-2, 49	29R-2, 63	24.43	264.15	264.29	264.22	0.07
T *Chiasmolithus gigas*	NP15b	29R-2, 63	29R-2, 70	44.12	264.29	264.36	264.33	0.03
Planktonic foraminifers								
T *Globorotalia truncatulinoides*		3R-CC	4R-CC	1.93	14.76	27.16	20.96	6.20
T *Globoquadrina altispira*	PL5	5R-CC	6R-CC	3.47	32.70	48.14	40.42	7.72
T *Sphaeroidinellopsis seminulina*	PL4	6R-CC	7R-CC	3.59	48.14	51.80	49.97	1.83
T *Hirsutella margaritae*	PL3	7R-CC	8R-CC	3.85	51.80	68.08	59.94	8.14
T *Globoturborotalita nepenthes*	PL2	10R-CC	11R-CC	4.37	87.57	96.80	92.19	4.61
B *Globorotalia plesiotumida*	M14	24R-CC	25R-CC	8.58	223.23	233.50	228.37	5.13
T *Paragloborotalia siakensis*	M13a	24R-CC	25R-CC	10.46	223.23	233.50	228.37	5.13
T *Fohsella fohsi lobata*	M10	25R-CC	26R-CC	11.79	233.50	240.05	236.78	3.28
B *Fohsella robusta*		28R-2, 74–76	28R-4, 72–73	13.13	255.74	258.72	257.23	1.49
Tc *Globigerinoides primordius*		28R-2, 74–76	28R-4, 72–73	23.50	255.74	258.72	257.23	1.49

Table 5.2 Microfossil datums and chrons used to construct Site U1506 age model (Sutherland et al., 2018).

Fig. 5.3 Age model and sediment accumulation over time at IODP Hole U1506A. On the left: core recovery and images of cores. On the bottom: compacted LSR and total mass accumulation rate (MAR). Green triangles are new calcareous nannofossil data from this study (modified after Sutherland et al., 2018)

5.2. Benthic foraminifera

**General characteristics of benthic foraminiferal assemblages at IODP Site 1506**

The results of the benthic foraminiferal counts, showing the percentage of the 91 identified taxa across the studied interval, are included in supplementary material (see attached CD).

Benthic foraminiferal assemblages are strongly dominated by calcareous taxa (ca. 85 % through most of the section), and only one sample (U1506A-12R-1, 110-112 cm, 101.41 m) contains abundant (25 %) agglutinated taxa. Infaunal morphogroups clearly dominate over epifaunal ones, and their abundance fluctuates between 65 % and 85 %, with only one sample (U1506A-16R-3, 140-142 cm, 142.81 m) containing more than 40 % of epifaunal taxa, mainly *Osangularia culter*, *Planulina wuellestorfi, Gyroidina* spp. and *Anomalinoides* spp. (Fig. 5.5) The diversity of the assemblages (Fisher- α index) ranges between 20 and 33. It reaches the maximum values in the lowermost part of the studied interval and it gradually decreases upwards, with a positive peak between 105 and 130 m.

The Shannon-Weaver heterogeneity index H(S) ranges between 2.8 and 3.7. It reaches its maximum values in the lower part of the studied interval, at 161.86 and 184.07 m, and its minimum value it is reached in the upper part, at 95.05 m.

Multivariate analyses were based on a dataset of species with a relative abundance > 5 % in at least one sample. R-mode (species) hierarchical cluster analyses were performed to identify groups of species with similar distribution. The unweighted pair-group average algorithm (UPGMA) and the Pearson correlation, as similarity coefficient, were used.

Two clusters (A, B) and four subclusters (A1, A2, B1, and B2) of benthic foraminifera were identified in the R-mode cluster analysis (Fig 5.4). The relative abundance of each subcluster is plotted in Fig. 5.6, and the percentage of all the species within each subcluster is represented in Fig. 5.7, 5.8, 5.9a and 5.9b.
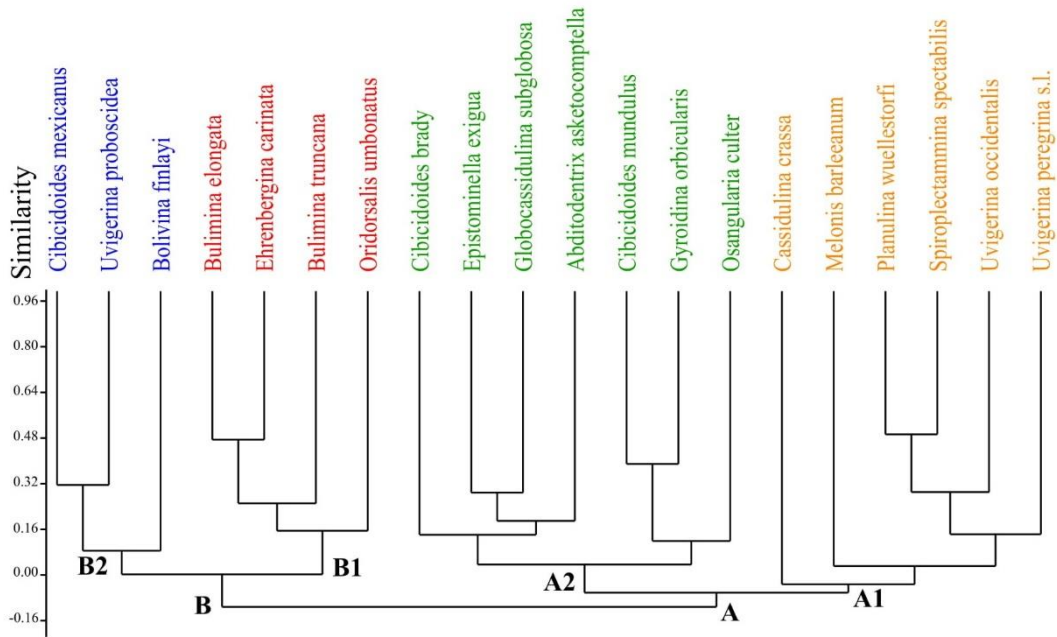
Fig. 5.4 Subdivision of the taxa into four subcluster based on R-mode cluster analysis.
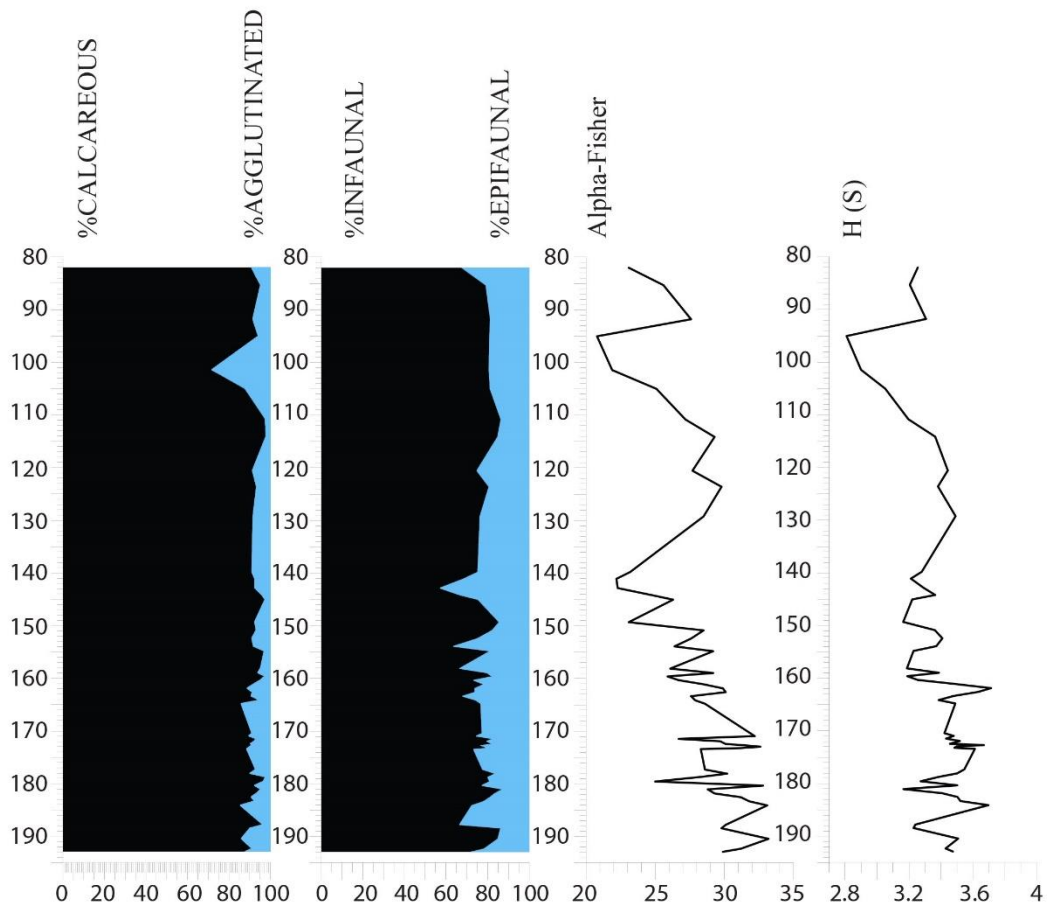
Fig. 5.5 Plot of the relative abundance of calcareous/agglutinated and infaunal/epifaunal taxa and plot of the alpha-Fisher and H(S) indices. Divesity and heterogeneity reach the maximum values in the lowermost part of the studied interval.
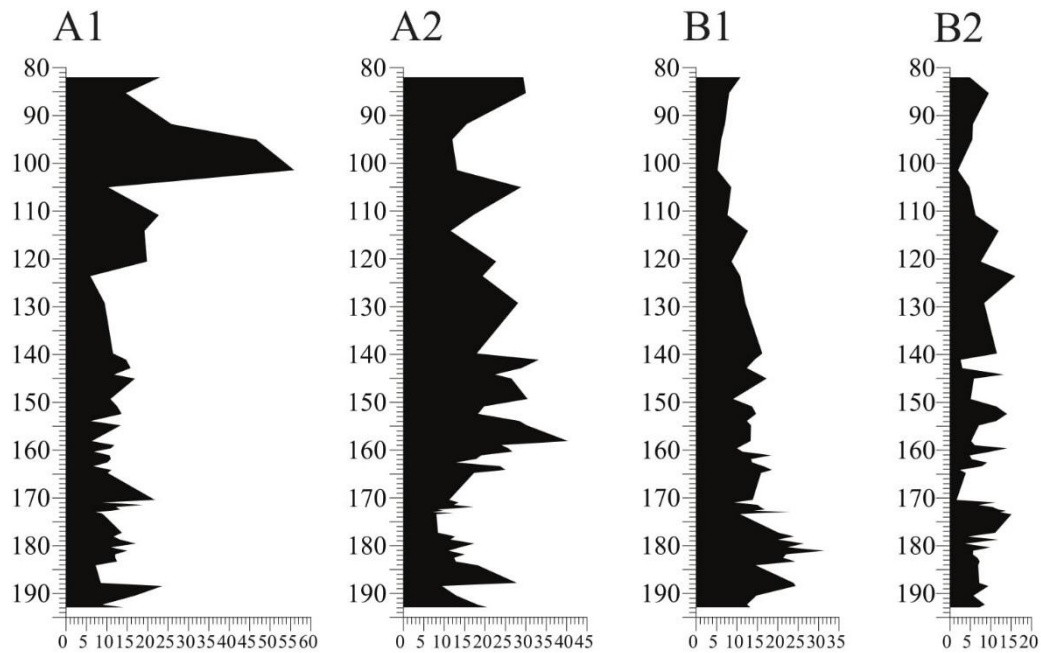
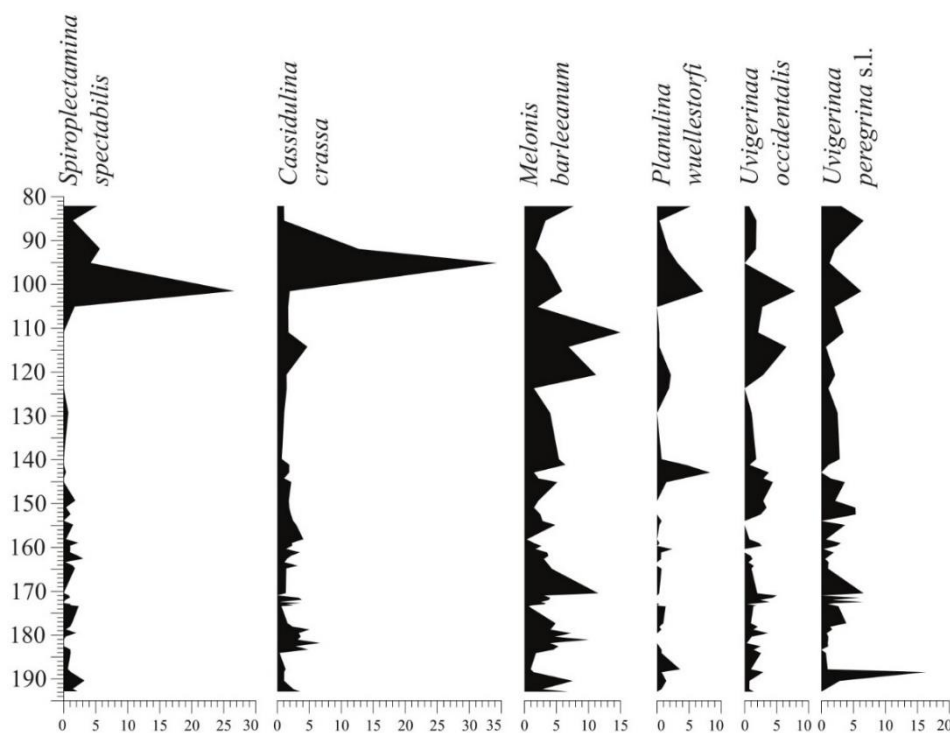**Fig. 5.6** Relative abundance of the four subclusters.

Cluster A includes more species than cluster B, and a similar percentage of infaunal and epifaunal species. Cluster B shows less species and is dominated by infaunal taxa (Fig. 5.6).

Subcluster A1 (Fig. 5.7) is dominated by infaunal species, and it contains only one epifaunal species, *Planulina wuellestorfi*. In the lower part, the abundance is relatively low, however there is a significant abundance peak in *U. peregrina* s.l. Near the middle of the section (ca. 143 m), there is a peak of *P. wuellestorfi* that coincides with a smaller decline in diversity. A1 is more abundant in the upper most part, this is related mostly to an abundance peak of both *Cassidulina crassa* (ca. 95 m) and *Spiroplectamina spectabilis* (ca. 101 m), although these two species reach their highest peaks in abundance at different levels. The peak of *C. crassa* seems to coincide with a drop in diversity, instead *S. spectabilis* peaks slightly earlier. The decline in diversity also coincides with a drop in *Uvigerina occidentalis* and *Uvigerina peregrina* s.l.

Subcluster A2 (Fig. 5.8) has the highest number of species and it is dominated by epifaunal foraminiferal taxa. Subcluster A2 is most abundant in the middle part, mainly related to the increase in *Epistominella exigua* and *Globocassidulina subglobosa*. The upper part of the studied interval shows a peak in *G. subglobosa* (ca. 105 m), followed by a decrease in abundance that coincides with a drop in diversity; in the upper most part (ca. from 95 m), the relative abundance of the subcluster increases again, the main contribution coming from *Cibicidoides mundulus*, *G. subglobosa* and *O. culter*.

Subcluster B1 (Fig. 5.9a) is composed of four infaunal taxa, and it is most abundant in the lower part of the studied interval, mainly due to the contribution of *Bulimina elongata*, *Bulimina truncana* and *Oridorsalis umbonatus*; the relative abundance decreases upwards.

Subcluster B2 (Fig. 5.9b) is represented by two infaunal species and an epifaunal one (i.e. *Cibicidoides mexicanus*). The abundance is relatively low throughout the section, and the most common species is *Uvigerina proboscidea*.

Fig 5.7 Relative abundance of benthic foraminifera of subcluster A1
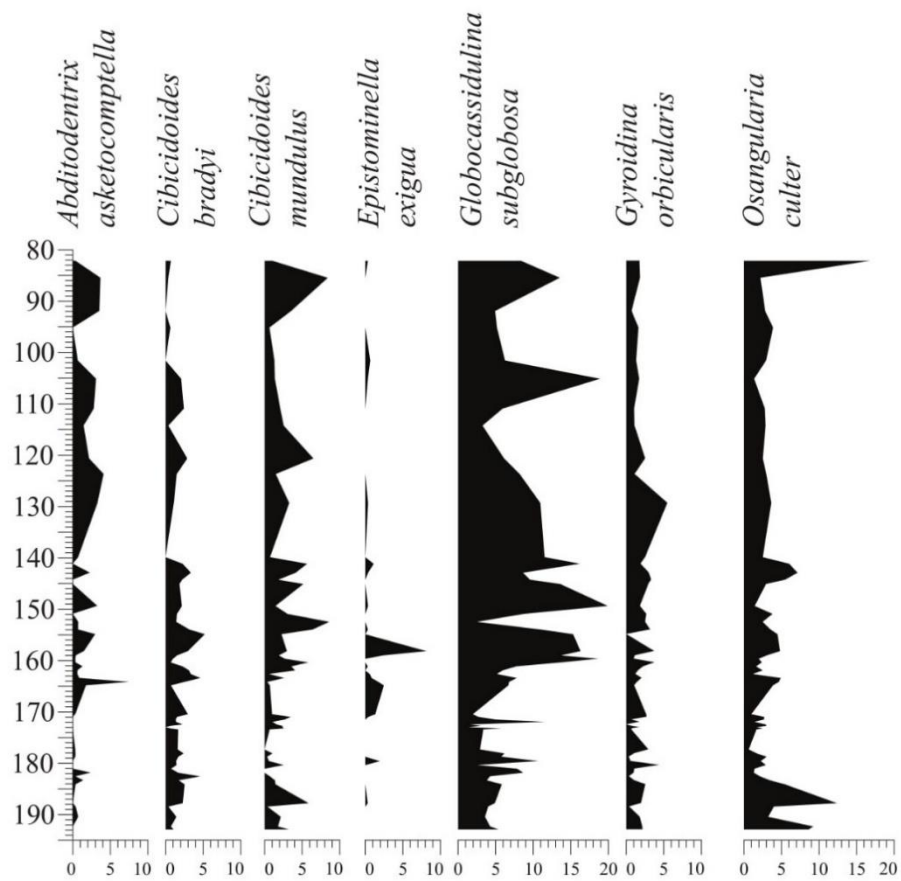
Fig. 5.8 Relative abundance of benthic foraminifera of subcluster A2
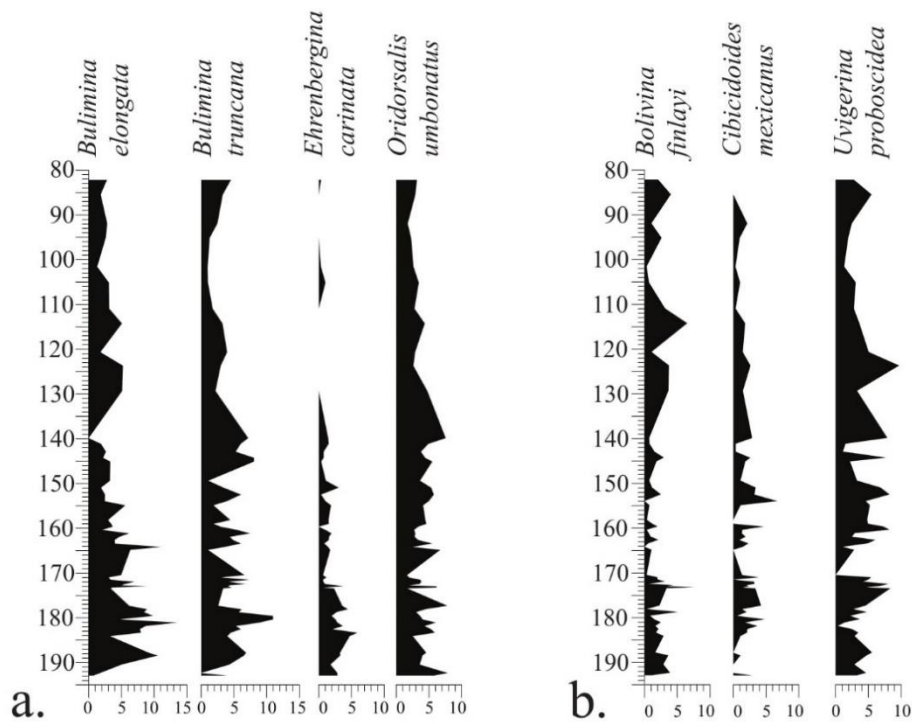
Fig. 5.9 Relative abundance of benthic foraminifera of subcluster B1 (a.) and B2 (b.)

5.2.1. Subdivision of the study section

Taking into account the benthic foraminiferal assemblages composition and diversity, and the distribution of the subclusters, three main intervals have been differentiated and are here described (Fig. 5.10).
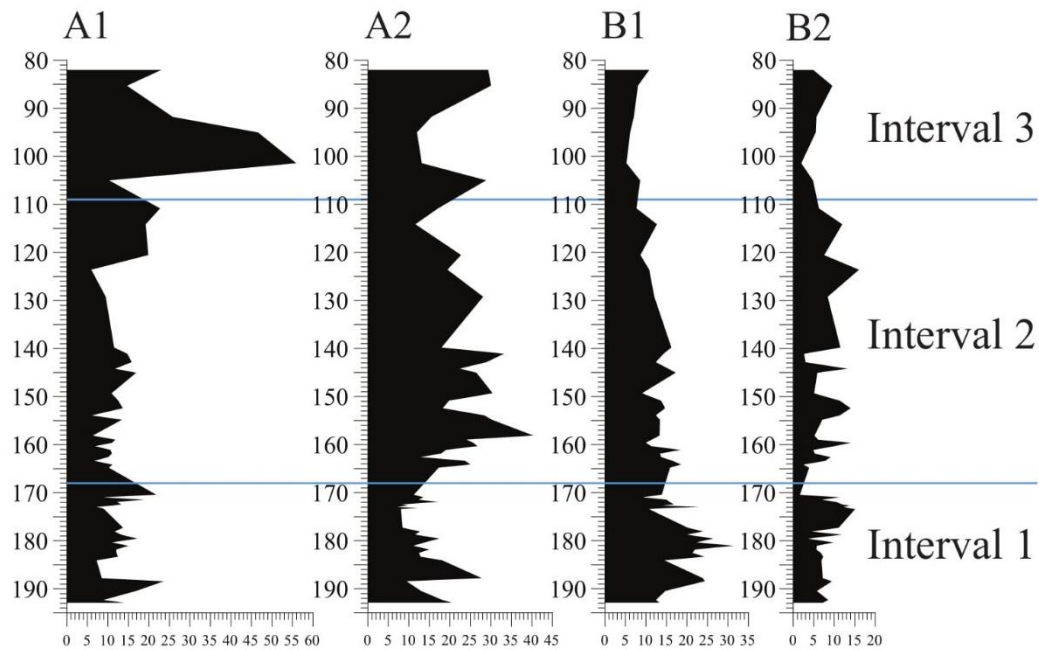
Fig. 5.10 The four subclusters of species subdivided into the three identified intervals.

The lower interval 1 (from 192.91 to 168 m) (Fig. 5.10) is characterized by a high abundance of subcluster B1, with a minor contribution from subcluster A2 (Fig. 5.8-5.9a)

In this part of the section, there is a high percentage of buliminids (up to 40 %, mainly *Bulimina truncana, Bulimina elongata* and *Bolivina finlayi*), a minor peak in *Osangularia culter* and moderate abundance of *Oridorsalis umbonatus*.

The presence of abundance peaks in buliminids may point to high productivity or low oxygenation (Hayward et al., 2010), probably the former since the diversity in this part of the section is high and this does not agree with a low oxygenation hypothesis. However, abundance peaks in *Uvigerina* and *Ehrenbergina* also characterize this interval (Fig. 5.7 and 5.9a-5.9b), and these two genera are usually associated with lowered oxygen content (Lohmann, 1978; Streeter and Shackleton, 1979; Schnitker, 1979; Douglas, 1981; Miller and Lohmann, 1982).

The species *U. peregrina* s.l. is a good proxy for increased productivity and is often associated with lowered oxygen content (Lohmann, 1978).

The presence of quantitative peaks in the relative abundance of both *Uvigerina* spp. and buliminids s.l. (Fig.5.11), inhabitants of present-day OMZs (Nomura, 1991; Hermelin, 1992) between 191.00 and 187.40 m, point to the presence of the biogenic bloom since an increase in paleo-productivity leads to increased carbonate dissolution and expansion of the OMZs (Dickens and Owen, 1994).

The middle interval 2 (from 168 to 109 m) (Fig. 5.10) is characterized by the dominance of subcluster A2 (mainly *Globocassidulina subglobosa*, with a contribution of *Epistominella exigua* and, in the lower part, a minor contribution of *Abditodentrix asketocomptella*). This interval does not show any uniform trends but fluctuations in the relative abundance of several species. The dominance of *O. umbonatus* and *G. subglobosa*, which are thought to be indicative of high oxygen, carbonate corrosive bottom environments (e.g., Murray, 1988; Mackensen et al., 1995; Hayward et al., 2004b), points to an increase in oxygen concentration.

One of the largest fluctuations in this interval coincides with a drop in the percentage of *G. subglobosa,* associated with an increase in the relative abundance of buliminids s.l. (*B. truncana, B. finlayi, U. peregrina s.l.,* and *Uvigerina proboscidea*) and *C. mundulus*. There is also a slight drop in diversity that seems to coincide with the peak in epifaunal species, however it is not a dramatic drop since the heterogeneity does not show significant changes.

The upper interval 3 (from 109 to 82.01 m) (Fig. 5.10) is dominated by subcluster A1, with a minor contribution of subcluster A2. Diversity is high in this interval but there is a minor drop in the upper most part (at ca. 95 m) that seems to be associated with a peak in abundance of *Cassidulina crassa*, a species that is reported to thrive in areas of sustained carbon flux (Mackensen et al., 1995; Smart, 2008). The drop in diversity also coincides with a significant decrease in the relative abundance of *Uvigerina* spp., buliminids s.l. and *Spiroplectamina spectabilis*. The decrease of buliminids and *Uvigerina* spp. may indicate good oxygenation and low supply of labile organic matter to the sea floor (this is characteristic of *Bulimina truncana* and *Uvigerina peregrina* s.l.; Hayward et al., 2010; Lohmann, 1978; Streeter and Shackleton, 1979; Schnitker, 1979; Douglas, 1981; Miller and Lohmann, 1982).

In the upper part, there is also a relatively small peak (ca. 25 %) in agglutinated foraminifera, mostly related to a peak of *Spiroplectamina spectabilis.*

Overall this interval is characterized by increases in taxa associated with increased oxygen concentration and decreased influx of organic matter, i.e. *C. crassa, O. culter, G. subglobosa, P. wuellestorfi, M. pompilioides* (Murray, 2009).

The occurrence of *Ehrenbergina glabra* only in this interval supports the interpretation of increased oxygen concentration (Hayward et al., 2010).
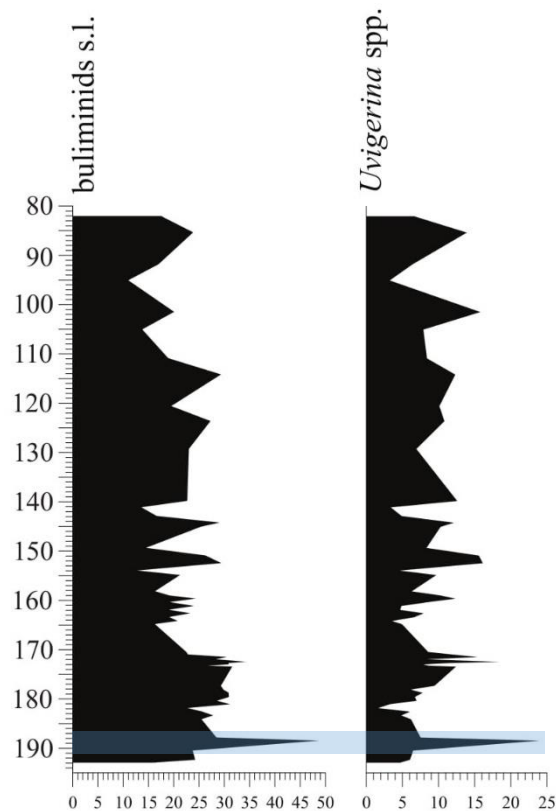
Fig. 5.11 Relative abundance of buliminids s.l. and *Uvigerina* spp., the blue band marks the peaks located in Interval 1, which are used to recognize the biogenic bloom.

5.2.2. DCA analysis

As an attempt to identify the environmental variables that may have controlled the distribution pattern of benthic foraminifera, a detrended correspondence analysis (DCA) in R-mode (species) and in Q-mode (samples) was performed on the same dataset (Fig. 5.12 and Fig. 5.13).

Q-mode (samples)

The DCA analysis in Q-mode (samples) is shows in Fig. 5.12, where sample depths in meters CSF-A have been used instead of the samples IDs (i.e. sample U1506A-10R-1, 100-102 cm corresponds to 82.01 m). Samples are clearly arranged in stratigraphic order in the DCA analysis, which supports the definition of the three intervals (1, 2 and 3) based on benthic foraminiferal assemblages. Outliers are marked in red.

Interval 1 (168 to 192.91 m) is located at low values along axis 1 and axis 2. This interval is characterized by the high relative abundances of taxa typical of high nutrient influx and low oxygen conditions, suggesting high productivity conditions. Interval 2 (from 168 to 109 m) is located at low values along axis 1 and high values along axis 2. This interval is defined by presence of taxa typical of high oxygen and low nutrient conditions, and characterizes a low productivity environment. Lastly, Interval 3 (from 109 to 82.01 m) is located at high values along axis 1. It is similar to the Interval 2 and is characterised by taxa typical of oxic and oligotrophic environments.

Based on this subdivision and on the characteristics of each sample, we suggest that axis 2 is mainly controlled by productivity, which is higher at low values and progressively decreases at higher values. Interpretation of axis 1 is not straightforward though, and further work on geochemical proxies might throw some light into its paleoenvironmental interpretation.
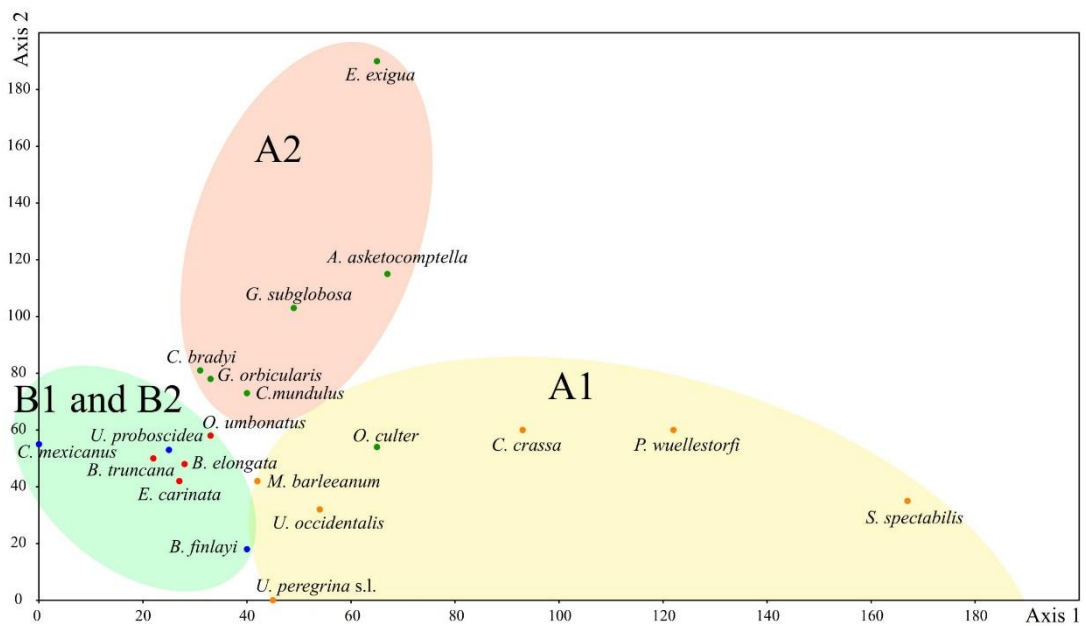
R-mode (species)

The R-mode DCA analysis was made using species with a relative abundance > 5 % in at least one sample (Fig. 5.13). Species from subclusters B1 and B2, including *Bulimina elongata, Bolivina finlayi* and *Ehrenbergina carinata* are located at lower values along axis 1.

These species are typical of eutrophic environments and suggest a high nutrient supply to the seafloor. Subcluster A1 dominates at high values along axis 1, with species that are common in oligotrophic environments (*O. culter*, *C. crassa* and *P. wuellestorfi*). The only exception is *S. spectabilis*, typical of increased carbon flux, but also known as an opportunistic species, e.g. occurring just above the Cretaceous/ Paleogene boundary at ODP Site 959 in the equatorial Atlantic (Kuhnt et al., 1998) and at Gubbio, Italy (Kuhnt and Kaminski, 1996). Species from subclusters B1 and B2 occur at lower values along axis 2 (*B. finlayi, B. elongata* and *E. carinata*), and are typical of environments with low oxygen concentration. Subcluster A2 dominates at high values along axis 2, with species that are related to environments with high oxygen concentration (*E. exigua* and *G. subglobosa*).

Axis 1 has been interpreted as controlled by nutrient supply, with eutrophic conditions at low values and oligotrophic conditions at high values. Axis 1 is not related to oxygen concentration because *C. mexicanus,* which has big pores and is typical of oxic environments, is located at low values among the suboxic-dysoxic species. Axis 2 is probably related to changes in bottom-water oxygenation, at high values the oxygen concentration is high, and it decreased towards low values along axis 2. This interpretation agrees with the one made for the three intervals: Interval 1 is characterized by species associated with low oxygenation and high carbon influx and is dominated by subcluster B1, this is consistent with the interpretation since in the R-mode DCA graph this subcluster is placed in the low oxygenation-high food supply sector. Interval 2 is more difficult to interpret since it shows fluctuations, however it seems to be characterized by an increase in oxygen concentration and by the dominance of subcluster A2; once again the interpretation is consistent because in the DCA, subcluster A2 is found in a sector characterized by high oxygenation. Lastly, Interval 3 is defined by high oxygen concentration and low nutrient supply. This interpretation fits with the DCA plot, since this interval is dominated by subcluster A1, characterized by taxa typical of oxic and oligotrophic environments.
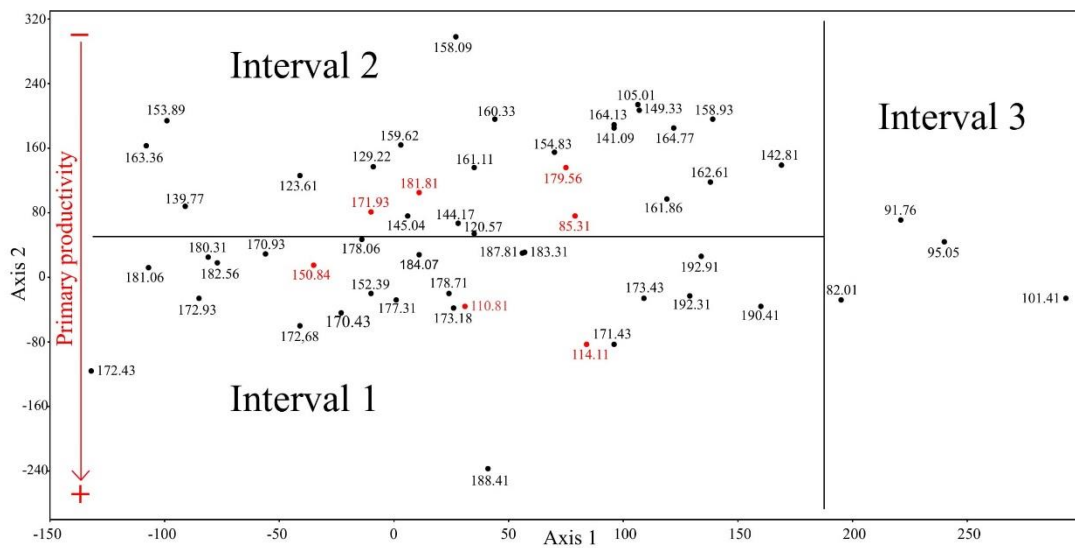
Fig. 5.12 Q-mode (samples): the graph shows all the analysed samples and their subdivision into the three intervals based on statistical analysis. Outliers are marked in red. Interval 1 is characterized taxa typical of high nutrient influx and low oxygen conditions, suggesting high productivity conditions. Interval 2 and 3 are defined by taxa typical of low productivity environment. Based on this we suggest that axis 2 is mainly controlled by productivity

Fig. 5.13 R-mode (species): the graph shows the subdivision of the species into the four subclusters based on ecological parameters. Subcluster A1 dominates at high values along axis 1, with species that are common in oligotrophic environments; subcluster A2 dominates at high values along axis 2, with species that are related to environments with high oxygen concentration; meanwhile, species from subclusters B1 and B2 occur at lower values along axis 2 and are typical of environments with low oxygen concentration.

5.2.3. Paleoenvironmental conditions

As reported in § 5.2.1., the studied succession has been divided into three main intervals based on the benthic foraminiferal assemblages composition and statistical analysis (Q-mode). The integrated age model has allowed us to put the three intervals into a chronological framework: Interval 1 spans from ca. 7.28 to 6.50 Ma, Interval 2 from ca. 6.50 to 5.07 Ma, and Interval 3 from ca. 5.07 to 4.61 Ma.

Interval 1 shows the most interesting and promising features, which fits the expected conditions during the biogenic bloom. The paleo-ecological analysis points to eutrophic conditions at the seafloor and low oxygen concentration of bottom waters, and the Fisher- α index shows that diversity is higher compared to the other intervals. All these characteristics are typical of high productivity environments and suggest that this interval coincides with the biogenic bloom. This interpretation is supported by the DCA analysis, where Interval 1 is dominated by subcluster B1, which lies in the low oxygenation-high food supply area (Fig. 5.13). Furthermore, high paleo-productivity leads to increased carbonate dissolution and expansion of the OMZs (Dickens and Owen, 1994). Between 191.00 and 187.40 m peaks in relative abundance of *Uvigerina* spp. and buliminids has been observed and is indicative of low oxygen levels because, these taxa thrive in present-day OMZs (Nomura, 1991; Hermelin, 1992) and are thus ancillary evidences for the biogenic bloom (Fig. 5.11).

Based on this interpretation, the biogenic bloom at IODP Site U1506 is located between 192.91 and 168.00 m, and spans from ca. 7.28 to 6.50 Ma, a duration that is significantly shorter than the one previously suggested in the literature.

When stable carbon isotope will become available for this succession, a direct comparison between benthic foraminiferal data and $\delta^{13}C$ will confirm, in case of a synchronous timing, or disregard, in case of an offset, this hypothesis.

6. CONCLUSIONS

Calcareous nannofossil and benthic foraminiferal assemblages were investigated at IODP Site U1506, on one hand, calcareous nannofossil provide a biostratigraphic classification of the section as well as an implemented age model. On the other hand, benthic foraminiferal data has allowed to reconstruct the paleoenvironmental conditions at the sea floor.

The biostratigraphic analyses frame the succession within the standard biozonations, according to which the study section extends from Zone NN10 to Zone NN13 (Martini, 1971), and from Subzone CN8b to Subzone CN10c (Okada and Bukry, 1980). Based on the additional biozonation of Backman et al. (2012) the section comprises an interval between Zone CNM15 to Zone CNPL2. From the chronostratigraphic point of view, the analysed section spans from the Tortonian (late Miocene) to the Zanclean (early Pliocene).

The implementation of the age model, originally proposed by Sutherland et al. (2018), has allowed to date the base (8.45 Ma) and the top (4.53 Ma) of the section as well as to calculate the sedimentation rates along the section, which pointed to values up to ca. 40 m/Myr in the investigated section during the biogenic bloom.

The studied succession has been divided into three main intervals based on benthic foraminiferal quantitative data and statistical analyses. Interval 1 has a slightly higher diversity if compared with Intervals 2 and 3.

In addition, paleo-ecological affinity of benthic foraminiferal taxa present in the assemblages suggests a high nutrient supply to the seafloor and a relatively low oxygen concentration of bottom waters during Interval 1. These features depict a high productivity environmental conditions that well fit with the biogenic bloom.

Moreover, the DCA analysis is coherent with this interpretation since Interval 1 is characterized by the dominance of subcluster B1, which is placed in the low oxygenation-high food supply area. Furthermore, the abundance peaks in the relative abundance of *Uvigerina* spp. and buliminids, inhabitants of present-day OMZs (Nomura, 1991; Hermelin, 1992), between 191.00 and 187.40 m CSF-A, support an increase in paleo-productivity leading to increased carbonate dissolution and expansion of the OMZs (Dickens and Owen, 1994), which also indicate a biogenic bloom phase.

In conclusion, our data indicate that the biogenic bloom is recognizable at Site U1506 between 192.91 and 168.00 m (7.28 to 6.50 Ma) based on the changes in the benthic foraminiferal assemblages. However, to better comprehend this event further analyses are required such as additional investigation on benthic foraminiferal assemblages below 192.91 m, quantitative study on calcareous plankton microfossil, redox analyses, and last but not least, a high resolution oxygen and carbon stable isotope study. These would further constrain the position of the biogenic bloom and help in better understanding the dynamics and the processes involved during the biogenic bloom.

REFERENCES

Agnini, C., Fornaciari, E., Raffi, I., Catanzariti, R., Pälike, H., Backman, J., Rio, D., 2014. *Biozonation and biochronology of Paleogene calcareous nannofossils from low to middle latitudes*. Newsletters on Stratigraphy, vol. 47 (2), pp.131-181.

Arnold, E., Leinen, M., King, J., 1995. *Paleoenvironmental variation based on the mineralogy and rock-magnetic properties of sediment from sites 885 and 886*. Proc. ODP, Sci. Results 145, 231–245.

Arreguín-Rodríguez, G. J., Alegret, L., Thomas, E., 2016. *Late Paleocene – middle Eocene benthic foraminifera on a Pacific Seamount (Allison Guyot, ODP Site 865): Greenhouse Climate and superimposed hyperthermal events*. Paleoceanography and Paleoclimatology, doi:10.1002/2015PA002837.

Backman, J., Raffi, I., 1997. *Calibration of Miocene nannofossil events to orbitally tuned cyclostratigraphies from Ceara Rise*. Proc. ODP Sci. Results 154, 83–99.

Backman, J., Raffi, I., Rio, D., Fornaciari, E., & Pälike, H., 2012. *Biozonation and biochronology of Miocene through Pleistocene calcareous nannofossils from low and middle latitudes.* Newsletters on Stratigraphy, 45(3), 221–244. doi:10.1127/0078-0421/2012/0022.

Berger, W.H., Leckie, R.M., Janecek, T.R., Stax, R., Takayama, T., 1993. *Neogene carbonate sedimentation on Ontong Java Plateau: highlights and open questions.* Proc. ODP, Sci. Results 130, 711–744.

Berger, W.H., Stax, R., 1994. *Neogene carbonate stratigraphy of Ontong Java Plateau (Western Equatorial Pacific): three unexpected findings.* Terra Nova 6, 520–534.

Berggren, W.A., and J.A. Van Couvering. 1978. *Biochronology.* In G.V. Cohee, M.F. Glaessner, and H.D. Hedberg (editors), Contributions to the geologic time scale: 39–55. Tulsa, OK: American Association of Petroleum Geologists.

Berggren, W.A., Miller, K.G., 1989. *Cenozoic bathyal and abyssal calcareous benthic foraminiferal zonation.* Micropaleontology 35, 308^320.

Berggren, W.A., Kent, D.V., Swisher, C.C.III, Aubry, M.-P., 1995. *A revised Cenozoic geochronology and chronostratigraphy*. In: Berggren, W.A., Kent, D.V., Aubry, M.-P., Hardenbol, J., Geochronology, time scales and global stratigraphic correlation: A unified temporal framework for an historical geology. Spec. Publ. Soc. Econ. Paleontol. Mineral., 54, 29–212.

Bernhard, J.M., 1986. *Characteristic assemblages and morphologies of benthic foraminifera from anoxic, organic-rich deposits: Jurassic through Holocene*. J. Foraminifer. Res. 16, 207-215.

Bijl, P.K., Schouten, S., Sluijs, A., Reichart, G.J., Zachos, J.C., and Brinkhuis, H., 2009. *Early Paleogene temperature evolution of the southwest Pacific Ocean*. Nature, 461 (7265):776-779. doi:10.1038/nature08399.

Brady, H. B. (1884). *Report on the Foraminifera dredged by H.M.S. Challenger during the Years 1873-1876. Report on the Scientific Results of the Voyage of H.M.S. Challenger during the years 1873–76.* Zoology. 9 (part 22): i-xxi, 1-814; pl. 1-115., available online at http://www.19thcenturyscience.org/HMSC/HMSC-Reports/Zool-22/htm/doc.html

Brewer, P. G., 1990. *Productivity of the Ocean. Present and Past.* W. H. Berger, V. S. Smetacek, and G. Wefer, Eds. Wiley-Interscience, New York, 1989. Xviii, 470 pp., illus. $146. Life Sciences Research Reports, vol. 44. From a workshop, Berlin, F.R.G., April 1988. Science, 247(4944), 865–865. doi:10.1126/science.247.4944.865.

Broecker, W.S., Peng, T. H., 1982. *Tracers in the Sea*. Eldigio Press, Palisades, NY

Brummer, G.J.A., Van Eijden, A.J.M., 1992. *''Blue-ocean'' paleoproductivity estimates from pelagic carbonate mass accumulation rates*. Mar. Micropaleontol. 19, 99–117.

Corliss, B.H., 1985. *Microhabitats of benthic foraminifera within deep-sea sediments*. Nature 314, 435-438.

Corliss, B.H., Chen, C., 1988. *Morphotype patterns of Norwegian Sea deep-sea benthic foraminifera and ecological implications*. Geology 16, 716-719.

Corliss, B.H., 1991. *Morphology and microhabitat preferences of benthic foraminifera from the northeast Atlantic Ocean*. Mar. Micropalontol. 17, 195-236.

Coxall, H.K., Pearson, P.N., 2007. T*he Eocene-Oligocene transition.* Williams, Mark, Haywood, A. M., Gregory, J. and Schmidt, D. N. (Eds). Deep-Time Perspectives on Climate Change: Marrying the Signal from Computer Models and Biological Proxies, Micropaleontology Society Special Publication, London, Geological Society, pp. 351-387.

Delaney, M.L., Filippelli, G.M., 1994. *An apparent contradiction in the role of phosphorus in Cenozoic chemical mass balances for the world ocean.* Paleoceanography 9, 513-527.

Dickens, G.R., Owen, R.M., 1994. *Late Miocene–Early Pliocene manganese redirection in the central Indian Ocean: expansion of the intermediate water oxygen minimum zone.* Paleoceanography 9, 169–181.

Dickens, G.R., Owen, R.M., 1996. *Sediment geochemical eviŽ. dence for an Early–Middle Gilbert Early Pliocene productivity peak in the North Pacific Red Clay Province*. Marine Micropaleontol. 27, 107–120.

Dickens, G. R., Owen, R. M., 1999. *The Latest Miocene-Early Pliocene biogenic bloom: a revised Indian Ocean perspective.* Marine Geology 161 (1999) 75-91.

Dobson, D.M., Dickens, G.R., Rea, D.K., 1997. *Terrigenous sedimentation at Ceara Rise.* Proc. ODP, Sci. Results 154, 465–473.

Douglas, P.M.J., Affek, H.P., Ivany, L.C., Houben, A.J.P., Sijp, W.P., Sluijs, A., Schouten, S., and Pagani, M., 2014. *Pronounced zonal heterogeneity in Eocene southern high-latitude sea surface temperatures.* Proceedings of the National Academy of Science of the United States of America, 111(18):6582-6587. doi:10.1073/pnas.1321441111.

Eade, J. V., 1967. *New Zealand recent Foraminifera of the families Islandiellidae and Cassidulinidae.* New Zealand Journal of Marine and Freshwater Research, 1:4, 421-454, doi:10.1080/00288330.1967.9515217.

Falkowski, P.G., Katz, M.E., Knoll, A.K., Quigg, A., Raven, J.A., Schofield, O. & Taylor, F.J.R. 2004. *The evolution of modern eukaryotic phytoplankton*. Science 305, 354–360.

Farrell, J.W., Janecek, T.R., 1991. *Late Neogene paleoceanography and paleoclimatology of the northeast Indian Ocean site 758*. Proc. ODP, Sci. Results 121, 297–355.

Farrell, J.W., Ra, I., Janecek, T.R., Murray, D.W., Levitan, M., Delaney, M., Dadey, K.A., Emeis, K.-C., Lyle, M., Flores, J.-A., Hovan, S., 1995. *Late Neogene sedimentation patterns in the eastern equatorial Pacific*. Proc. ODP Sci. Res. 138, 717-756.

Filippelli, G.M., 1997. *Intensification of the Asian monsoon and a chemical weathering event in the Late Miocene–Early Pliocene: implications for Late Neogene climate change*. Geology 25, 27–30.

Fisher, R. A., Corbet, A. S., & Williams, C. B., 1943. *The Relation Between the Number of Species and the Number of Individuals in a Random Sample of an Animal Population*. The Journal of Animal Ecology, 12(1), 42. doi:10.2307/1411.

Fontanier, C., Jorissen, F.J., Licari, L., Alexandre, A., Anschutz, P., Carbonel, P., 2002. *Live benthic foraminiferal faunas from the Bay of Biscay: faunal density, composition and microhabitats.* Deep-Sea Res. I 49, 751-785.

Gooday, A.J., Turley, C.M., 1990. *Responses by benthic organisms to inputs of organic material to the ocean floor: a review.* Philos. Trans. R. Soc. Lond. 331, 119-138.

Gooday, A.J., 2003. *Benthic foraminifera (Protista) as tools in deep-water paleoceanography: a review of environmental influences on faunal characteristic.* Adv. Mar. Biol. 46, 1-90.

Gornitz V., 2008. *Encyclopedia of Paleoclimatology and Ancient Environments*.Springer Science & Business Media, Oct 31, 2008 – Science.

Grant, K. M., & Dickens, G. R., 2002. *Coupled productivity and carbon isotope records in the southwest Pacific Ocean during the late Miocene–early Pliocene biogenic bloom*. Palaeogeography, Palaeoclimatology, Palaeoecology, 187(1-2), 61–82. doi:10.1016/s0031-0182(02)00508-4.

Hammer, O., Harper, D.A.T., Ryan, P.D., 2001. *Past: paleontological statistics software package for education and data analysis.* Paleontologia Electronica.

Hays, J.D., Opdyke, N.D., 1967. *Antarctic radiolaria, magnetic reversals and climate changes*. Science 158, 1001–1011.

Hayward B. W., Buzas, M. A., 1979. *Taxonomy and Paleoecology of Early Miocene Benthic Foraminifera of Northern New Zealand and the North Tasman Sea.* Smithsonian Contributions to Paleontology, no. 36.

Hayward, B. W., Sabaa, A., & Grenfell, H. R., 2004. *Benthic foraminifera and the late Quaternary (last 150 ka) paleoceanographic and sedimentary history of the Bounty Trough, east of New Zealand.* Palaeogeography, Palaeoclimatology, Palaeoecology, 211(1-2), 59–93. doi:10.1016/j.palaeo.2004.04.007.

Hayward, B. W., Grenfell, H. R., Sabaa, A. T., Neil, H. L., Buzas, M.A., 2010. *Recent New Zealand deep-water benthic foraminifera: Taxonomy, ecology distribution, biogeography, and use in paleoenvironmental assessment.* GNS Science monograph 26

Hayward, B. W., Sabaa, A. T., Grenfell, H. R., Neil, H. L., Bostock, H., 2013. *Ecological distribution of recent deep-water foraminifera around New Zealand.* Journal of Foraminiferal Research, v. 43, no. 4, p. 415-442.

Hermelin, J. O. R., 1989. *Pliocene benthic foraminifera from the ontong-java plateau (western equatorial pacific ocean): faunal response to changing paleoenvironment.* Cushman Foundation for foraminiferal research, special publication no. 26.

Hermelin, J.O.R., 1992. *Variations in the benthic foraminiferal fauna of the Arabian Sea: a response to changes in upwelling intensity?* In: Summerhayes, C.P., Prell, W.L., Emeis, K.-C. Eds., Upwelling Systems: Evolution since the Early Miocene. Geol. Soc. Spec. Publ., London, 64, 151–166.

Hermoyian, C.S., Owen, R.M., 2001. *Late Miocene-early Pliocene biogenic bloom: Evidence from low-productivity regions of the Indian and Atlantic Oceans.* Paleoceanography 16, 95-100.

Hodell, D.A., Benson, R.H., Kent, D.V., Boersma, A., RacicEl Bied, K., 1994. *Magnetostratigraphic, biostratigraphic, and stable isotope stratigraphy of an upper Miocene drill core from the Sale Briqueterie (Northwestern Morocco): A high resolution chronology for the Messinian stage.* Paleoceanography 9, 835-855.

Holbourn, A., Henderson, A. S., MacLeod, N., 2013. *Atlas of Benthic Foraminifera.* Wiley-Blackwell, Natural History Museum.

Jones, R.W., Charnock, M.A., 1985. *'Morphogroups' of agglutinated foraminifera: Their life positions and feeding habits and potential applicability in (paleo)ecological studies.* Rev. Paleobiol. 4, 311-320.

Hollis, C. J., Handley, L., Crouch, E. M., Morgans, H. E. G., Baker, J. A., Creech, J., Collins, K.S., Gibbs, S.J., Huber, M., Schouten, S., Zachos, J.C.,and Pancost, R. D., 2009. *Tropical sea temperatures in the high-latitude South Pacific during the Eocene.* Geology, 37(2), 99–102. doi:10.1130/g25200a.1.

Hollis, C.J., Taylor, K.W.R., Handley, L., Pancost, R.D., Huber, M., Creech, J.B., Hines, B.R., Crouch, E.M., Morgans, H.E.G., Crampton, J.S., Gibbs, S., Pearson, P.N., and Zachos, J.C., 2012. *Early Paleogene temperature history of the Southwest Pacific Ocean: reconciling proxies and models.* Earth and Planetary Science Letters, 349-350:53-66. doi:10.1016/j.epsl.2012.06.024.

Jorissen, F.J., Stigter, H.C., Widmark, J.G.V., 1995. *A conceptual model explaining benthic foraminiferal microhabitats.* Mar. Micropaleontol. 26, 3-15.

Kaminski, M.A., Gradstein, F.M., 2005. *Atlas of Paleogene Cosmopolitan Deep-water Agglutinated Foraminifera*, ISBN – 83-912385-X, The Grzybowski Foundation.

Kennett, J.P., Von der Borch, C.C., 1986. *Southwest Pacific Cenozoic paleoceanography.* Initial Rep., DSDP 90, 1493– 1517.

Koizumi, I., 1986. *Pliocene and Pleistocene diatom levels related with paleoceanography in the Northwest Pacific.* Mar. Micropaleontol. 10, 309– 325.

Krijgsman, W., Hilgen, F.J., Raffi, I., Sierro, F.J., Wilson, D.S., 1999. *Chronology, causes and progression of the Messinian salinity crisis*. Nature 400, 652-655.

Kuhnt, W., Moullade, M., & Kaminski, M. A., 1996. *Ecological structuring and evolution of deep sea agglutinated foraminifera — a review*. Revue de Micropaléontologie, 39(4), 271–281. doi:10.1016/s0035-1598(96)90119-1.

Kuhnt, W., Moullade, M., Kaminski, M.A., 1998. *Upper Cretaceous, K/T boundary, and Paleocene agglutinated foraminifers from Hole 959D (Côte d'Ivoire-Ghana Transform Margin).* Proceedings of the Ocean Drilling Program: Scientific Results 159. doi:10.2973/odp.proc.sr.159.039.1998.

Leinen, M., 1979. *Biogenic silica accumulation in the central equatorial Pacific and its implications for Cenozoic paleoceanography*. Geol. Soc. Am. Bull. 90, 1310–1376.

Lisiecki, L.E., Raymo, M.E., 2005. *A Plio–Pleistocene stack of 57 globally distributed benthic d180 records*. Paleoceanography 20, PA1003. doi:10.1029/2004PA001 071

Lohmann, G.P., 1978. *Abyssal Benthonic Foraminifera as Hydrographic Indicators in the Western South Atlantic Ocean.* Journal of Foraminiferal Research, v. 8. (1), 6-34.

Lourens, L.J., Hilgen, F.J., Shackleton, N.J., Laskar, J., Wilson, D., 2004. *The Neogene Period.* In: Gradstein, F.M., Ogg, J.G., Smith, A.G. (Eds.), A Geological Time Scale 2004. Cambridge University Press, Cambridge, 409–440.

Lyle, M., Pisias, N., 1990. *Ocean circulation and atmospheric CO changes: coupled use of models and paleoceanographic 2 data*. Paleoceanography 5, 15–41.

Mackensen, A., Harloff, J., 1995. *Recent benthic foraminiferal associations and ecology of the Scotia Sea and Argentine Basin*. Marine Micropaleontology, 31(1-2), 1-29.

Martini, E., 1971. Standard Tertiary and Quaternary calcareous nannoplankton zonation. In: Farinacci, A. (Ed.), Proceedings 2nd International Conference Planktonic Microfossils Roma: Rome (ed. Tecnosci.) 2, 739-785.

Miller, K.G., Wright, J.D., and Fairbanks, R.G., 1991. *Unlocking the ice house: Oligocene-Miocene oxygen isotopes, eustasy, and margin erosion.* J. Geophys. Res., 96(B4), 6829–6848.

Milliman, J.D. 1993: *Production and accumulation of calcium carbonate in the ocean: budget of a nonsteady state.* Global Biogeochemical Cycles 7, 927–957.

Mikkelsen, N., 1990. *Cenozoic diatom biostratigraphy and paleoceanography of the western equatorial Indian Ocean.* Proc. ODP, Sci. Results 115, 411–432

Mortimer, N., Campbell, H.J., Tulloch, A.J., King, P.R., Stagpoole, V.M., Wood, R.A., Rattenbury, M.S., et al., 2017. *Zealandia: Earth's hidden continent.* GSA Today, 27(3):27-35. doi:10.1130/GSATG321A.1.

Munsell Color Company, Inc., 1994. *Munsell Soil Color Chart* (revised edition): Newburgh, MD (Munsell Color).

Murray, J.W., 1991. *Ecology and Palaeoecology of Benthic Foraminifera.* Elsevier, Amsterdam.

Murray, J.W., 2001. *The niche of benthic foraminifera, critical thresholds and proxies.* Mar. Micropaleontol. 41, 1-8.

Murray, J.W., 2009. *Ecology and applications of benthic foraminifera.* Cambridge University Press. doi:10.1017/CBO9780511535529.

Nees, S., Struck, U., 1999. *Benthic Foraminieral response to major paleoceanographic changes. Reconstructing Ocean History: A Window into the Future.* Abrantes F, Mix A (eds), Kluwer Academic/Plenum Publishers, pp. 195–216.

Nicolo, C.S., Dickens, G.R., Hollis, C.J., and Zachos, J.C., 2007. Multiple early *Eocene hyperthermals: their sedimentary expression on the New Zealand continental margin and in the deep sea.* Geology, 35(8):699-702. doi:10.1130/G23648A.1

Nigrini, C., 1991. *Composition and biostratigraphy of radiolarian assemblages from an area of upwelling Northwestern Arabian.* Sea, Leg 117. Proc. ODP, Sci. Results 117, 89–126.

Nomura, R., 1991. *Oligocene to Pleistocene benthic foraminiferal assemblages at sites 754 and 756, eastern Indian Ocean.* Proc. ODP, Sci. Results 121, 31–76.

Okada, H., Burky, D., 1980. *Supplementary modification and introduction of code numbers to the low-latitude coccolith biostratigraphic zonation* (Burky 1973, 1975). Marine Micropaleontology 5, 321-325.

Olson, D.B., Hitchcock, G.L., Fine, R.A., Warren, B.A., 1993. *Maintenance of the low-oxygen layer in the central Arabian Sea. Deep-Sea Res*., Part II 40, 673–685.

Pälike, H., Norris, R.D., Herrle, J.O., Wilson, P.A., Coxall, H.K., Lear, C.H., Shackleton, N.J., Tripati, A.K., Wade, B.S., 2006. *The heartbeat of the Oligocene climate system.* Science 314, 1894–1898. doi:10.1126/science.1133822.

Pälike, H., et al., 2007. *Ceara Rise Oligocene–Miocene ODP926B Stable Isotope Data.* IGBP PAGES/World Data Center for Paleoclimatology. Data Contribution Series # 2007-017 NOAA/NCDC Paleoclimatology Program, Boulder CO, USA.

Perch-Nielsen, K., 1985. *Cenozoic calcareous nannoplankton*. In: Bolli, H.M., Saunders, J.B., Perch Nielsen, K., (Eds.), Plankton Stratigraphy, Cambridge University Press, pp. 427-554.

Peterson, L.S., Backman, J., 1990. *Late Cenozoic carbonate accumulation rates of ODP Leg 115 samples*. PANGAEA. doi:10.1594/PANGAEA.755788.

Peterson, L.C., Murray, D.W., Ehrmann, W.U., Hempel, P., 1992. *Cenozoic carbonate accumulation and compensation depth changes in the Indian Ocean.* In: Duncan, R.A., Rea, D.K., Kidd, R.B., Von Rad, U., Weissel, J.K.

Eds. , Synthesis of Results From Scientific Drilling in the Indian Ocean. Am. Geophys. Union, Geophys. Monogr. 70, 311–333.

Pross, J., Contreras, L., Bijl, P.K., Greenwood, D.R., Bohaty, S.M., Schouten, S., Bendle, J.A., et al., 2012. *Persistent near-tropical warmth on the Antarctic continent during the early Eocene epoch*. Nature, 488(7409):73-77. doi:10.1038/nature11300.

Raffi, I. and Flores, J.-A., 1995. *Pleistocene through Miocene calcareous nannofossils from eastern equatorial Pacific Ocean (Leg 138).* In Pisias, N.G., Mayer, L.A. Janecek, T.R., Palmer-Julson, A., and van Andel, T.H. (Eds), *Proc. ODP, Sci. Repults*, 138: College Station, TX (Ocean Drilling Program), 223-286.

Raffi, I., Backman, J., & Rio, D., 1998. *Evolutionary trends of tropical calcareous nannofossils in the late Neogene.* Marine Micropaleontology, 35(1-2), 17–41. doi:10.1016/s0377-8398(98)00014-0.

Raffi, I., Backman, J., Fornaciari, E., Pälike, H., Rio, D., Lourens, L., & Hilgen, F., 2006. *A review of calcareous nannofossil astrobiochronology encompassing the past 25 million years.* Quaternary Science Reviews, 25(23-24), 3113–3137. doi:10.1016/j.quascirev.2006.07.007.

Rea, D.K., 1992. *Delivery of Himalayan sediment to the Northern Indian Ocean and its relation to global climate, sea level, uplift, and seawater strontium.* In: Duncan, R.A., Rea, D.K., Kidd, R.B., Von Rad, U., Weissel, J.K. Eds. , Synthesis of Results From Scientific Drilling in the Indian Ocean. Am. Geophys. Union, Geophys. Monogr. 70, 387–402.

Rea, D.K., Basov, I.A., Krissek, L.A. et al., 1995. *Scientific results of drilling the North Pacific transect.* Proc. ODP, Sci. Results 145, 577–596.

Reid, J.L., 1965. *Intermediate waters of the Pacific Ocean.* Johns Hopkins Oceanographic Studies No. 2, Baltimore, 85 pp.

Resig, J.M., 1993. *Cenozoic stratigraphy and paleoceanography of biserial planktonic foraminfers, Ontong Java Plateau*. Proc. ODP, Sci. Results 130, 231–244.

Rind, D., Chandler, M., 1991. *Increased ocean heat transports and warmer climate*. J. Geophys. Res. 96, 7437–7461.

Ruddiman, W.F., 2008. *Earth's climate, Past and Future (2nd edition).* Eds. W.H. Freeman and Company, New York.

Salvador, A., 1994. *International Stratigraphic Guide.* Second Edition. The International Union of Geological Sciences and The Geological Society of America, Inc.

Saraswati, P.K. and Srinivasan, M.S., 2016. *Micropaleontology principles and applications.* Springer Inter. Pub., Switzerland, 224 p.

Savin, S.M., Douglas, R.G., and Stehli, F.G., 1975. *Tertiary marine paleotemperatures.* Geol. Soc. Am. Bull., 86, 1499–1510.

Schneider, D.A., 1995. *Paleomagnetism of some Leg 138 sediments: Detailing Miocene magnetostratigraphy.* In: Pisias, N.G., Mayer, L.A., Janecek, T.R., Palmer-Julson, A., van Andel, T.H., et al., Proceedings ODP, Scientific Results 138 (Ocean Drilling Program, College Station, TX), 69–72. doi:10.2973/odp.proc.sr.138.105.1995.

Schroeder, C., Scott, D.B., Medioli, F.S., 1987. *Can smaller benthic foraminifera be ignored in paleoenvironmental analysis?* J. Foraminifer. Res. 17, 101-105.

Seisser, W.G., 1995. *Paleoproductivity of the Indian Ocean during the Tertiary Period.* Global Planet. Change 11, 71–88.

Shackleton, N.J., and Kennett, J.P., 1975. *Paleotemperature history of the Cenozoic and the initiation of Antarctic glaciation: Oxygen and carbon isotope analyses in DSDP sites 277, 279, and 281.* Init. Rep. DSDP Proj., 29, 743–755.

Shackleton, N.J., Baldauf, J., Flores, J.A., Iwai, M., Moore, T.C., Raffi, I., Vincent, E., 1995. *Biostratigraphic summary for Leg 138.* In Pisias, N.G., Mayer, L.A., Janecek, T.R., Palmer-Julson, A., van Andel, T.H., et al., Proceedings ODP, Scientific Results 138 (Ocean Drilling Program, College Station, TX), 517–536. doi:10.2973/ odp.proc.sr.138.127.1995.

Shackleton, N.J., Crowhurst, S., 1997. *Sediment fluxes based on an orbitally tuned time scale 5 Ma to 14 Ma, Site 926.* In: Curry, W.B., Shackleton, N.J., Richter, C., Bralower, T.J., et al., Proceedings ODP, Scientific Results 154 (Ocean Drilling Program, College Station, TX), 69–82. doi:10.2973/odp.proc.sr.154.102.1997.

Smart, C.W., King, S.C., Gooday, A.J., Murray, J.W., Thomas, E., 1994. *A benthic foraminiferal proxy of pulsed organic matter paleofluxes.* Mar. Micropaleontol. 23, 89-99. doi:10.1016/0377-8398(94)30002-7.

Slotnick, B.S., Dickens, G.R., Nicolo, M.J., Hollis, C.J., Crampton, J.S., Zachos, J.C., and Sluijs, A., 2012. *Large-amplitude variations in carbon cycling and terrestrial weathering during the latest Paleocene and earliest Eocene: the record at Mead Stream, New Zealand.* The Journal of Geology, 120(5):487-505. doi:10.1086/666743.

Sutherland, R., Dickens, G.R., Blum, P., and the Expedition 371 Scientists, 2019. *Proceedings of the International Ocean Discovery Program Volume 371.* publications.iodp.org, doi:10.14379/iodp.proc.371.102.2019.

Takayama, T., 1993. *Notes on Neogene calcareous nannofossili biostratigraphy of the Ontong Java Plateau and size variations of Reticulofenestra coccoliths.* In Berger, W.H., Kroenke, L.W. Mayer, L.A., et al., *Proc. ODP, Sci. Results*, 130: College Station, TX (Ocean Drilling Program), 179-229.

Tarduno, J.A., 1994. *Temporal trends of magnetic dissolution in the pelagic realm: gauging paleoproductivity?* Earth Planet. Sci. Lett. 123, 39–48

Theyer, F., Mayer, L.A., Barron, J.A., Thomas, E., 1985. *The equatorial Pacific high-productivity belt: elements for a synthesis of Deep Sea Drilling Project Leg 85 results.* Initial Rep., DSDP 85, 971–985.

Treguer, P., Nelson, D.M., Van Bennekom, A.J., DeMaster, D.J., Leynaert, A., Queguiner, B., 1995. *The silica balance in the world ocean*; a reestimate. Science 268, 375–379.

Van Andel, T.H., Heath, G.R., Moore Jr., T.C., 1975. *Cenozoic history and paleoceanography of the central equatorial Pacific Ocean: a regional synthesis of Deep Sea Drilling Project data.* Geol. Soc. Am., Mem. 143, 143 pp.

Van Morkhoven, F.P.C.M., Berggren, W.A., Edwards, A.S., 1986. *Cenozoic cosmopolitan deep-water benthic foraminifera.* Bull. Cent. Rech. Explor.-Product. Elf-Aquitaine, Mem. 11, 421 pp.

Wade, B.S., Pearson, P.N., Berggren, W.A., Pälike, H., 2011. *Review and revision of Cenozoic tropical planktonic foraminiferal biostratigraphy and calibration to the geomagnetic polarity and astronomical time scale.* Earth-Science Reviews 104, 111–142. doi:10.1016/ j.earscirev.2010.09.00.

Westerhold, T., Röhl, U., Donner, B., and Zachos, J.C., 2018. *Global extent of early Eocene hyperthermal events: a new Pacific benthic foraminiferal isotope record from Shatsky Rise (ODP Site 1209).* Paleoceanography and Paleoclimatology, 33(6):626-642. doi:10.1029/2007GC001710.

Woodruff, F., 1985. *Changes in Miocene deep-sea benthic foraminiferal distribution in the Pacific Ocean: relationship to paleoceanography.* Geol. Soc. Am. Bull., Mem. 143, 131–175.

Woodruff, F., Douglas, R.G., 1981. *Response of deep-sea benthic foraminifera to Miocene paleoclimatic events, DSDP site 289.* Mar. Micropaleontol. 6, 617–632.

Wright, Miller, 1996. *Control of North Atlantic Deep Water circulation by the Greenland–Scotland Ridge.* Paleoceanography 11, 157–170.

Wyrtki, K., 1971. *Oceanographic Atlas of the International Indian Ocean Expedition.* National Science Foundation, Washington, DC, 351 pp.

Zachos, J.C., Flower, B.P., Paul, H. 1997. *Orbitally paced climate oscillations across the Oligocene/Miocene boundary.* Nature. 1997, Vol. 388, p. 567-570.

Zachos, J.C., Pagani, M., Sloan, L., Thomas, E., Billups, K., 2001. *Trends, rythyms, and aberrations in global climate 65 Ma to Present.* Science, vol. 292, pp. 686-693.

Zachos, J.C., Dickens, G.R., and Zeebe, R.E., 2008. *An early Cenozoic perspective on greenhouse warming and carbon-cycle dynamics.* Nature, 451(7176):279-283. doi:10.1038/nature06588
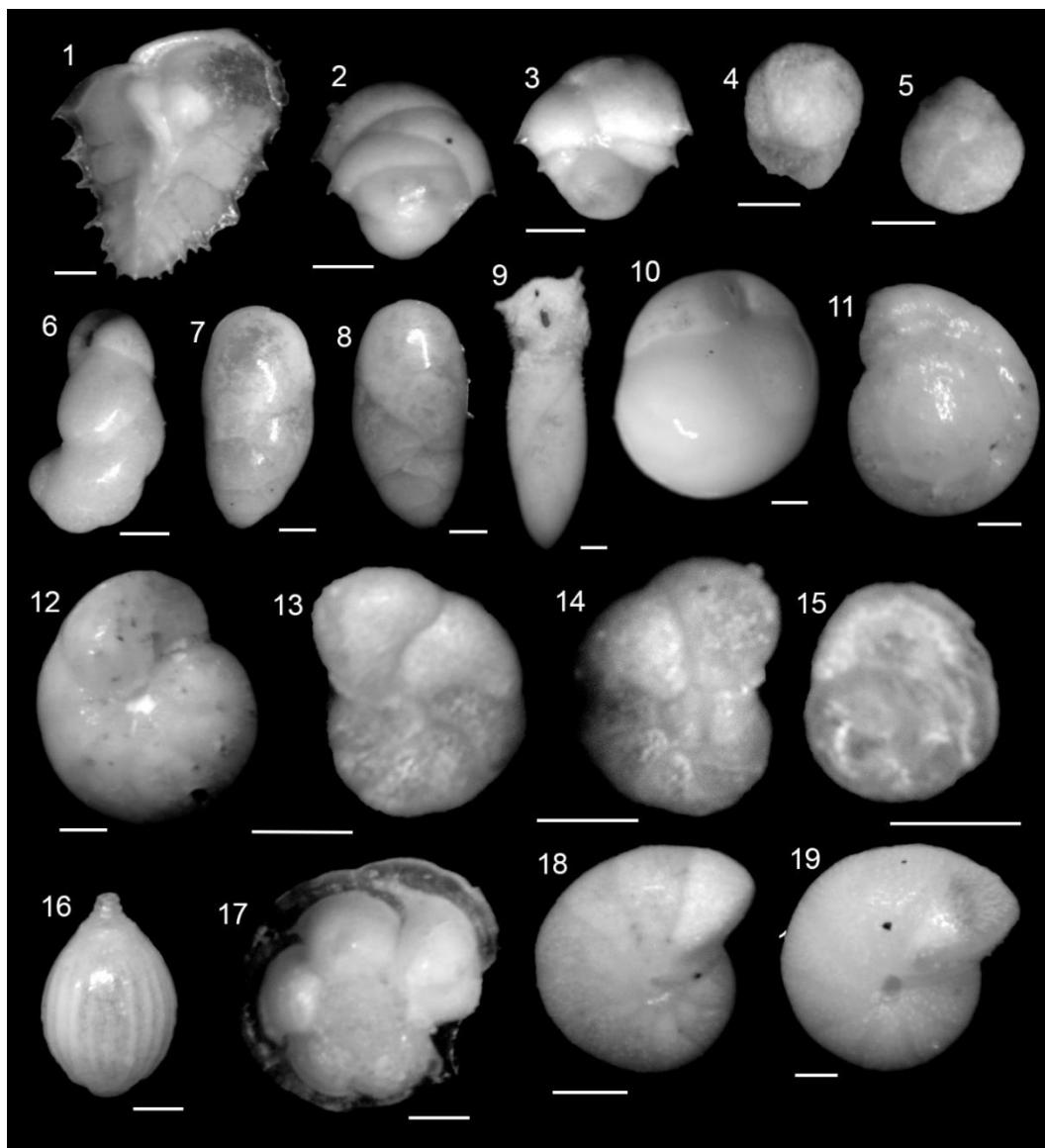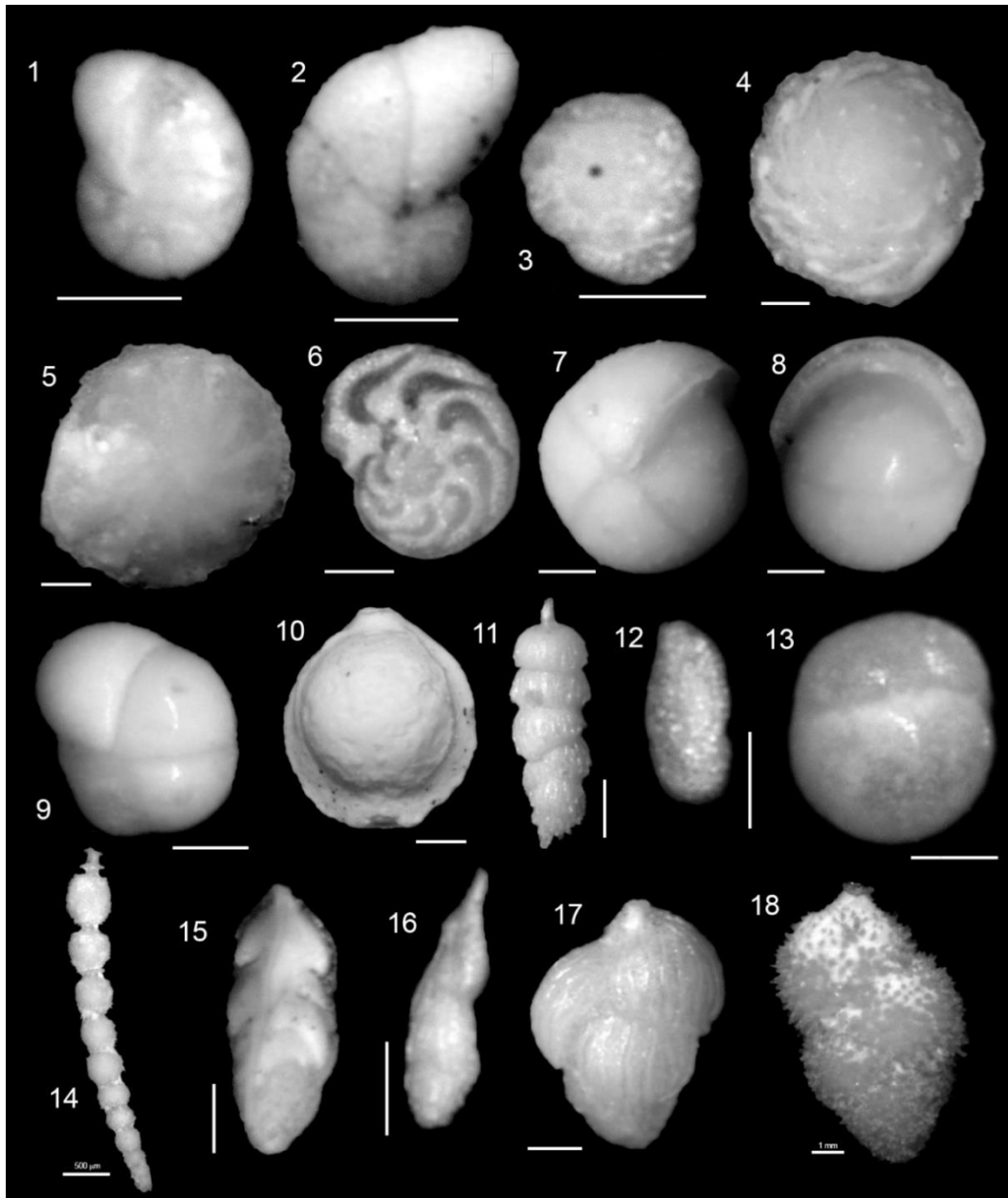
APPENDIX I - PLATES

PLATE I
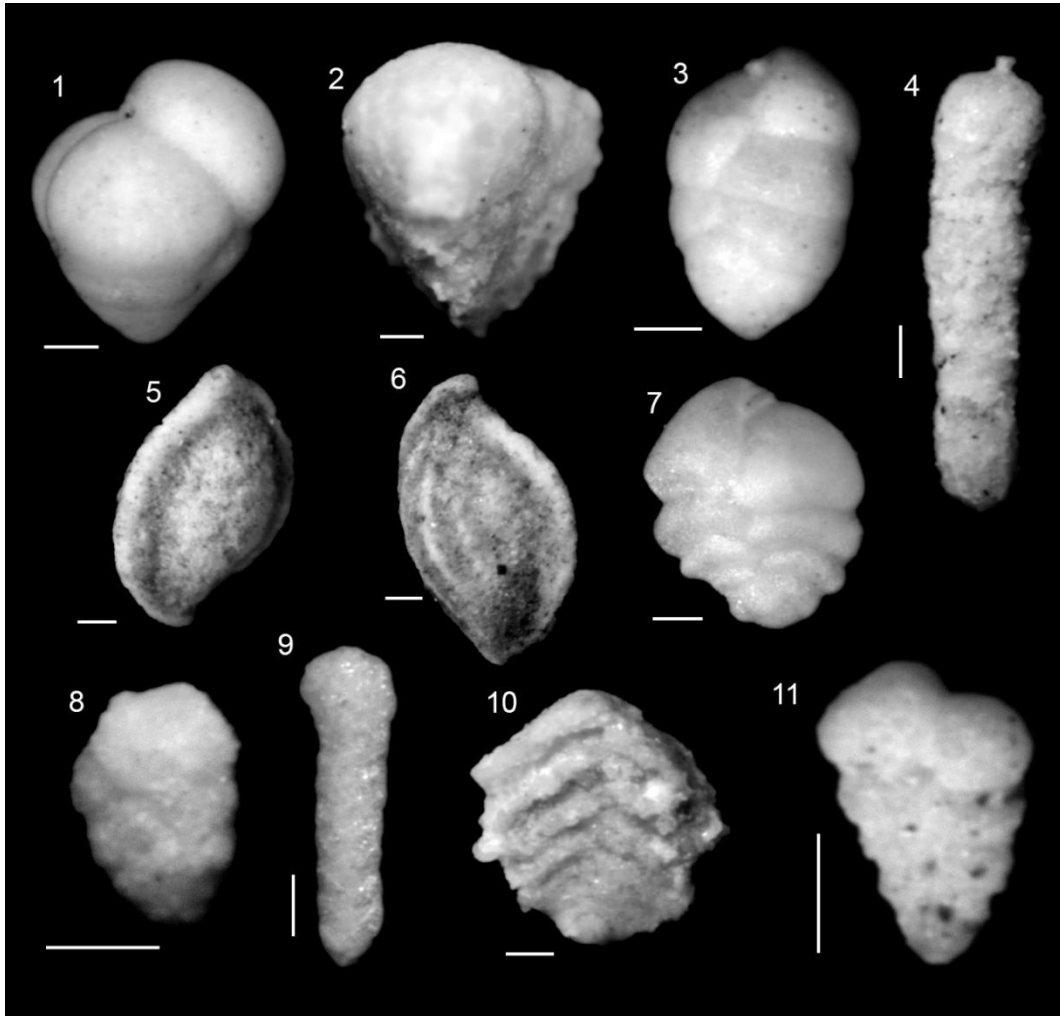
Plate I. Microphotographies of benthic foraminifera from IODP Site U1506A. Binocular stereoscopic microscope. Scale-bar = 100 μm.

1. *Eggerella bradyi*, U1506A-19R-3(122-124)-n.44; **2.** *Gaudryna* sp. 1, U1506A-19R-5(22-24)-N.44 ; **3.** *Karreriella bradyi*, U1506A-17R-2(133-135)-n.47; **4.** *Martinotiella petrosa*, U1506A-17R-3(138-140)-n.48; **5, 6.** *Sigmoilina schlumbergeri*, U1506A-19R-4(22-24)-n.47;

7. *Siphotextularia flintii*, U1506A-19R-4(147-149)-n.47; **8.** *Siphotextularia foliosa*, U1506A-21R-2(50-52)-n.47; **9.** *Spiroplectamina spectabilis*, U1506A-12R-1(110-112)-n.39;

10. *Textularia lythostrota*, U1506A-19R-3(122-124)-n.46; **11.** *Textularia* sp., U1506A-21R-4(140-142)-n.45.

PLATE II
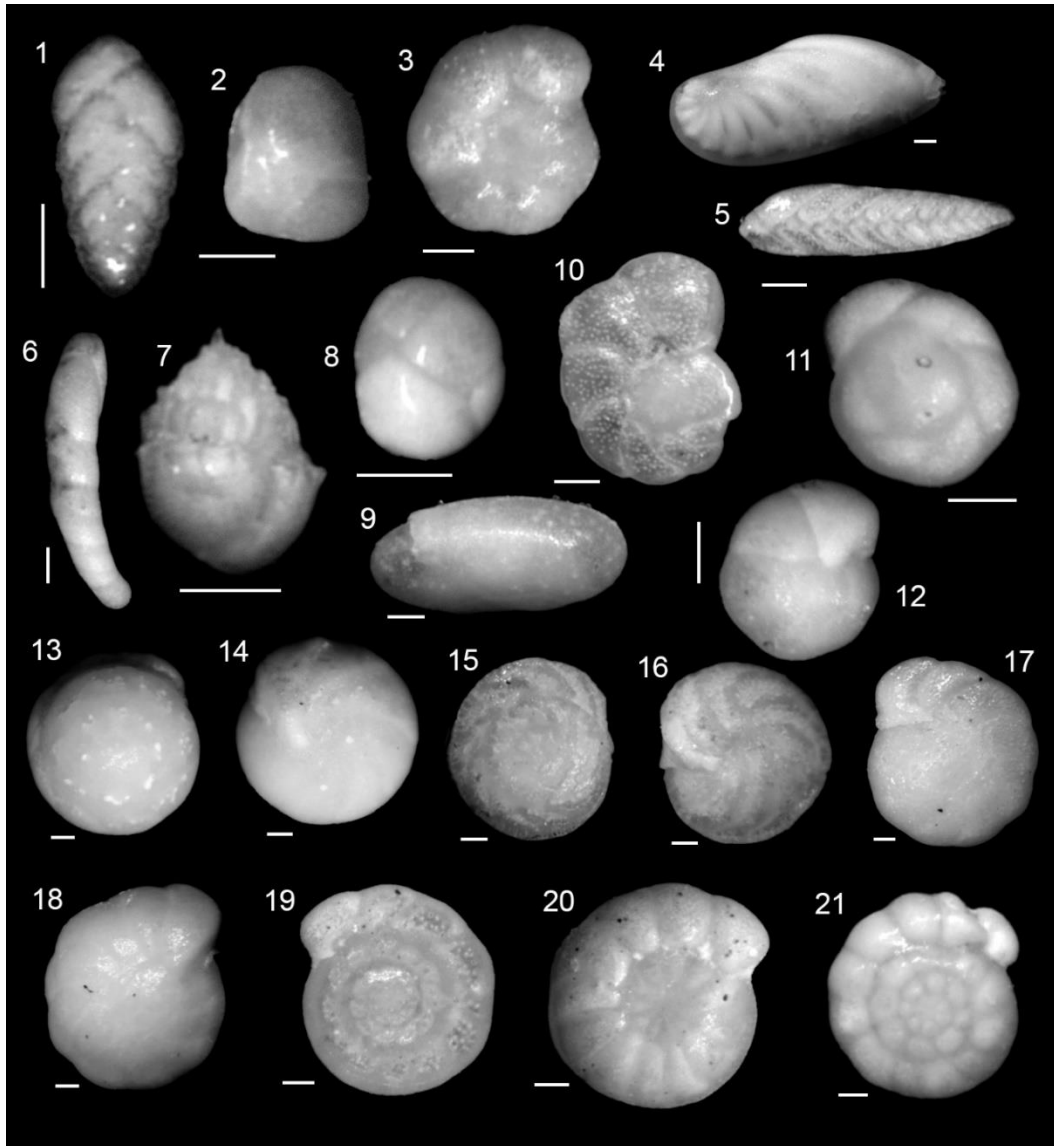
Plate II. Microphotographies of benthic foraminifera from IODP Site U1506A. Binocular stereoscopic microscope. Scale-bar = 100 µm.

1. *Abditodentrix asketocomptella*, U1506A-18R-1(48-50)-n.24; **2.** *Allomorphina pacifica*, U1506A-17R-2(133-135)-N.43; **3.** *Anomalinoides globulosus*, U1506A-19R-3(122-124)-n.24; **4.** *Astacollus*, U1506A-19R-4(122-124)-n.55; **5.** *Bolivina finlayi*, U1506A-14R-3(130-132)-n.55; **6.** *Bulimina elongata*, U1506A-18R-3(50-52)-n.39; **7.** *Bulimina striata*, U1506A-18R-5(116-118)-n.41; **8.** *Cassidulina crassa*, U1506A-11R-3(130-132)-n.08; **9.** *Chilostomella oolina*, U1506A-18R-2(51-53)-n.57; **10.** *Cibicides lobatulus*, U1506A-19R-4(22-24)-n.24; **11, 12.** *Cibicidoides bradyi*, U1506A-11R-3(130-132)-n.04; **13, 14.** *Cibicidoides havanensis*, U1506A-20R-3(50-52)-n.14; **15, 16.** *Cibicidoides mexicanus*, U1506A-13R-3(130-132)-n.13; **17, 18.** *Cibicidoides mundulus*, U1506A-17R-3(138-140)-n.02; **19, 20.** *Cibicidoides robertsonianus*, U1506A-21R-2(50-52)-n.05; **21.** *Cibicidoides robertsonianus*, U1506A-20R-3(50-52)-n.12.

PLATE III

Plate III. Microphotographies of benthic foraminifera from IODP Site U1506A. Binocular stereoscopic microscope. Scale-bar = 100 µm.

1. *Ehrenbergina carinata*, U1506A-19R-4(22-24)-n.54; **2, 3.** *Ehrenbergina glabra*, U1506A-12R1(110-112)-n.40; **4, 5.** *Epistominella exigua*, U1506A-18R-1(48-50)-n.26; **6.** *Evolvocassidulina*, U1506A-17R-1(132-134)-n.52; **7, 8.** *Francesita advena*, U1506A-20R-5(50-52)-n.56; **10.** *Globocassidulina subglobosa*, U1506A-11R-1(105-107)-n.24; **11, 12.** *Gyroidina orbicularis*, U1506A-21R-4(140-142)-n.21; **13, 14.** *Hanzawaia ammophila*, U1506A-18R-3(50-52)-n.21; **15.** *Heronallenia unguiculata*, U1506A-16R-5(63-65)-n.55; **16.** *Lagena*, U1506A-16R-4(126-128)-n.62; **17.** *Laticarinina altocamerata*, U1506A-10R-1(100-102)-n.36; **18.** *Melonis barleeanum*, U1506A-16R-1(136-138)-n.07; **19.** *Melonis pompilioides,* U1506A-10R-1(100-102)-n.06.

PLATE IV

Plate IV. Microphotographies of benthic foraminifera from IODP Site U1506A. Binocular stereoscopic microscope. Scale-bar = 100 μm.
1. *Nonion*, U1506A-11R-1(105-107)-n.36; **2.** *Nonionella*, U1506A-20R-5(50-52)-n.37; **3.** *Nuttalides umbonifera*, U1506A-14R-3(130-132)-n.09; **4, 5.** *Osangularia culter*, U1506A-10R-1(100-102)-n.24; **6.** *Planulina* sp. 1, U1506A-18R-3(125-127)-n.41; **7, 8.** *Pullenia bulloides*, U1506A-10R-1(100-102)-n.56; **9.** *Pullenia quinqueloba*, U1506A-13R-1(100-102)-n.30; **10.** *Pyrgo murrhina*, U1506A-19R-4(22-24)-n.61; **11.** *Rectuvigerina multicostata*, U1506A-20R-5(50-52)-n.26; **12.** *Seabrookia pellucida,* U1506A-20R-5(50-52)-n.63; **13.** *Sphaeroidina bulloides*, U1506A-16R-4(126-128)-n.03; **14.** *Stillostomella*, U1506A-17R-1(132-134)-n.34; **15.** *Trifarina bradyi*, U1506A-13R-1(100-102)-n.44; **16.** *Uvigerina occidentalis*, U1506A-16R-4(126-128)-n.41; **17.** *Uvigerina peregrina* s.l., U1506A-16R-4(126-128)-n.41; **18.** *Uvigerina proboscidea*, U1506A-16R-5(63-65)-n.40.

PLATE V
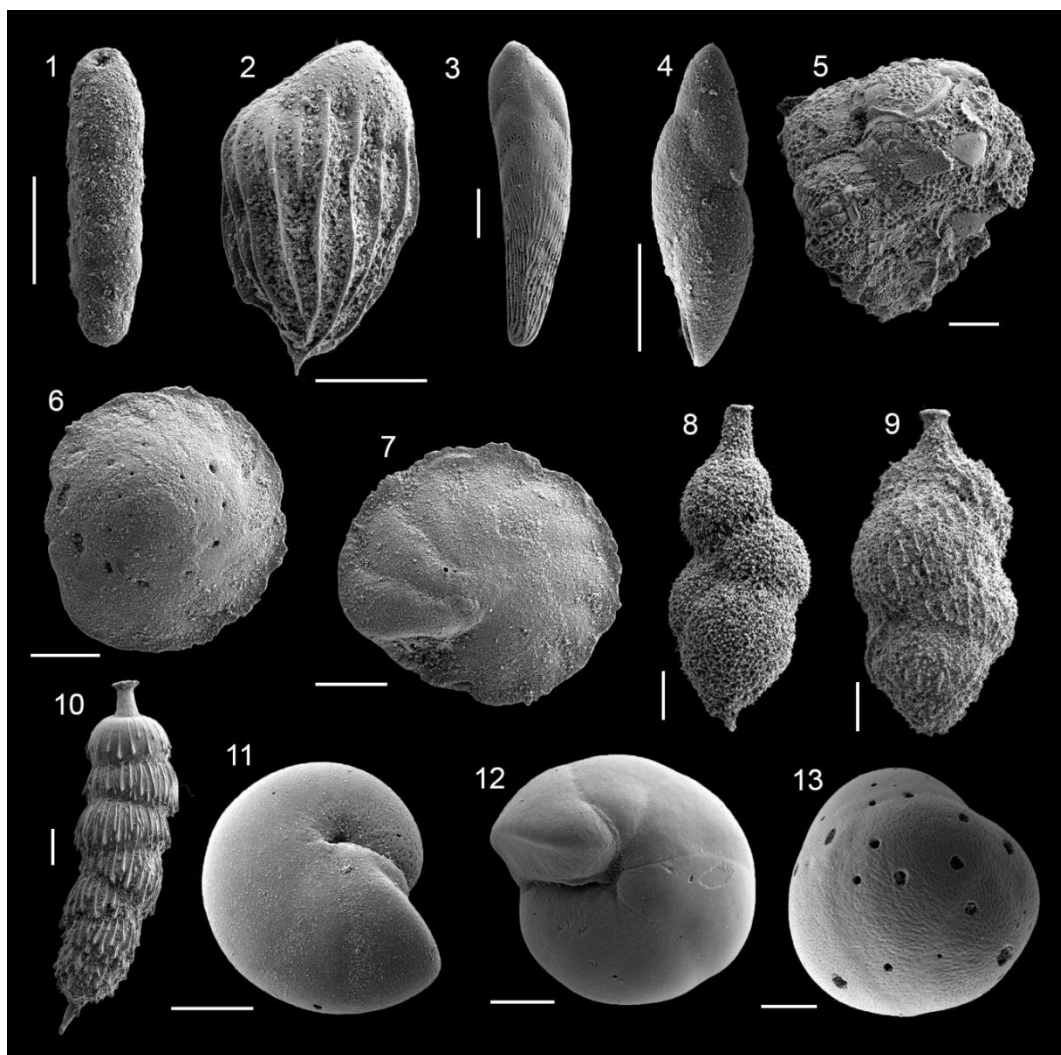
Plate V. Scanning electron (SEM) micrographs of selected benthic foraminiferal species from IODP Site U1506A sample 21R-1(140-142) (Credit Lucía Rivero-Cuesta). Scale-bar = 100 µm. **1.** *Fursenkoina*; **2.** *Bulimina truncana*; **3.** *Bolivina finlayi*; **4.** *Pleurostomella*; **5.** *Gaudryna* sp. 1; **6, 7.** *Osangularia culter*; **8.** *Uvigerina proboscidea*; **9.** *Uvigerina peregrina* s.l.; **10.** *Rectuvigerina semicostata*; **11.** *Melonis barleeanum*; **12.** *Gyroidina soldanii*; **13.** *Globocassidulina subglobosa*.

PLATE VI
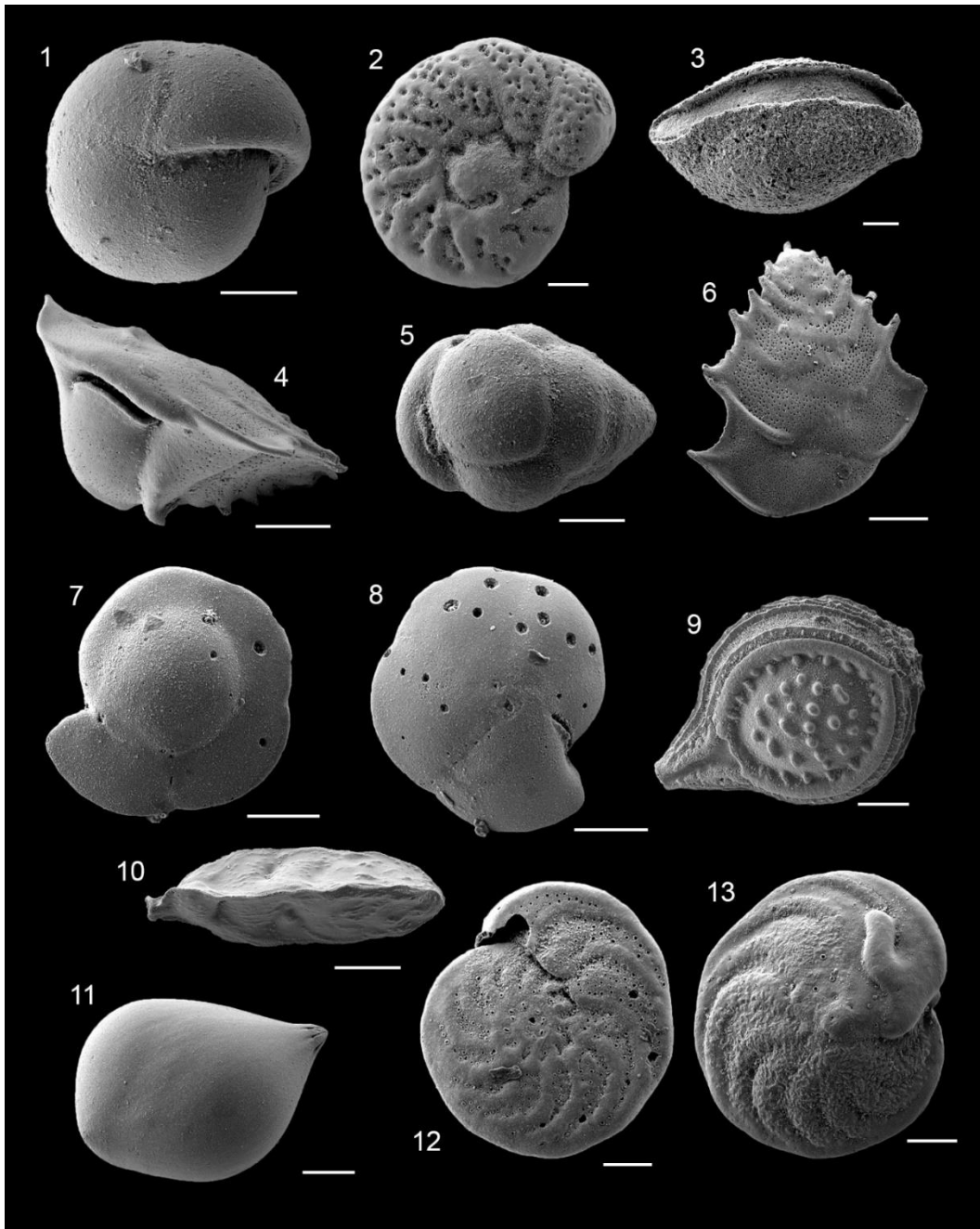
Plate VI. Scanning electron (SEM) micrographs of selected benthic foraminiferal species from IODP Site U1506A sample 21R-1(140-142) (Credit Lucía Rivero-Cuesta). Scale-bar = 100 µm. **1.** *Pullenia bulloides*; **2.** *Anomalinoides* sp.; **3.** *Sigmoilina schlumbergeri*; **4, 6.** *Ehrenbergina carinata*; **5.** *Eggerella bradyi*; **7, 8.** *Oridorsalis umbonatus*; **9.** *Fissurina*; **10.** *Trifarina bradyi*; **11.** *Polymorphinid*; **12, 13.** *Planulina wuellestorfi*.

PLATE VII
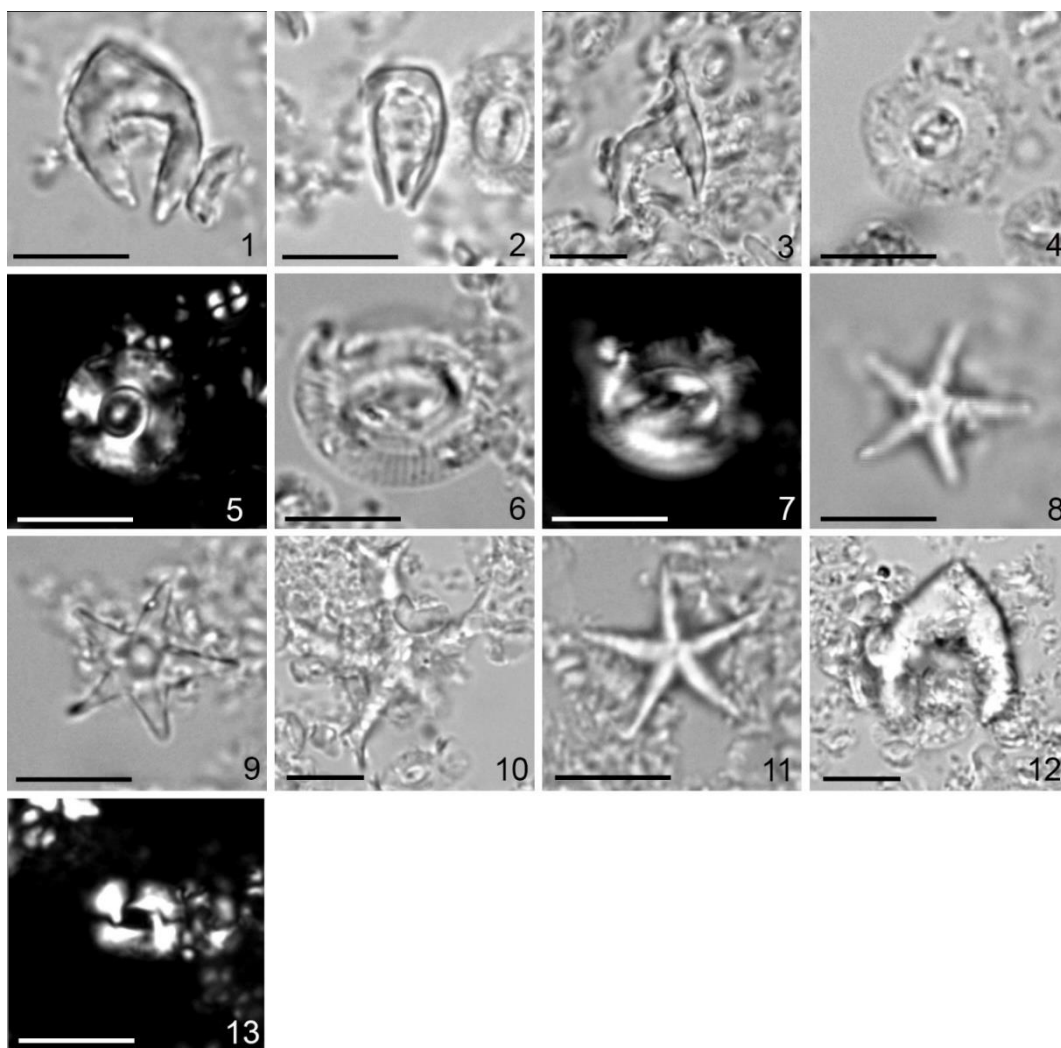
Plate 7. Microphotographies of calcareous nannofossils from IODP Site U1506A. Optical polarizing microscope (1250 magnifications), parallel and crossed nicols. Scale-bar = 5 µm.
1. *Amaurolithus primus*, U1506A-20R-2W, 74 cm; **2.** *Amaurolithus primus*, U1506A-17R-CC, 05 cm; **3.** *Amaurolithus tricorniculatus*, U1506A-11R-CC, 05 cm; **4, 5.** *Calcidiscus macintyrei*, U1506A-25R-CC, 05 cm; **6, 7.** *Coccolithus miopelagicus*, U1506A-25R-CC, 05 cm; **8, 9.** *Discoaster berggrenii*, U1506A-24R-2W, 75 cm; **10.** *Discoaster pentaradiatus*, U1506A-13R-CC, 05 cm; **11.** *Discoaster quinqueramus*, U1506A-17R-CC, 05 cm; **12.** *Nickilithus amplificus*, U1506A-17R-CC, 05 cm; **13.** *Reticulofenestra pseudoumbilicus*, U1506A-17R-CC, 05 cm.

APPRENDIX II - TAXONOMIC LIST

Alphabetical list of taxa mentioned in this thesis.

Benthic foraminifera

Eggerella bradyi (Cushman 1911)
Gaudryina sp. 1
Gaudryina spp.
Karreriella bradyi (Cushman 1911)
Karreriella spp.
Martinotiella petrosa (Cushman and Bermúdez 1937)
Martinotiella sp.
Sigmolina schlumbergeri (Silvestri 1904)
Siphotextularia flintii (Cushman 1911)
Siphotextularia foliosa Zheng 1988
*Spiroplectammina spectabilis (*Grzybowski 1898) emend. Kaminski, 1984
Textularia lythostrota (Schwager 1866)
Textularia spp.
Vulvulina sp.
Abditodentrix asketocomptella (Patterson 1985)
Alabamina spp.
Allomorphina pacifica Cushman and Todd 1949
Anomalinoides globulosus (Chapman and Parr 1937)
Anomalinoides spp. Brotzen 1942
Astacolus spp.
Bolivina finlayi Hornibrook 1961
Bulimina spp.
Bulimina elongata d'Orbigny 1846
Bulimina marginata d'Orbigny 1826
Bulimina striata d'Orbigny 1843
Bulimina truncana Gümbel 1868
Chilostomella oolina Schwager 1878
Cassidulina crassa d'Orbigny 1839
Cibicides lobatulus (Walker and Jacob 1798)
Cibicidoides bradyi (Trauth 1918)
Cibicidoides havanensis (Cushman and Bermúdez 1937)
Cibicidoides mexicanus (Nuttall 1932)
Cibicidoides micrus (Bermúdez 1949)
Cibicidoides mundulus (Brady, Parker and Jones 1888)
Cibicidoides robertsonianus (Bradyi 1881)
Cibicidoides spp.
Ehrenbergina carinata Eade 1967
Ehrenbergina glabra Heron-Allen and Earland 1922
Ehrenbergina marwicki Finlay 1939
Ehrenbergina spp.
Epistominella exigua (Brady 1884)
Evolvocassidulina sp.
Fissurina spp.

Francesita advena (Cushman 1922)
Francuscia extensa (Cushman 1923)
Fursenkoina sp.
Globocassidulina subglobosa (Brady 1881)
Globulina spp.
Gyroidina orbicularis d'Orbigny in Parker, Jones and Brady 1865
Gyroidina soldani (d'Orbigny 1826)
Gyroidina spp.
Gyroidina sp.1
Hanzawaia ammophila (Guembel 1868)
Heronallenia sp.
Heronallenia unguiculata (Sidebottom 1918)
Lagena spp.
Laticarinina altocamerata (Herron-Allen and Earland 1922)
Laticarinina pauperata (Parker and Jones 1865)
Lenticulina spp.
Melonis barleeanum (Williamson 1858)
Melonis pompolioides (Fichtel and Moll 1798)
Melonis spp.
Miliolids
Nodosariids
Nonion spp.
Nonionella spp.
Nuttallides umbonifera (Cushman 1933)
Nuttallinella spp.
Oridorsalis spp.
Oridorsalis umbonatus (Reuss 1851)
Osangularia culter (Parker and Jones 1865)
Osangularia spp.
Planulina wuellestorfi (Schwager 1866)
Planulina spp.
Planulina sp.1
Planulina sp.2
Pleurostomella spp.
Polymorphinids
Pullenia bulloides (d'Orbigny 1846)
Pullenia quinqueloba (Reuss 1851)
Pullenia sp.
Pyrgo murrhina (Schwager 1866)
Rectuvigerina multicostata (Cushman & Jarvis, 1929)
Seabrookia pellucida Brady 1890
Sphaeroidina bulloides d'Orbigny in Deshayes 1828
Stillostomellids
Trifarina bradyi Cushman 1923
Uvigerina occidentalis Cushman 1923
Uvigerina peregrina s.l. Cushman 1923
Uvigerina proboscidea Schwager 1866
Uvigerina spp.
Valvulineria minuta (Schubert 1904)

Calcareous nannofossil

Amaurolithus Gartner and Bukry, 1975
Amaurolithus delicatus Gartner and Bukry, 1975
Amaurolithus primus (Bukry and Percival, 1971) Gartner and Bukry, 1975
Amaurolithus tricorniculatus (Gartner, 1967) Gartner and Bukry, 1975

Calcidiscus Kamptner, 1950
Calcidiscus leptoporus (Murray & Blackman 1898) Loeblich & Tappan, 1978
Calcidiscus macintyrei (Bukry and Bramlette, 1969) Loeblich and Tappan, 1978

Ceratolithus Kamptner, 1950
Ceratolithus acutus Gartner & Bukry 1974
Ceratolithus atlanticus Perch-Nielsen, 1977
Ceratolithus rugosus Bramlette & Wilcoxon 1967

Coccolithus Schwartz 1894
Coccolithus miopelagicus Bukry 1971

Discoaster Tan 1927
Discoaster bergenii Russell and Firth, 1989
Discoaster berggrenii Bukry, 1971
Discoaster bellus Bukry and Percival, 1971
Discoaster pentaradiatus Tan, 1927
Discoaster quinqueramus Gartner, 1969

Nickilithus
Nickilithus amplificus (Bukry and Percival, 1971) Raffi, Backman and Rio 1998

Reticulofenestra Hay *et al.* 1966
Reticulofenestra pseudoumbilicus (Gartner, 1967) Gartner, 1969

SUPPLEMENTARY MATERIAL

The attached CD contains:

1. An Excel file (**Benthic foraminifera counting**) with the counts performed on benthic foraminifera. The following are the abbreviations referenced in the file:

- **300**: counting on 300 specimen of benthic foraminifera;
- **% 300**: counting on 300 specimen of benthic foraminifera converted into percentage;
- **H(S)**: data derived from the counting and used to obtain the Shannon-Weaver heterogeneity index.

2. An Excel file (**Calcareous nannofossil counting**) with the counts performed on calcareous nannofossil. The following are the abbreviations referenced in the file:

- **mm^2**: number of specimens belonging to the same taxon present on an area of 1 mm^2;
- **biohorizons**: biohorizons and the biostratigraphic classification

3. A PDF file (**% 300**) with the graphs derived from % 300

ACKNOWLEDGEMENT